Dissecting the heterogeneity of murine mesenchymal bone marrow stromal cells

Dissertation

zur Erlangung des akademischen Grades

doctor rerum naturalium

(Dr. rer. nat.)

im Fach Biologie

eingereicht an der

Lebenswissenschaftlichen Fakultät

der Humboldt-Universität zu Berlin

von

M.Sc. Daniel Lenz (geboren Schulz)

Präsidentin der Humboldt-Universität zu Berlin

Prof. Dr.-Ing. Dr. Sabine Kunst

Dekan der Lebenswissenschaftlichen Fakultät

Prof. Dr. Bernhard Grimm

Gutachter: 1. Andreas Radbruch

2. Andreas Thiel

3. Enrico Klotzsch

Tag der mündlichen Prüfung: 17.12.2019

DRFZ BERLIN
Deutsches Rheuma-Forschungszentrum
Ein Institut der Leibniz-Gemeinschaft

HUMBOLDT-UNIVERSITÄT ZU BERLIN

Dissecting the heterogeneity of murine mesenchymal bone marrow stromal cells

Doctoral thesis to acquire the Dr. rer. nat.

Handed in by

Daniel Lenz,

1st reviewer: Andreas Radbruch

2nd reviewer: Andreas Thiel

3rd reviewer: Enrico Klotzsch

Abstract

Stromal cells of the murine bone marrow receive increasing amounts of attention lately. They have been shown to support survival of hematopoietic stem cells as well as memory lymphocytes. Furthermore, their multipotency is the research foundation of contemporary regenerative therapies. Among these stromal properties their support of memory lymphocytes is of great importance when targeting the perseverance of autoimmune diseases. In the murine bone marrow, long-lived plasma cells reside in close proximity to a subset of VCAM-1^+ stromal cells that secrete CXCL12. A similar pattern of interaction was observed for $CD4^+$ memory T lymphocytes in contact with VCAM-1 expressing stromal cells which provide them with survival signals such as Interleukin-7 constituting a subset within $CXCL12^+$ stroma.

Herein, a protocol was developed to quantitatively obtain VCAM-1^+ and VCAM-1^+ IL-$7^{+/-}$ stromal cells via enzymatic/mechanic digestion and cytoskeleton-inhibition. *Ex vivo* gene expression analysis was performed from sorted, pure cells with good recovery. Candidate genes/markers like CD1d, gas6 or ANXA2R were validated in (high-throughput) flow cytometry and histological analysis including subsequent semi-automated colocalization was performed. CD1d was found to be good surrogate marker for VCAM-1^+PECAM-1^- non-endothelial stroma while the population of $CD200^{int}$/BP-1^+/$CD73^+$/$CD105^-$ stromal cells is greatly enriched in IL-7 producers which was equally true for the stromal transcription factor Prrx1. CD55, BP-1 and Cadherin-11 were found to be differentially expressed in differing IL-7 reporter mice haplotypes that mimic IL-7 abundance. For BP-1 and Cadherin-11, the resulting absence of mature lymphocytes could be ruled out as the reason. The reporter mice haplotypes revealed monoallelic expression features of IL-7. Regardless of haplotype, many hitherto lymphoid-associated markers such as PDC-TREM or CMKLR1 could be observed to be expressed on bulk stroma. Expression of gas6, ANXA2 or CD1d is not restricted to bone marrow stroma but was also observed in spleen albeit with less overlap and architectural differences. ANXA2 and its receptor ANXA2R were implicated in a new interaction between stroma and early B cell lineage in the bone marrow.

All methodologies suggest that VCAM-1^+ as well as IL-$7^{+/-}$ stromal cells are heterogeneous by marker expression yet don't cluster extensively in flow cytometry co-stains. The functional relevance of the marker diversity described in this thesis remains to be tested but insinuates a broad repertoire for bone marrow stroma cells for new interaction pathways with lymphocyte subsets. Ultimately, this knowledge will hopefully feedback to clinical questions of autoimmunity for targeted treatment of stromal niches.

Zusammenfassung

Stromazellen des murinen Knochenmarks sind in den letzten Jahren aus vielerlei Hinsicht in den Fokus der Forschung gerückt. Es konnte gezeigt werden, dass sie durch Bereitstellung von Überlebenssignalen essenziell für die Erhaltung hämatopoetischer Nischen sind – von der Stammzelle über Vorläuferzellen bis hin zu T-/B-Gedächtniszellen sowie Plasmazellen. Ein weiterer Forschungsansatz beruht auf deren Multipotenz, die man sich in regenerativen Therapien zunutze macht, aber die mangelhafte Klassifizierung der Ausgangszellen oft die Vergleichbarkeit von Studien erschwert. Besondere Relevanz haben die Stromazell-Nischen in der Ätiologie vieler Autoimmunerkrankungen. In Erkrankungen wie dem systemischen Lupus erythematosus (SLE) können maligne Plasmazellen, welche Antikörper gegen körpereigene Epitope sezernieren, Jahrzehnte überdauern und das eigene Gewebe nachhaltig schädigen. Während langlebige Plasmazellen zu CXCL12-positiven Knochenmarks-Stromazellen migrieren, konnte Interleukin-7 (IL-7) für T-Zellen als Überlebenssignal identifiziert werden, welches von etwa 50% der Stromazellen exprimiert wird. Gemeinsam ist allen Stromazellen die Expression des Oberflächenmarkers CD106/VCAM-1.

Die Isolation von VCAM-1^{+} Stromazellen wurde mechanisch wie enzymatisch – u.a. durch Inhibition des Cytoskeletts via Latrunculin B – optimiert und erlaubte die quantitative und qualitative Gewinnung der Zellen in Einzelzellsuspensionen. Die *ex vivo* Heterogenität wurde via Genexpressionsstudien und ergründet und *in situ* in der Histologie verifiziert. Besonderes Interesse galt den IL-7^{+} Stromazellen zur Klärung der Fragestellungen, ob Gedächtnis-T-Zellnischen weiter unterteilt werden können oder alle Zellen um dieselbe Nische konkurrieren.

Ein effizientes Protokoll erlaubte die qualitative wie quantitative Isolation von Stromazellen aus dem murinen Knochenmark mit anschließender *ex vivo* Microarray-Analyse. Die auf diese Weise ermittelten Kandidaten-Marker konnten auf Proteinebene via Histologie und (Hochdurchsatz-) Durchflusszytometrie validiert werden. Dazu gehören z-B. die Marker CD1d, gas6 or ANXA2R. CD1d wurde als guter Interimsmarker für VCAM-1^{+}PECAM-1^{-} nicht-endotheliale Stromazellen identifiziert werden, wohingegen die IL-7-Produzenten in der Population von $CD200^{int}$/BP-1^{+}/$CD73^{+}$/$CD105^{-}$ Stromazellen angereichert ist. Gleiches gilt für den Transkriptionsfaktor Prrx1. CD55, BP-1 and Cadherin-11 zeigten eine Expressionsmuster in Abhängigkeit des verwendeten IL-7-Reportermaus-Haplotyps, welcher die An-/Abwesenheit von IL-7 imitiert. Für BP-1 und Cadherin-11 konnte die Abwesenheit von reifen Lymphozyten als Ursache des Feedbacks ausgeschlossen werden. Die Haplotypen der Reportermaus legten auch eine monoallele Expression des IL-7 nahe. Viele Marker wie PDC-TREM oder CMKLR1 wurden unabhängig vom Haplotyp auf Stromazellen exprimiert. Die Expression von gas6, Annexin A2 (ANXA2) oder CD1d ist nicht auf das Knochenmarksstroma beschränkt, sondern wurde auch in der Milz beobachtet; dort jedoch mit geringerem Überlapp und

architektonischen Unterschieden. Darüber hinaus legen histologische Ergebnisse von ANXA2 und dessen Rezeptor ANXA2R eine mögliche Interaktion von Stroma- und B-Vorläuferzellen im Knochenmark nahe.

Die Ergebnisse dieser Arbeit zeigen VCAM-1^{+} (IL-$7^{+/-}$) Stromazellen als heterogene Population, wenn es nach der Vielzahl der möglichen exprimierten Marker geht. Zwischen vielen dieser Marker gibt es aber wiederum auf Zelloberflächenebene einen großen Überlapp. Die funktionelle Relevanz dieser Oberflächenmarker-Diversität wird in weiteren Arbeiten zu klären sein, gibt aber den Stromazellen ein breites Repertoire vor, um Interaktionen mit Lymphozyten zu initiieren, modulieren und inhibieren. Abschließend bleibt zu hoffen, dass diese Erkenntnisse in die klinische Behandlung der Stroma-Nischen in Autoimmun-Fragestellungen einfließen.

Contents

Abbreviations & Acronyms

Abbreviation/ Acronym	Meaning	Abbreviation/ Acronym	Meaning
A405... A647	Alexa Fluor™ 405... 647	**IL-…**	Interleukin …
		LatB	Latrunculin B
ACAM	Adipocyte adhesion molecule	**MACS**	Magnetic cell sorting
APC	Allophycocyanin	**MCAM**	Melanoma cell adhesion molecule
CFU-F	Fibroblast Colony-forming unit	**MFI**	mean fluorescence intensity
AU	Airy Unit	**MMP**	Matrix metalloproteinase
BM	Bone marrow	**MSC**	Mesenchymal stromal/stem cell
BMSC	Bone marrow stromal cell	**PacB**	Pacific Blue™
BSA	Bovine serum albumin	**PBS**	Phosphate-buffered saline
BST-…	Bone marrow stromal cell antigen …	**PDGFR**	Platelet-derived growth factor receptor
CD	Cluster of differentiation	**PE**	Phycoerythrin
CSF	Colony-stimulating factor	**PECAM**	Platelet endothelial cell adhesion molecule
CXCL /CXCR/ CCL/CCR	CXC/CC motif ligand/receptor family	**PerCP**	Peridinin chlorophyll complex
DAPI	4',6-Diamidino-2-phenylindole	**PMA**	Phorbol-12-myristate-13-acetate
EDTA	Ethylenediaminetetraacetic acid	**RBCs**	Red blood cells, erythrocytes
FN	Fibronectin	**PTPRD**	Protein tyrosine phosphatase, receptor type, D
DAF	Decoy accelerating factor	**RFP/GFP**	Red/green fluorescent protein
FACS™	Fluorescence-activated cell sorting	**RIN**	RNA integrity number
FCS	Fetal calf serum	**ROI**	Region of interest
FITC	Fluorescein isothiocyanate	**SA**	Streptavidin
FMO	fluorescence minus one	**lo; int; hi**	low; intermediate; high
HSC	Hematopoietic stem cell	**vSMC**	Vascular smooth muscle cell
ICAM	Intercellular adhesion molecule	**T-PMT**	Transmissive channel (photon multiplier tube

Antibodies

Cognate (Murine) Antigen(s)	Supplier	Hybridoma clone or catalogue ID (polyclonals)
Lineage • **CD3** • **Ly-6G/Ly-6C** • **CD11b** • **CD45R/B220** • **Ly-76**	BioLegend	i.e. • 17A2 • RB6-8C5 • M1/70 • RA3-6B2 • Ter-119
CD4	DRFZ	GK1.5 or YTS19.1
Gr-1 (Ly6G)	DRFZ	RB6-8C5

Ly-76	DRFZ	Ter-119
F4/80	DRFZ	F4/80
CD45R (B220)	DRFZ	RA3-6B2
CD31 (PECAM-1)	BioLegend	MEC13.3
CD31 (PECAM-1)	eBioScience	390
CD106 (VCAM-1)	eBioScience	429
CD106 (VCAM-1)	DRFZ	6C71
CD44	DRFZ	IM7
Sca-1 (Ly6A/E)	eBioScience	D7
CD54 (ICAM-1)	eBioScience	eBioKAT-1
BP-1 (Ly51)	eBioScience	6C3
CD105 (Endoglin)	eBioScience	MJ7/18
CD45	eBioScience	30-F11
Sca-1 (Ly6A/E)	eBioScience	D7
Ly-76	eBioScience	Ter-119
Viability (DAPI)	Sigma	-
Streptavidin conjugates	invitrogen	-
Anti-rat IgG	invitrogen	-
Anti-rabbit IgG	invitrogen	-
Anti-goat IgG	invitrogen	-
Anti-RFP-Biotin	Rockland	Rabbit polyclonal, 600-406-379
hIL10 (IgG2a,k isotype)	DRFZ	JES3-19F1
IgG2a	BioLegend	RTK2738
Surface Marker Screen	BioLegend	see Materials / Methods
Gas6	R&D	Goat polyclonal, AF986
Annexin A2	abcam	Rabbit polyclonal, ab41803
CD1d	BioLegend	CD1.1
Annexin A2 Receptor	Novus	Rabbit polyclonal, NBP2-49008
Cadherin-11	Sigma Aldrich	Rabbit polyclonal, ABT283
CD317/BST2	BioLegend	129C1
Fibronectin	Sigma Aldrich	Rabbit polyclonal, F3648
IgM	BioLegend	RMM-1
IgD	BioLegend	11-26c.2a
Kappa light chain	BioLegend	RMK-12
lambda light chain	BioLegend	RML-42
CD90/Thy1	BioLegend	G7

Figures & Tables

1 Introduction

1.1 Architecture of the murine long bones

Bones are the scaffold of the vertebral organism and fulfill several functions within the body. While the most prominent is their supportive role for locomotion by offering anchoring points to tendons and muscles they also protect inner organs from traumatic events.

In contrast to avian hollow bones, the mammalian counterparts contain bone marrow in their inner cavities which serve as the major site for generation of blood cells (explained in section *1.4*) postnatally. Moreover, besides harboring a pool of progenitor blood cells the bone marrow recently was identified to be home to immune memory cells.

The anatomy of a bone will be described by help of the murine femoral bone representative of all murine long bones. Generally, the bone is a mineralized cortex that is synthesized by osteoblasts in the bone marrow among other cell types. Moreover, there are two types of mineralized osseous tissue. While the dense cortical bone is making up the shaft of the bone it transitions into the so-called trabecular bone with a sponge-like appearance towards the joints (see *Fig 1.1*A).

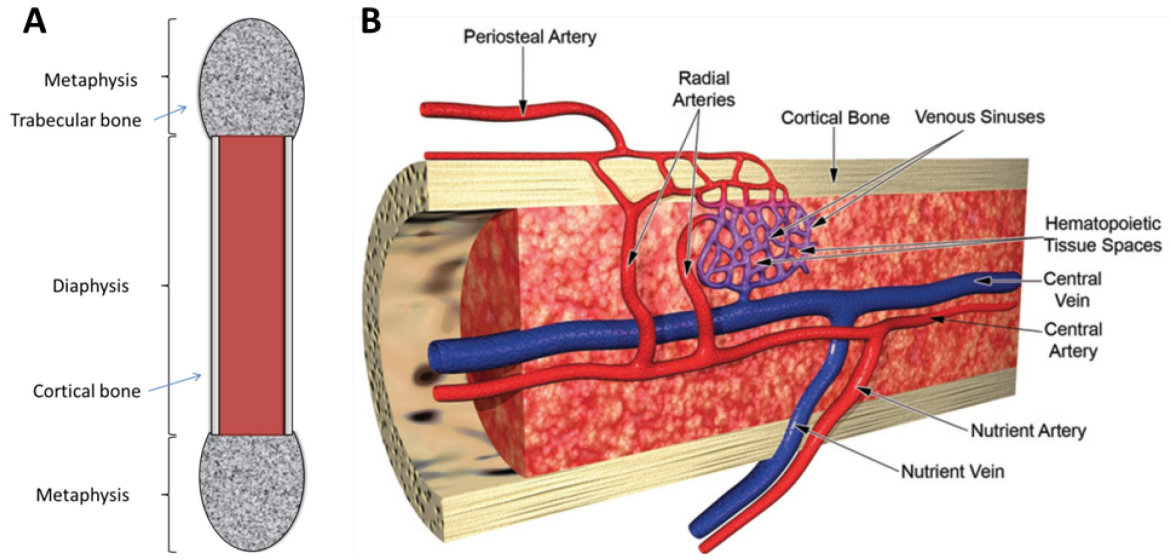

Fig. 1.1: Architecture and vascularization of the murine long bones A: Schematic depiction of long bone terminology and bone type distribution; **B:** Organization of the vasculature in the murine bone marrow of long bones as taken from Travlos et al.[1]

Bone marrow is also connected to the blood circulation. Nutrient arteries enter the bone through the cortex (*Fig. 1.1B*). Similarly, periosterial arteries and veins were only recently identified to contribute substantially to blood exchange by crossing the cortex. In the bone marrow they form dense capillary networks termed the sinusoids that ultimately drain into the largest venous vessel that is the central

vein. Interestingly, bone marrow is not drained by the lymphatic system[2] despite its pivotal role as the primary lymphoid organ in the generation, selection & maintenance of immature lymphocytes.

Sinusoidal networks make up most of the space in bone marrow consisting of a luminal endothelial layer that is partially lined by adventitial reticular stromal cells[3]. The bone marrow parenchyma comprises a well-connected network of reticular stromal cells. These cells do not only act as connective tissue but also provide specialized microenvironments for cells of the early or late hematopoietic lineage as described below. Although murine bone marrow also contains adipocytes it is not divided into red and yellow bone marrow (containing mostly hematopoietic cells or adipocytes, respectively) as in the human equivalent[3].

Bone marrow is also densely innervated. While nerve fibers located in periarterial sheaths are thought to regulate vessel tone many nerve fibers terminate in the intersinusoidal areas. There, the fibers contact reticular stromal cells which were shown to carry β2- and β3-adrenergic receptors[4, 5]. Innervation together with gap-junctional communication of stromal cells regulates hematopoietic stem cell release by stress and in a circadian manner[5, 6].

1.2 Cellular composition of the bone marrow

Cells of the bone marrow can be easily divided into the hematopoietic and the non-hematopoietic cell types. While the latter will be discussed further below the following paragraphs will deal with cells on the mesenchymal lineage that are non-hematopoietic and how they contribute individually to the various biological functions of bone marrow.

1.2.1 Reticular stromal cells

Reticular stromal cells make up the reticular scaffold of the bone marrow and are responsible for secretion of extracellular matrix (ECM) proteins. Much like fibroblasts, they show a spindle-shaped phenotype with long processes in culture. In addition, reticular stroma is connected via gap junctions[7, 8] and partly innervated by the sympathetic system as summarized earlier.

Reticular stroma seems to be highly heterogeneous in terms of surface marker expression and differentiation potential. Due to its ability to differentiate into cells of the non-hematopoietic mesenchymal lineage (i.e. osteoblasts, adipocytes, chondroblasts) *in vitro* and *in vivo*[9], the term "mesenchymal stem cell (MSC)" is sometimes used interchangeably for stromal subsets meeting certain requirements[10]. Multipotency was first observed in the 1970s by Friedenstein and coworkers[11] who used an adherence-based culture to characterize their clonogenicity and differentiation potential *in vitro*[12]. Even broader differentiation diversity could be shown *in vitro* including trans-differentiation capacity to ectodermal tissue (e.g. neurons[13]) in the presence of unphysiological media additives.

Hence, MSCs are increasingly considered for regenerative therapies. Nevertheless, their *in situ* lifestyle has not been fully elucidated, yet.

Surface marker expression varies among reticular stromal cells as mentioned earlier. The lack of a stroma-specific marker contributes to the difficulties of studying their diversity. Several publications begin to shed light on the distribution of stromal subsets by assessing their enhanced proliferation *in vitro* as introduced by Friedenstein's fibroblast colony-forming unit (CFU-F) assay[12].

Morikawa et al. reported a population of perivascular PDGFRα$^+$/Sca-1$^+$ stromal cells (PαS) that show increased CFU-F frequency *in vitro* and gave rise to perivascular cells and osteoblasts in a transplantation approach[14]. Using reporter mice expressing GFP under control of the promoter for the intermediate filament protein Nestin, another rare candidate MSC subset was defined[15]. Interestingly, Nestin is considered a neuronal or neuron-related protein[16] contradicting the proposed mesenchymal phenotype of MSCs and might hint at a neural crest origin[17]. However, Nestin-GFP$^+$ stromal cells were found in perivascular (periarteriolar for Nestin-GFP^{bright}; perisinusoidal for Nestin-GFP^{dim}) as well as endosteal areas of the bone marrow. When kept in culture, only CD45$^-$Nestin$^+$ cells were able to differentiate into osteoblasts, adipocytes and chondroblasts. Fate-mapping revealed that their *in vivo*-potential was restricted to osteoblasts/osteocytes and chondrocytes. The expression of HSC support factors CXCL12, Interleukin-7, Angiopoietin-1, VCAM-1, stem cell factor (SCF) and Osteopontin hints at a highly versatile stromal subset[15]. Nestin as a defining stromal marker however is highly controversial in the field as summarized in a review by Xie recently[18].

A third study identified a pivotal role of *Myxovirus resistance-1* promoter active (Mx1$^+$) cells in stromal biology[19]. They could show that Mx1$^+$ cells exhibit tri-lineage potential *in vitro* while only committing to the osteogenic lineage *in vivo*. Furthermore, Mx1$^+$ cells could be serially transplanted and were highly motile in case of bone fracture to constantly replenish the osteoblast pool at the site of injury[19].

In contrast to the clonogenicity used in the studies before, a set of stromal cells was characterized regarding its high expression of CXCL12 / stromal derived factor 1 (SDF-1). Hence, those cells were termed CXCL12-abundant reticular (CAR) cells[20, 21]. They are scattered throughout the bone marrow[20] and associated with endothelial cells at the sinusoids, thus encompassing perivascular reticular cells[21]. CAR cells show bi-lineage potential differentiation behavior towards adipocytes and osteoblasts in culture and homogenously express the surface markers PDGFRα/β, VCAM-1, CD44 and Integrin αV (CD51)[22]. They contact several stage-specific cells of the hematopoietic lineage in the bone marrow such as HSCs, B cell progenitors and plasma cells[20, 21] reflecting their vital role in B cell lymphopoiesis[23, 24] in particular. In addition to the lymphoid lineages, myeloid cells similarly rely on stromal cues for their differentiation and survival.

In addition to CXCL12-expressing reticular stroma, another subset secreting Interleukin-7 (IL-7) was described[20]. IL-7 producers are found among PDGFRα^{+}Sca-1$^{+/-}$ as well as VCAM-1$^{+/-}$ cells while only half of the VCAM-1^{+} stromal population expresses it[25]. Mostly overlapping with CAR cells[26], IL-7^{+} stromal cells are also involved in early lymphopoiesis[27, 28]. Recent studies demonstrate their involvement in memory lymphocyte maintenance.

Most recently, Leptin receptor (LepR) – previously thought to only be expressed on adipocytes – was proven to be a *bona fide* stroma marker as well as it is enriched for most CFU-F and marks most of the mesenchymal lineage while also being involved in HSC maintenance[29, 30].

While several stromal subsets have thus been described, the question arises whether they share similarities, overlap or even belong to the same subset. Considering the different degrees of multipotency of mentioned subsets it could be possible that LepR^{+} cells are the most stem-like cells, while bi-lineage potential PαS and osteogenic Mx1^{+} cells might represent more committed stromal phenotypes. Although CAR cells are more abundant than Nestin^{+} cells the subsets share similar characteristics[15, 21, 22] indicating a certain overlap as well.

1.2.2 Pericytes

In vivo, many of the reticular stromal cells contact the endothelial layer of sinusoids and arterioles[3, 31] while their cell bodies can also be found distant from the vessels. Whether those perivascular stromal cells are identical or of different origin is still a matter of debate[32, 33, 34].

Some have argued for a common perivascular origin of all reticular stroma[34, 35, 36] but depletion experiments[37] with neural/glial antigen 2 (NG2) – a widely recognized, murine pericyte marker – showed that pericyte replenishment can even occur by endoderm-mesoderm transition (EMT) from endothelial cells casting into doubt such concepts in favor of more adaptive ancestors.

Given that virtually all stromal cells express PDGFRs while endothelial as well as smooth muscle cells (characterized by α smooth muscle Actin) are a major source of PDGF as their ligand, stromal/pericyte proximity to vessels could merely reflect a survival benefit as PDGFRs are the mesenchymal maintenance receptors.

In the context of the hematopoietic niche, it is by now widely accepted that ligand contributions to the HSC niche differ with regards to whether they are reticular, endosteal, perisinusoidal or periarteriolar[38, 39, 40, 41].

1.2.3 Osteoblasts, osteocytes & osteoclasts

Osteoblasts develop out of mesenchymal progenitor cells discussed above. They are short-lived and non-mitotic[19]. Their main function is to secrete the proteinaceous ECM that ultimately leads to bone

mass after mineralization[42]. Several transcription factors have been identified to be expressed during the progenitor-osteoblast-transition such as Runx2 or Osterix[43, 44]. Bone is constantly remodeled throughout the entire organism's life. Thus, osteogenesis by osteoblasts is in strict balance with bone resorption by osteoclasts – macrophage descendants – and tightly regulated (e.g. by the WNT signaling pathway[45]).

Besides modeling of the bone cortex osteoblasts have shown to be involved in HSC maintenance by expressing factors like Osteopontin, CXCL12, Angiopontin-1 or membrane-bound stem cell factor[46]. Consequently, depletion of osteoblasts by conditional models or disease results in mobilization of HSCs into the blood[47, 48, 49]. However, recent results question the necessity of osteoblasts for HSC support as hematopoiesis may alternatively occur in extramedullary sites[47] and modulating the osteoblast pool size does not alter HSC numbers[50, 51].

Osteocytes are osteoblasts that have been encapsulated in the bone matrix. They are connected with each other via long processes – called canaliculi – for communication and nutrient exchange with the bone marrow[52].

1.2.4 Adipocytes

Adipocytes are fat cells that are found scattered throughout the murine bone marrow in contrast to human white bone marrow as described earlier. They develop from mesenchymal progenitors such as CAR or Nestin$^+$ cells that were shown to undergo adipogenesis *in vivo*[22]. Adipogenesis might be triggered by lack of mechanical signals[53, 54] and is accompanied by expression of the adipogenic transcription factor PPARγ[55]. Adipocytes were shown to negatively regulate HSC maintenance [56].

1.2.5 Endothelial cells

Endothelial cells build up the inner lining of the vessels meandering the bone marrow and are covered by adventitial reticular stromal cells[31]. As such, they form a barrier to control molecule exchange and cell trafficking. Marrow endothelial cells express Laminin, von Willebrand factor (vWF) and Collagen IV[3]. Furthermore, they carry the surface proteins VCAM-1, E-Selectin and PECAM-1 that mediate leukocyte transmigration[57]. Similar to reticular stromal cells there is heterogeneity in expression of some markers. Sca-1 is found in arteriolar endothelium whereas it is not found on sinusoidal endothelial cells[58].

1.3 Bone marrow as the site of hematopoiesis

In addition to the aforementioned cell types the bone marrow is the major site of hematopoiesis in mammals after birth[59]. Blood as a regenerative tissue undergoes a constant turnover of cells. Thus there is a need for long-lived stem cells that in hematopoiesis are called long-term hematopoietic stem cells (LT-HSC[60]). The HSCs reconstitute the diverse set of blood cells in a step-wise manner while

gradually losing multipotency. Short-term HSCs which originate from LT-HSCs differentiate into the common myeloid progenitor (CMP) – accounting for subsequent maturation of megakaryocytes, erythrocytes and myeloblasts – and the common lymphoid progenitor (CLP) whose offspring include natural killer, natural killer T (NKT), T-, B- and innate lymphocytes (ILC) with varying responsibilities. Lineage commitment is tightly regulated by expression of several antagonistic transcription factors[61].

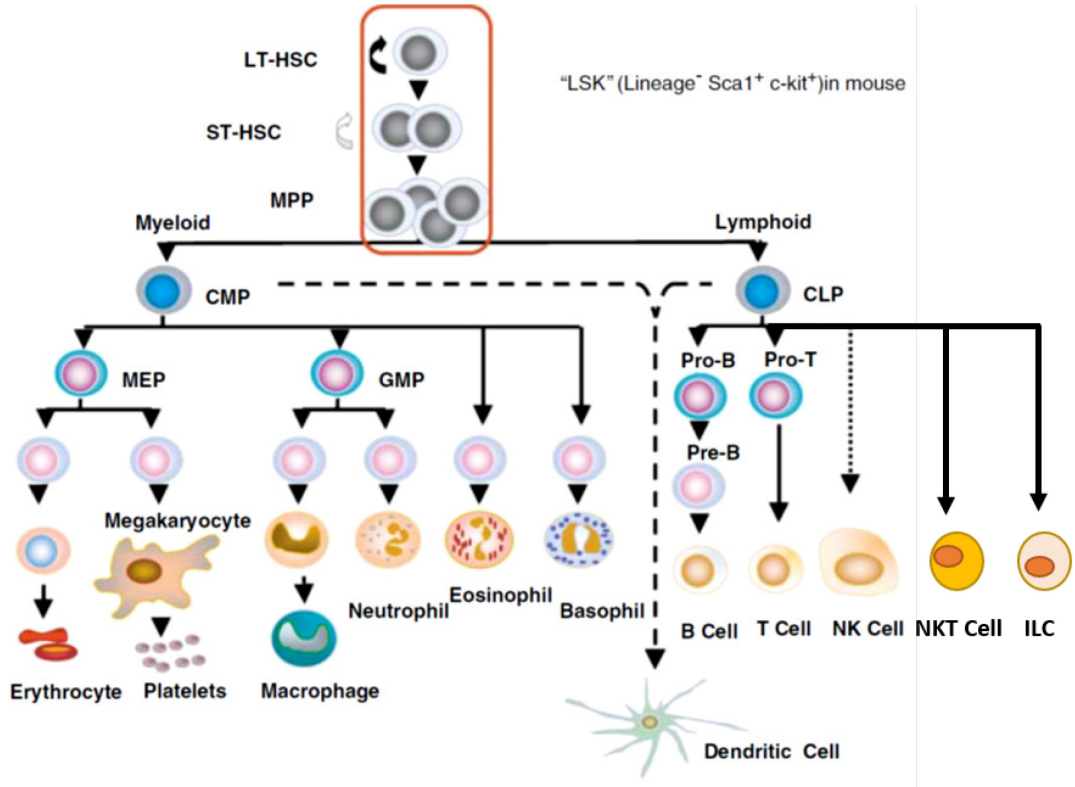

Fig. 1.3: Developmental pathway of the hematopoietic lineage Modified depiction of the developmental lineage from multipotent hematopoietic stem cell in the bone marrow over committed progenitors to mature cells inside and out of the bone marrow (Larsson & Karlsson, 2005, modified). LT/ST-HSC = long-/short-term hematopoietic stem cell; MPP = multipotent progenitors; CMP/CLP = common myeloid/lymphoid progenitor; NK(T) = natural killer (thymocyte); ILC = innate lymphoid cell

HSCs are maintained in the bone marrow by reticular stroma in a specialized microenvironment. Over the last couple of years additional cell types including macrophages and the sinusoidal endothelium were found to be crucial in regulation of quiescence, self-renewal and differentiation of HSCs[46]. Furthermore, HSC cycling and release into the blood stream is under control of the sympathetic nervous system in a circadian rhythm[4, 46].

1.4 The mammalian immune system

The mammalian immune system protects the organism from pathogens by discriminating molecules between self and non-self. Whereas germline-encoded canonical motifs are used at the level of innate immunity to identify potentially harmful microbiota it's the plethora of antigen-specific receptors on immune cells of the adaptive immunity – i.e. T and B cells - that provide protection against antigens not yet encountered. The required receptor diversity is possible due to DNA recombination

mechanisms that each lead to genomic changes on the single-cell level during maturation of antigen-specific immune cells in the lymphoid organs.

1.4.1 Immunological memory

Apart from its ability to recognize a vast number of antigens in an acute situation upon primary encounter, one particularly important function of the immune system is its enhanced response behavior when rechallenged with an already encountered antigen. As this feature is preserved over months in small vertebrates and decades in humans, the term “immunological memory” was coined.

Whether it’s residual antigen that enables survival of antigen-specific cells or maintenance of reactive cells in the absence of antigen – as the strict definition of ‘memory’ requires – was a matter of debate. Meanwhile, the latter theory of antigen-independent maintenance was verified by switching the antigen-specificity of memory B lymphocytes[62], memory T cells[63] and long-lived plasma cells that produce antibodies regardless of antigenic instruction. In contrast, memory cells rather seem to depend on cytokine signals for survival[64]. Studies revealed that molecules of interest include IL-7 for CD4 memory cells[65], both IL-7 and IL-15 for CD8 memory cells[66, 67, 68, 69] and BAFF in combination with APRIL for memory B cell subsets[70]. Furthermore, other experiments identified CXCL12 (also known as SDF-1), ligands of CD44 and IL-6 to be able to promote survival at least *in vitro*[71, 72].

It hasn’t been until recent years that the underlying mechanisms for establishing immunological memory have been explored. When looking at acute immune responses it is observed that all antigen-specific lymphocyte subsets readily divide after receiving appropriate receptor stimuli in follicles of mostly spleen and lymph nodes which lead to a fast, clonal expansion in terms of cell numbers. This is followed by a contraction phase in which most of the clonal lymphocytes undergo apoptosis[73]. However, when tracking experiments were performed with $CD4^+$ cells in a primary immune response to determine the localization during and after the expansion it could be seen that a small percentage of $CD4^+$ cells relocate to the bone marrow while decreasing numbers were observed in the periphery[74].

1.4.2 Establishing the lymphocyte memory niche in the bone marrow

In the bone marrow, CD4 memory T cells have been shown to contact VCAM-1 expressing stromal cells that also secrete IL-7 comprising about 1% of total bone marrow cells[20] constituting a subset of $VCAM\text{-}1^+CXCL12^+$ plasma niche stromal cells (see *Fig 1.4.2*). Although the term niche originally stems from ecological theory where it’s defined as "a range of environmental conditions and resources needed for population persistence"[75] it is meanwhile used to describe the spatially and temporally defined microenvironments needed for maintenance and survival of memory lymphocytes.

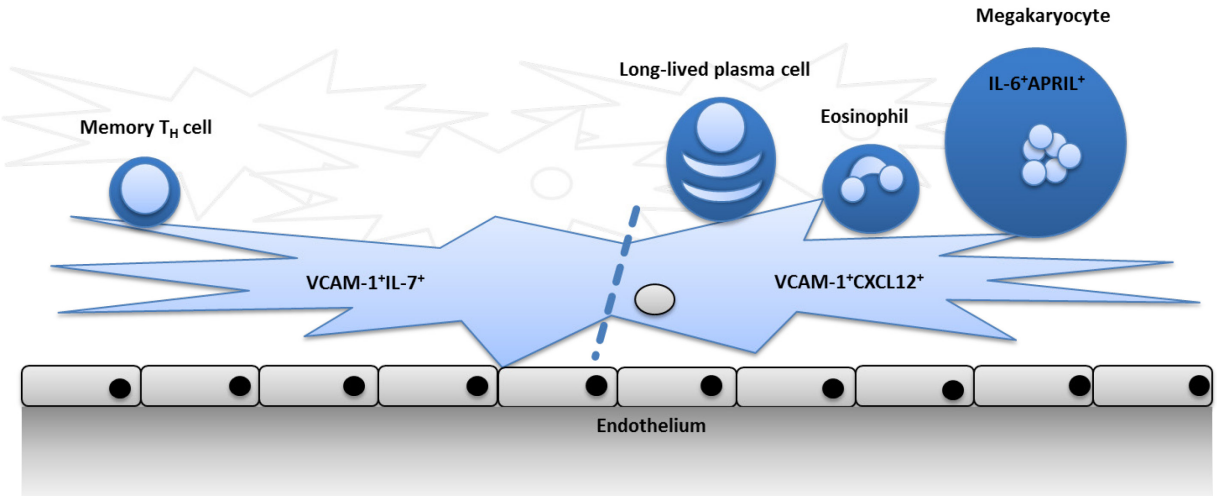

Fig. 1.4.2: Cellular and molecular composition of distinct BM stromal niches for memory lymphocyte subsets according to recent data Proposed composition of IL-7 dependent $CD4^+$ T_H memory cell (left) and long-lived plasma cell niche homing to $CXCL12^+$ stromal subsets. Dashed line indicates uncertainty in how overlapping these sub-populations are.

As memory $CD4^+$ cells have been shown to be resting in terms of proliferation and migration the memory lymphocyte pool size is only maintained by the numbers of stromal cells rather than homeostatic proliferation.

These findings bear clinical implications. Memory cells can also act pathophysiologically if specific for self-antigens. In this setting, the treatment of choice involves either immunosuppression or immunoablation - both putting the patient at high risk due to increased susceptibility for pathogens. However, memory cells - being resting both in terms of migration and proliferation – still fail to respond to the treatment methods targeting proliferating cells such as Cyclosporin A or total body irradiation[76].

1.4.3 Isolation of mesenchymal stromal cells

It is desirable to target stromal cells involved in the maintenance and survival of memory lymphocyte subsets therapeutically to address the aforementioned disease-promoting abilities. Historically, this is a problem due to the accessibility of stroma itself. Adding to this comes the fact that studies often rely on adherence-cultured CFU-Fs[12]. The method takes advantage of the self-renewing capacity and multi-lineage differentiation potential of mesenchymal stromal cells.

This approach has flaws. While on the one hand non-adherent progenitors[77] might be missed it has also been shown that surface marker expressions in CFU-Fs changes throughout passaging[78, 79, 80]. That might be due to transfer of stromal cells from a 3D to a 2D environment presumably lacking some of the *in vivo* triggers found in the extracellular matrix[81]. Additionally, the amount of marker combinations attributed to stromal cells hints at a high degree of heterogeneity with several subsets of stromal populations presumably involved in differing biological contexts as is the case for CXCL12 and/or IL-7 expressing $VCAM\text{-}1^+$ cells. Proposed marker sets include Sca-1/PDGFRα[14], CD146[82],

CD271[83, 84] or Nestin[15] amongst others described. Another dimension of confusion is added to the matter when trying to distinguish clearly between cell types of the bone marrow – especially across species. Markers as CD105/Endoglin are mainly expressed on endothelial cells[85] but were also used for proper MSC isolation in human context[86]. PDGFRβ is a similar example as it was used for definition of both pericytes[87] and MSCs[88] in the murine model.

1.5 Motivation

In this thesis, the role and diversity of VCAM-1 and memory lymphocyte supporting IL-7 expressing stromal cells in particular stand to be analyzed. Until today, only a handful of signals were identified to be involved in the maintenance of memory lymphocytes such as CXCL12 or IL-7. Hence, one goal is the search for additional stroma-derived molecules that could interact with memory lymphocytes in the murine bone marrow niches or chemotactic signals keeping or guiding them there. Ultimately, finding surrogate surface markers that comprise several stromal subsets are another appealing goal as they would allow for future research on the particular function of these subsets especially in the case of autoimmune diseases where only cells of a certain function are ideally targeted.

2 Materials & Methods

2.1 Mice

For general analyses in flow cytometry and for sorting of cells C57BL/6J mice aged between 7-12 weeks were used. Where indicated, IL-7 knock-in reporter mice [89] of 12-20 weeks were sacrificed. Both homozygous (IL7KI$^{-/-}$) and heterozygous (IL7KI$^{+/-}$) were used. Additionally, chimeric (C57BL/6J --> Ubiquitin:GFP or RFP) with fluorescent radioresistant cells or stroma reporter mice, i.e. B6.Cg-Tg(Prrx1-cre)1Cjt/J x Gt(ROSA)26Sor^{tm1Hjf} (PrxRFP), with fluorescent stromal cells were used for certain histological experiments (both Jackson Laboratory, Freiburg). These mice bred within the context of the dissertation of Sandra Zehentmeier [90] and provided by the workgroup of Anja Hauser (DRFZ).

Where stated, mice deficient for Recombinase activating gene 1 (RAG1) from Jackson Laboratory (B6.129S7-*Rag1*^{tm1Mom}/J) were used and further denoted as RagKO.

2.1 Cell preparation

Male C57BL/6J or chimeric mice aged between 7-12 weeks were sacrificed by cervical dislocation. The hind legs were prepared and the bones cleaned from muscle and tendon tissue and stored in PBS on ice.

For flushing, the bones were then transferred to a petri dish filled with medium (RPMI 1640 GlutaMAX™, Invitrogen, Carlsbad/USA) and the bones were cut close to the epiphyses. After that, a medium-filled syringe with appropriate needle sizes (i.e. 25G x 1'' for femora, 22G x 1 ¼'' for tibiae; Sterican®, B. Braun Melsungen, Melsungen) was used to flush out the bone marrow strings as intact as possible.

When crushing bones with pestle and mortar, 2 mL of PBS were put into a mortar pre-cooled on ice. The bones were crushed and brought to single-cell suspension by pipetting up and down several times. The suspension was then filtered (70 µm pore size, Nylon) into a 15 mL Falcon tube on ice.

2.2 Enzymatic digestion

The bone marrow flush-out and the empty bones (see section *2.1*) were each transferred to one well of a 24-well culture plate each containing 400 µL of digestion buffer (RPMI 1640 GlutaMAX™ [Invitrogen], Penicillin/Streptomycin; 0.5 mg/mL Collagenase IV [Sigma-Aldrich, Taufkirchen]; 1 mg/mL DNase I [Sigma-Aldrich]; 0.25 mg/mL Dispase II [Roche, Grenzach-Wylen]; where indicated 2.5 µg/mL Cytochalasin D [Sigma-Aldrich] and 5 µg/mL Latrunculin B [Sigma-Aldrich] were added to the digestion buffer). After the marrow was cut into small pieces the plate was incubated at 37 °C and 5% CO_2 for 15 min. Subsequently, another 400 µL of digestion buffer were added to each well. Marrow samples were

gently resuspended with a pipette while the bones were flushed through with the digestion buffer. Again, the plate was incubated for 15 min at 37 °C and 5% CO_2. Following that, 200 µL of PBS/BSA with 10 mM EDTA were added to each well to stop digestion. Bone marrow samples were resuspended with a pipette and then filtered through a 70 µm Nylon mesh into 15 mL Falcon tubes to remove clumps. Additionally, the wells were washed with 1 mL of PBS/BSA/EDTA. The hollow bones were thoroughly flushed out with a syringe through a 22G needle. The resulting suspension was added to the corresponding tube.

2.3 Flow cytometry and fluorescence-activated cell sorting (FACS™)

Firstly, cell suspensions obtained from digestion were spun at 320 x g for 7 min at 4 °C. The supernatant was discarded and the pellet were resuspended in 300 µL of F_cγ-receptor-Block (Clone 2.4G2, 10 µg/mL in PBS/BSA/EDTA). Following that, samples were incubated for 30 min on ice. When staining in 1.5 mL reaction tubes, an aliquot of ca. $2x10^7$ cells was transferred from the initial sample.

In the next step, the staining mix was added (see antibody list). Staining was performed for 20-30 min on ice in a darkened environment. After that, tubes were filled up to 1 mL or 10 mL according to a staining in a 1.5 mL reaction tube or a 15 mL Falcon tube, respectively. Samples were centrifuged for 7 min at 4 °C, either at 320 x g or 973 x g according to the tubes used as aforementioned.

The supernatants were discarded and pellets gently resuspended in 100-500 µL of PBS/BSA/EDTA and stored on ice. All samples were filtered before measuring (70 µm pore size, Nylon mesh). Additionally, compensation was carried out immediately before every analysis. This was done by measuring fresh cells only stained with antibody-dye-conjugates for each of the available channels with the corresponding dye of interest and software-side compensation between channels.

When using DAPI for viability staining, it was added only before measuring at the given concentration. Cells were measured at 10,000 events per second at maximum. Data was analyzed by FlowJo software (v7.6.5, Tree Star Inc.). If not stated otherwise, gatings included single live cells and were also negative for lineage markers (see antibody list) or at least for RBCs ($Ter119^-$).

After staining and centrifugation, cell samples were resuspended in 500 µL PBS/BSA/EDTA and filtered (Pre-Separation filters, 30 µm, Miltenyi Biotec, Bergisch Gladbach) into a sorting tube. The tubes used for the initial cell suspension as well as for the sorted fractions were coated with RPMI + 10% FCS 3-4 h before sort at room temperature. The tube for the total BM cell suspension was washed briefly with PBS/BSA/EDTA prior to adding the cell suspension whereas about 200 µL of medium were left in the fraction tubes (12x75 mm, 5 mL, PP, Sarstedt, Nümbrecht) to sort the cells into. Fluorescence-activated cell sorting was done at the Flow Cytometry Core Facility of the MPI/DRFZ at the Influx™ cell sorter (Becton Dickinson, Heidelberg).

Gatings were set to include 3 fractions, i.e. CD45$^-$VCAM-1$^-$PECAM-1$^-$; CD45$^-$VCAM-1$^+$PECAM-1$^-$ and CD45$^-$VCAM-1$^+$PECAM-1$^+$. In case of sorting IL7KI stroma, gatings were CD45$^-$VCAM-1$^+$GFP$^+$PECAM-1$^-$, CD45$^-$VCAM-1$^+$GFP$^-$PECAM-1$^-$ and CD45$^-$VCAM-1$^+$GFP$^-$PECAM-1$^+$, respectively. Sorting speed did not exceed 15,000 events per second. Additionally, the hose system and the used buffers/ sheath fluid were cooled to 4 °C for sorting. Cells belonging to any of the mentioned fractions were then simultaneously sorted into the previously coated FACS™ tubes.

After sorting, the cell counts and purity were determined on the flow cytometer (MACSQuant Analyzer, Miltenyi Biotec) with an aliquot of 30 µL. The suspensions were transferred into a 2 mL reaction tube and spun at 1520 x g for 5 min at 4 °C. Supernatants were discarded and the cells resuspended in lysis buffer of the appropriate RNA isolation kit (see 2.5). Lysed samples were stored at -80 °C until further RNA isolation.

High-throughput surface marker screening via LEGENDScreen™ (Mouse Kit, BioLegend, Koblenz) was carried out as per manufacturer's instructions. Bone marrow of long bones of three mice (aged 9-12 weeks) per haplotype was pooled for the experiment. To account for comparison of IL7-GFP knock-in heterozygous vs. homozygous mice' cells, only half the recommended volumes and cell numbers were used and the pre-titrated antibody solutions split into two. Samples were acquired sequentially on a flow cytometer (MACSQuant Analyzer 10, Miltenyi Biotec) with plate reader function and resuspended briefly before measurement. Depicted gates were set according to isotypes and fluorescence-minus-one (FMO) controls included in the kit.

2.4 RNA isolation & purity assessment

RNA isolation was carried out by using the ZR RNA Miniprep (Zymo Research, Freiburg), the NucleoSpin® RNA II or XS kit (both Macherey-Nagel, Düren) mostly according to the manufacturers' instructions. Changes to the protocol included heating up the water used for elution to 60 °C and reducing the elution volume in the recommended range.

RNA concentrations were checked by measuring an aliquot of 1-2 µL at the NanoDrop (ND 1000, Thermo Scientific, Darmstadt) blanked with distilled water using the RNA-40 program. In addition, an aliquot of 2 µL was checked via electropherogram (BioAnalyzer 2100, Agilent Technologies, Santa Clara/USA) to assess RNA quality and integrity as seen by signal peaks specific for the 18S and 28S ribosomal RNA subunits. RNA samples were then stored at -80 °C.

2.5 MicroArray analysis

Total RNA isolates from 3 sorting experiments with a target population purity >80% were chosen to be used in MicroArray analysis. Fractions of interest were VCAM-1$^+$PECAM-1$^-$ and VCAM-1$^+$PECAM-1$^+$. For analysis of IL7KI mice, sorted populations were VCAM-1$^+$PECAM-1$^-$GFP$^+$, VCAM-1$^+$PECAM-1$^-$GFP$^-$ and

VCAM-1^{+}PECAM-1^{+}. Genome-wide analysis was done with the GeneChip Mouse Genome 430 2.0 Array from Affymetrix (Santa Clara/USA) according to manufacturer's instructions.

Chipset data was analyzed by applying the HPCDA algorithm as previously described [91, 92].

2.6 Immunofluorescence

2.6.1 Tissue preparation

Fixation

Bones obtained from freshly sacrificed mice were transferred to 15 mL Falcon tube containing about 4 mL of 4% Paraformaldehyde (diluted from 20% PFA, Electron Microscopy Sciences, Hatfield/USA). Cells were allowed to be fixed for 4 h at 4 °C. To dehydrate the tissues the samples were transferred to a 10% sucrose solution. The sucrose content was increased 10%-step-wise every 24 h until 30% sucrose were reached. The bones stayed in 30% sucrose solution until the freezing procedure.

Freezing

For freezing, a steel plate was cooled to temperatures below 0 °C by placing it on dry ice in a container. While still at room temperature, embedding medium (SCEM, Section-Lab, Hiroshima/Japan) was added to specimen molds (Standard, Sakura Finetek, Netherlands). Subsequently, tissue samples were immersed in the embedding medium while avoiding air bubbles in the compound. The specimen molds were then transferred onto the pre-cooled plate for freezing. The frozen blocks were wrapped in tin foil and stored at -80 °C until further use.

Cutting

Frozen bone tissue samples in embedding medium were cut at the microtome (HM 560 CryoStar Cryostat, Thermo Scientific) at -24 °C or at -19 °C for soft tissue. Section thickness was set to 6 µm. Slices were taped onto object slides for staining and stored at -80 °C according to the Kawamoto method[93].

2.6.2 Staining

Object slides with tissue slices were thawed for 3 min in PBS. After drying the surrounding of the tissue, the area of interest was encircled with Dako Pen (Dako, Wiesentheid). In the next step, slides were blocked with PBS-T (PBS/0.1% Tween/5% FCS) for 30 min in a wet chamber. Staining mixes and corresponding isotype controls were prepared in 100 µL of PBS-T from which 50-75 µL were added according to the tissue. Incubation was performed in the wet chamber for 1 h at room temperature. Slides were washed three times with PBS/0.1% Tween in between staining steps. Ultimately, slides were incubated for 2 min in PBS and carefully dried afterwards. While avoiding bubble encapsulation, 7 µL Fluorescent Mounting Medium (Dako) were pipetted onto the slides. The application of a cover

slip was followed by brief observation in light microscopy. The slides were then stored at 4 °C until measurement in fluorescence microscopy.

2.6.3 Confocal Microscopy

Fluorescence microscopy measurements were done on a LSM710 (Carl Zeiss, Jena) using the Zen 2011 software. Averaging was set to Line 4, zoom to 1.0. The objective used was a Plan-Apochromat 20x with 0.8 numerical aperture. Z-stacks over 6 µm were acquired in a sequential manner with the pinhole set to 1 Airy Unit for each track – typically containing one channel. After merging z-layers to a 2D maximum intensity projection, contrast and brightness were adjusted in similar fashion for sample and isotype control slides.

2.6.4 Cell quantification of stromal cells in histology

The femora of 3 age-matched PrxRFP mice were prepared, fixed, embedded, cut & stained as described. 5 ROIs of equal size were arbitrarily set in the resulting tile scans. DAPI and RFP signals were subjected to thresholding by ImageJ with default presets. Subsequently, the cell count was determined via particle analysis (DAPI: default settings; Prx: size starting from 80 px^2 to only account for nucleated cell bodies).

2.6.5 Semi-automated image analysis

The semi-automated image analysis of confocal bone marrow pictures was done in collaboration with Ralf Köhler of the work group of Anja Hauser. In short, an ImageJ Java Macro calculates the respective overlap of two image fluorescence channels from Zeiss/ZEN *.lsm files.

Firstly, the image threshold is defined by the signal to noise ratio, subsequently generating masks of unified signal intensities. The macro then counts for overlap pixel-wise. Visualization is done in pseudo-colors of choice. The applet also provides an Euler diagram depicting overlapping and separate signal as part of the total pixels for better immediate depiction.

Additionally, advanced image segmentation was provided by Wimasis, Munich with proprietary algorithms.

3 Results

3.1 Obtaining viable stromal cells quantitatively via an optimized protocol

3.1.1 Stromal cell isolation is sheer-force-sensitive and requires enzymatic digestion

As is empirically proven, hematopoietic cell populations are effortlessly accessible in all of the commonly analyzed organs including spleen, lymph nodes and the bone marrow. To obtain a single cell suspension the tissues are disrupted mechanically via straining/crushing through a filter with defined pore size. Despite knowledge of potential losses due to these forces, the extent of loss was enigmatic as the total stromal content in the bone was unknown.

To assess this question, histological slides of PrxRFP femora were imaged. Since Prrx1 is a mesenchymal lineage-restricted transcription factor, RFP expression is only induced in the stromal lineage and subsequent tissues/cells (osteoblasts, chondrocytes, pericytes etc.), allowing for an accurate estimate of stromal contribution to total nucleated bone marrow cells. By assessing different regions of the bone marrow, we could observe that reticular stroma was evenly distributed throughout the bone marrow with a consistent percentage of around 2% (see *Fig. 3.1.1.1*) of nucleated cells in the organ.

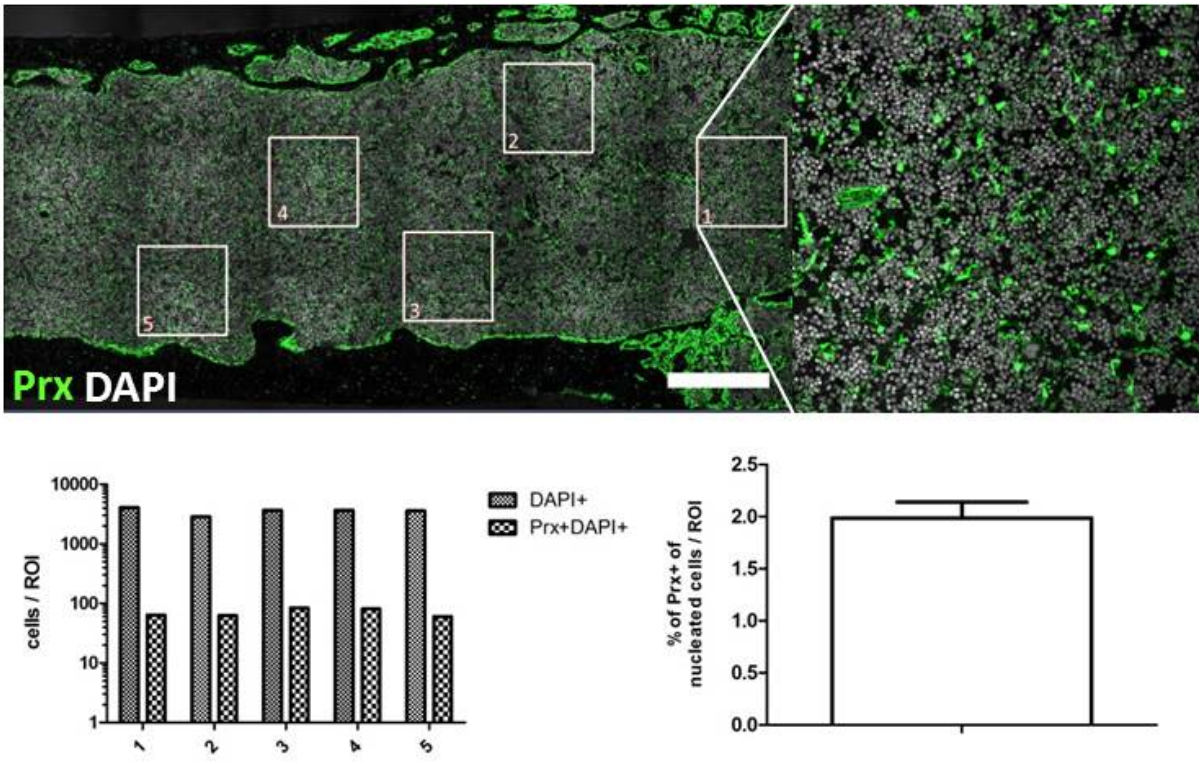

Fig. 3.1.1.1: Quantification of the stromal cell content in murine bone marrow Femur of PrxRFP mice were longitudinally cut and stained for RFP and nuclei; ROIs were chosen at random, inlet refers to magnified ROI 1; scale: 500 µm; bottom left: representative quantification of total nucleated and nucleated PrxRFP^{+} cells in one mouse; bottom right: Average frequency of stromal PrxRFP^{+} cells among nucleated cells per ROI; n=3 ; graph depicts ROI values (left) or mean ± SEM (right)

In terms of bone marrow stroma however, first experiments showed that for the proper isolation of stromal cells mechanical stress seems to have a negative impact on yield. Thus, several isolation

techniques were applied for comparison (see *Fig. 3.1.1.2*). This includes crushing the bones with mortar and pestle, flushing the bone with syringe and centrifugal flushing wherein the bone marrow is flushed out by using the centrifugal forces in a table-top centrifuge.

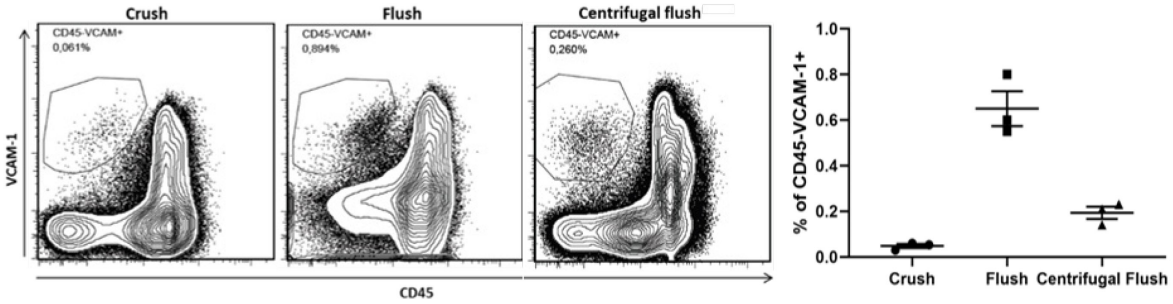

Fig. 3.1.1.2: Effect of isolation method on stromal yield Representative Contour plots with 5% contour levels and outliers; gated on single, live, non-lineage cells; **left:** crushed with mortar and pestle in PBS/BSA/EDTA; **center left:** bones were flushed with a syringe and then transferred to digestion medium; **center right:** cut bones were placed in a pierced 0.5 mL reaction tube in a 1.5 mL reaction tube containing digestion buffer, tubes were spun shortly to flush out BM strings; **right**: quantification of dot plot conditions; n=3, mean ± SEM

The lowest percentage was obtained with the crushed bones. Flushing the bones via centrifugation already increases the stromal percentage more than 4-fold compared to crushing. Nevertheless, the most prominent effect could be seen when flushing the bone with a syringe leading to an increase that is more than 10 times that of the crushed bones and still 3-fold more than similar flushing by centrifugation.

As the stroma forms a three-dimensional network throughout the bone marrow it is necessary to extract the bone marrow as intact as possible in order to prevent the loss of stromal cells. Also, it remained unclear whether there were still considerable amounts of stromal cells left in the hollow bones. This problem was addressed by flushing the bone and then looking at stromal percentages in bone and/or flush after digestion (*Fig. 3.1.1.3*). Here, samples were prepared in different fashion. Firstly, a bone with removed metaphyses was incubated in digestion buffer. In a second approach, bones were flushed out as described before but instead digested separately from the empty bone. Stromal percentages were then assessed in each alone or both combined. To check for stromal cells that were still lining the inner surface of the bone empty bones were washed a second time with PBS/BSA/EDTA only.

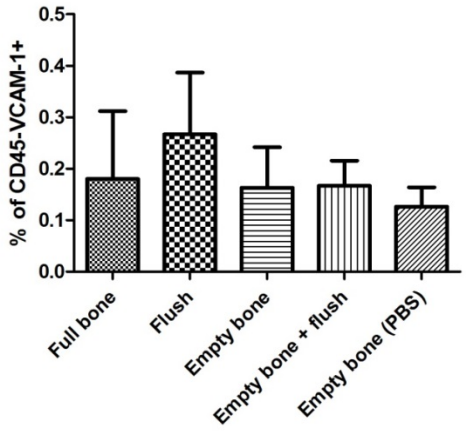

Fig. 3.1.1.3: Distribution of stroma cells in the bone marrow and contribution to digestion yield BM samples of different origins cells were pre-gated according to scatter/singlets/viability/Ter119$^-$; bones were incubated with cut ends only, flushed before digestion, incubated empty, or washed with PBS after second digestion incubation; percentages of CD45$^-$VCAM-1$^+$-cells of the parental populations are depicted in the plot. n=3; mean ± SEM

It can be seen that VCAM-1$^+$ stromal cells are found in every sample obtained albeit in low percentages which is reflected by percentage and subsequently numbers among total bone marrow cells. Apparently, even empty bone still contained notable amounts of VCAM-1 positive stromal cells that were still present after flushing as can be seen in the PBS-flushed sample. In line with these results the protocol was changed to flushing the bone marrow, digesting flush and empty bone separately but mixing both samples to achieve higher stromal cell counts for further analysis.

3.1.2 Stroma yield can be enhanced by Actin cytoskeleton-destabilizing agents

Stromal cells adhere strongly to plastic surfaces and this property was used for enrichment of stromal cells from total BM cells. It couldn't be ruled out that this would potentially decrease isolation outcome. As adherence is mainly depending on an intact actin cytoskeleton, drugs targeting F-Actin stability were chosen. Furthermore, attachment of cells to each other is prevented, thus potentially reducing doublets.

Cytochalasin D is a mycotoxin isolated from *Zygosporium mansonii* and a potent inhibitor of actin polymerization by binding to its barbed ends and preventing further growth of the filament [94, 95]. Latrunculin B, on the other hand, is a macrolide toxin derived from the red sea sponge *Latrunculia magnifica*. It disrupts the actin cytoskeleton by binding to the monomeric G-Actin in a 1:1 stoichiometry, subsequently altering its subunit interface[96] and reducing the amount of monomers available for polymerization[94].

In a pilot experiment not depicted the efficacy of both substances was tested in the designated concentration range on CD4$^+$ memory lymphocytes in spleen while monitoring the F-Actin cytoskeleton via Phalloidin staining. It could be confirmed that both reagents severely affected the structure of F-Actin.

In the next step, it remained to be evaluated how each of the inhibitors individually contributes to the effect observed earlier and whether one of them might already be sufficient to achieve a higher yield

in stroma isolation (*Fig 3.1.2*). For this, no inhibitors, one only or both combined were added to the digestion buffer and incubated with the cells as described earlier. Any subsequent buffers were free of inhibitors.

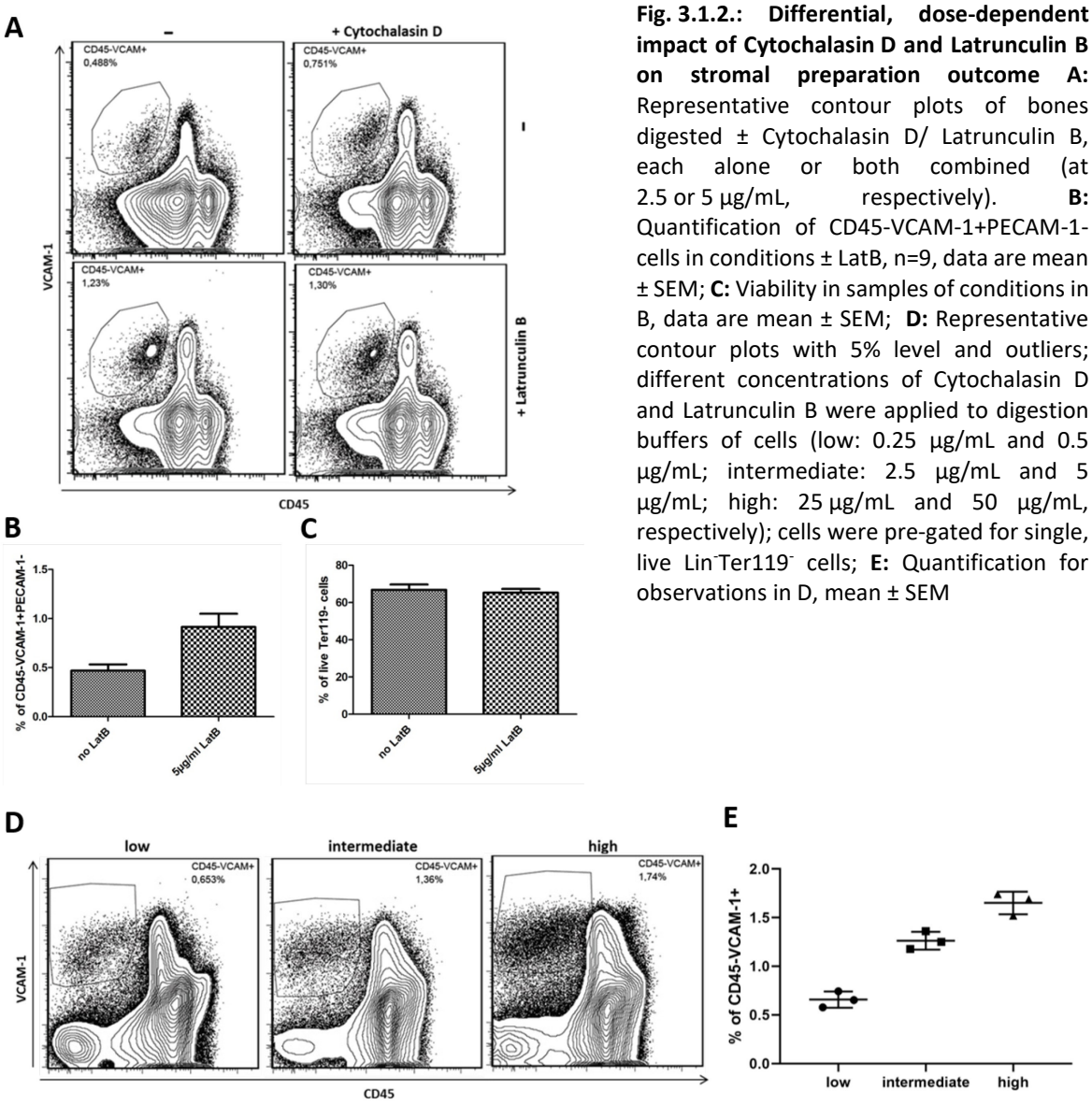

Fig. 3.1.2.: Differential, dose-dependent impact of Cytochalasin D and Latrunculin B on stromal preparation outcome A: Representative contour plots of bones digested ± Cytochalasin D/ Latrunculin B, each alone or both combined (at 2.5 or 5 µg/mL, respectively). **B:** Quantification of CD45-VCAM-1+PECAM-1- cells in conditions ± LatB, n=9, data are mean ± SEM; **C:** Viability in samples of conditions in B, data are mean ± SEM; **D:** Representative contour plots with 5% level and outliers; different concentrations of Cytochalasin D and Latrunculin B were applied to digestion buffers of cells (low: 0.25 µg/mL and 0.5 µg/mL; intermediate: 2.5 µg/mL and 5 µg/mL; high: 25 µg/mL and 50 µg/mL, respectively); cells were pre-gated for single, live $Lin^-Ter119^-$ cells; **E:** Quantification for observations in D, mean ± SEM

The control digestion without inhibitors reflects the yield variation of the isolation protocol. Nevertheless, a positive impact on digestion outcome can be observed with the cytoskeleton-destabilizing agents. Interestingly, Latrunculin B alone yields a percentage of VCAM-1^+ stroma cells that is comparable to both of the inhibitors added to digestion medium. However, Cytochalasin D also increases the stromal yield albeit in a lower manner. Importantly, survival of cells was not impaired in the absence of cytoskeleton inhibitors (*Fig 3.1.2B*). While according to the percentages obtained Latrunculin B would be sufficient for future isolation both inhibitors were chosen due to their differing modes of action on the cytoskeleton and published synergistic effects[97].

Reviews on the working principles of Cytochalasin D and Latrunculin B found them to exert a dose-dependent effect on cells. To find the optimal balance between increasing the stromal yield and risking loss of stroma due to the cytotoxic effect of both substances a titration was performed (*Fig. 3.1.2D-E*). Here, both toxins were added to the digestion buffer in a concentration range between 0.25-25 µg/mL (Cytochalasin D) and 0.5-50 µg/mL (Latrunculin B), respectively.

Although a yield increase can be seen in comparison from using 10-fold less inhibitor (low) than usually (intermediate), the difference between intermediate and 10-fold higher concentrations is only marginal. In addition, a slight decrease in viable cells could be observed in samples with high inhibitor concentrations proving the undesirable cytotoxic effects of Cytochalasin D and Latrunculin B (data not shown). In accordance with these data, an intermediate concentration of Cytochalasin D and Latrunculin B (2.5 or 5 µg/mL, respectively) was used for further isolations.

3.1.3 Pure stroma populations can be obtained via FACS™ with good recovery

The ultimate goal of the study is to characterize the stroma cells in terms of surface marker expression and their diversity. This is due to the lack of a clear stromal surface marker by which stromal cells could be stained. Additionally, it is of importance to analyze cytokine and chemokine expression of VCAM-1$^+$ stromal cells to understand their interaction with memory lymphocytes a little better.

To get pure populations of VCAM-1$^+$ stromal cells BM suspensions were sorted according to surface marker expression. The staining involved the same markers previously used for assessment of the enrichment with the cytoskeleton inhibitors. After gating out dead cells, doublets as well as Lin$^+$ cells three populations were sorted at the FACS™ machine. This included the stromal (CD45$^-$ VCAM-1$^+$PECAM-1$^-$) and endothelial fraction (CD45$^-$VCAM-1$^+$PECAM-1$^+$) as well as CD45$^-$VCAM-1$^-$PECAM-1$^-$ cells. Purity was assessed on a flow-cytometer (see *Fig. 3.1.3*).

Despite only few sorted cells due to the generally low percentage of the cells of interest high purity could be achieved for all fractions as seen in *Fig. 3.4.1*. It must be noted, however, that about 15% of sorted VCAM-1$^+$PECAM-1$^+$ cells are PECAM-1$^-$ most likely due to cells on the y-axis that could implicate clotting of the tubing system or a compensation issue. Latter could be excluded after checking the settings.

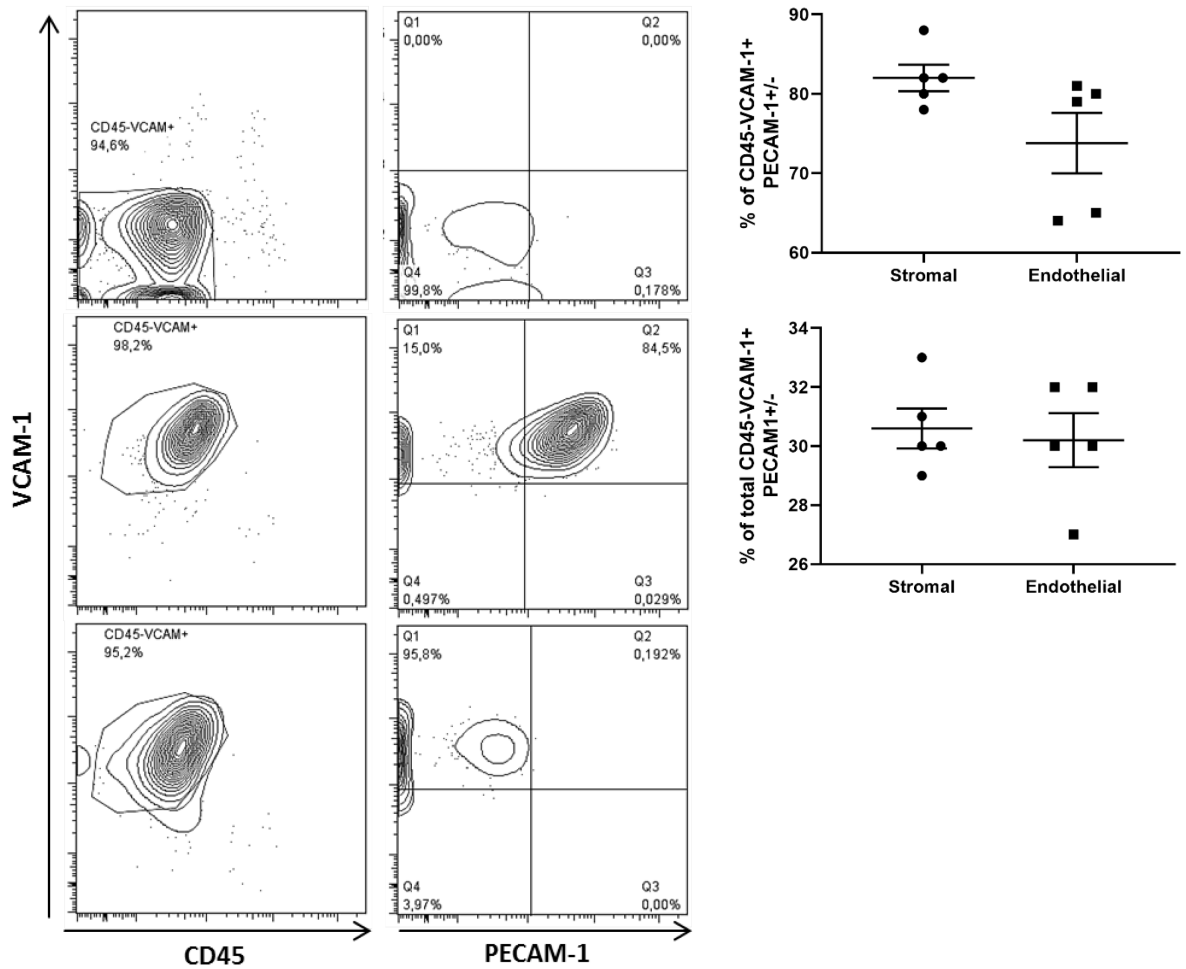

Fig. 3.1.3: Flow cytometric analysis of sorted murine BMSCs Aliquots from the fractions sorted at BD Influx were measured at the MACSQuant Analyzer and depicted as contour plots with 5% levels and outliers as modified in FlowJo software; **left column:** gated on Scatter/Singlets/Lineage$^-$Ter119$^-$Gr-1$^-$; **center column:** gated on Scatter/Singlets/Lineage$^-$Ter119$^-$Gr-1$^-$/CD45$^-$VCAM-1$^{-/+}$, respectively; **right:** quantification for purity (top) and total recovery from beginning of the isolation (bottom). Mean ± SEM

To rule out that the viability staining was washed out of dead cells additional dye was added before checking the purity. The experiment showed that the majority of the cells survive the long incubation step in the tube at the sorter (data not shown).

Stromal and endothelial cells that were sorted at the Influx according to the aforementioned gating strategy were afterwards lysed for RNA isolation in those cases when a sufficient purity was obtained. RNA content was measured via NanoDrop (*Tab. S1*). To assess the quality and integrity of the prepared RNA samples a small aliquot was run in an electropherogram (BioAnalyzer 2100, Agilent Technologies). The overall integrity was determined as RNA integrity number or RIN[98] (see *Tab. S1*).

3.1.4 Bulk stromal cells express a broad set of genes reminiscent of the mesenchymal lineage but enriched for cell adherence pathways

Cell populations sorted by FACS™ were lysed for RNA and subsequently checked for their gene expression in microarrays. Data is depicted in *Tab. S2* and derived from 3 different experiments for PECAM-1$^+$ and PECAM-1$^-$ each.

The excerpt of differentially expressed genes in *Tab. S2* shows only few of the several thousand genes that the HPCDA score ranked algorithm identified to be significant. Firstly, proteins that have been published to be expressed in stroma or endothelium could be shown here on the RNA level as well (see *Fig. 3.1.4*). That is true for CXCL12 as one of the key molecules in the plasma niche but also for PDGFRβ – a receptor that has been described to be involved in angiogenesis but also as a pericyte-defining surface marker in bone marrow (see *Fig. 3.1.4*). Other molecules such as Kit ligand were shown to be present on stroma cells as c-Kit$^+$ HSC are supported by Kit ligand MSCs[99]. For endothelium in contrast, genes like Endoglyx-1[100] or E-Selectin[101] were found to be highly expressed in PECAM-1$^+$ cell transcriptomes. Both are linked to endothelium almost exclusively.

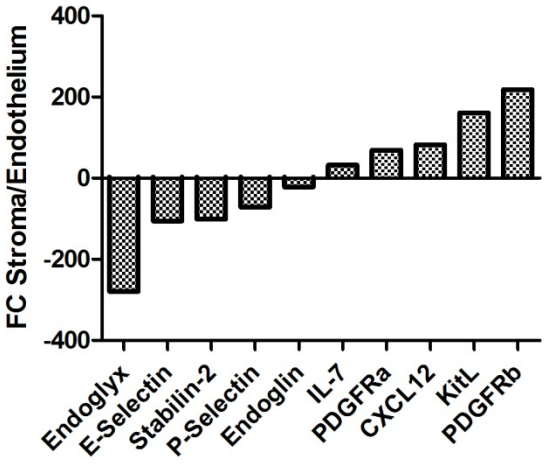

Fig. 3.1.4: Trends in gene expression and cell type distribution of genes highly expressed in stromal cells Fold change (FC) of representative endothelial (negative FC) and stromal (positive FC) genes that were differentially expressed in the micro arrays; data depicts mean of n=3

However, the transcriptomes did not only consist of genes that have been linked to reticular stromal cells or endothelium. Several markers of the mesenchymal lineage were present in both transcriptomes (*Fig. 3.1.4*). For example, gene expression in stromal cells is increased for genes related to adipogenesis (Adiponectin, Esm1[102], FABP4, ACAM[103, 104]) or osteogenesis (Osteoglycin, Bone sialoprotein, Runx2).

To get a broader idea which physiological pathway the differentially expressed genes are involved in, a gene-set enrichment assay (Cytoscape BiNGO) was performed (*Tab 3.1.4*).

Tab. 3.1.4: Gene-set enrichment analysis in GO category pathways among differentially expressed genes of stromal and endothelial cells Gene sets that were enriched in the micro arrays according to Cytoscape BiNGO; x: number of genes from GO category enriched; n: total number of reference genes in GO category

p-value	x	n	Description
1.58E-08	77	200	Focal adhesion
4.00E-07	27	50	Ribosome, eukaryotes
3.33E-05	72	218	Proteoglycans in cancer
8.81E-05	98	325	PI3K-Akt signaling pathway
1.28E-04	95	316	Pathways in cancer
3.92E-04	63	199	Endocytosis
7.72E-04	31	84	ECM-receptor interaction
1.24E-03	29	79	Gap junction
1.30E-03	9	15	Glycosaminoglycan biosynthesis - keratan sulfate
1.33E-03	32	90	Ribosome
1.51E-03	31	87	GnRH signaling pathway
2.69E-03	42	131	Axon guidance
3.51E-03	18	45	Sphingolipid metabolism
4.87E-03	60	206	Regulation of actin cytoskeleton
6.11E-03	48	160	Transcriptional misregulation in cancer
8.70E-03	19	52	Glutathione metabolism
8.80E-03	17	45	Notch signaling pathway
1.24E-02	24	72	Adherens junction
1.44E-02	28	88	Prostate cancer
1.45E-02	20	58	Long-term depression
1.63E-02	22	66	VEGF signaling pathway
1.85E-02	38	129	Tight junction
2.05E-02	67	249	MAPK signaling pathway
2.16E-02	4	6	Glycosaminoglycan biosynthesis, chondroitin sulfate backbone

It is apparent at first sight that many of the categories enriched either are involved cell-substrate (focal adhesion, ECM-receptor interaction, Regulation of Actin cytoskeleton) or cell-cell adhesion (gap junction, tight junction, adherens junction). Another recurring theme is cancer physiology (Proteoglycans, Pathways, Transcriptional misregulation in cancer). Some general signaling pathways are enriched (PI3K/Akt, Notch, VEGF, MAPK) as well. Stromal very active contribution to surrounding ECM is represented by Keratan and Chondroitin sulfate GAG synthesis.

Surprisingly, some rather neuron-affiliated processes (GnRH signaling, long-term depression and axon guidance) are also enriched.

3.1.5 Identification of possible memory niche interactions by complementary transcriptomics

As outlined briefly in the introduction, the concept of stromal niches is thought to be a recurring theme throughout the developmental stages of a hematopoietic cell.

Our group had already generated transcriptomes of several memory lymphocytes, including CD4, CD8, B and long-lived plasma cells. For the first time, we now had *ex vivo* transcriptomes of their elusive stromal binding partners of the corresponding niches at hand. We hypothesized that since survival and adherence factors must be based on the principle of receptor-ligand interactions, there should be a way to devise an algorithm that could scan each transcriptome for possible interactions between the cell populations (see scheme in *Fig. 3.1.5A*). Contrary to the depiction in the figure, those interactions do not necessarily have to be surface-surface but could well include secreted factors from one side. To make the visual presentation of these binding partners more appealing, the results were embedded into maps available via the Kyoto Encyclopedia of Genes and Genomes (KEGG). One such example is depicted in *Fig. 3.1.5B* for the complementary transcriptomics of bulk stromal cells and long-lived plasma cells, both generated in our group.

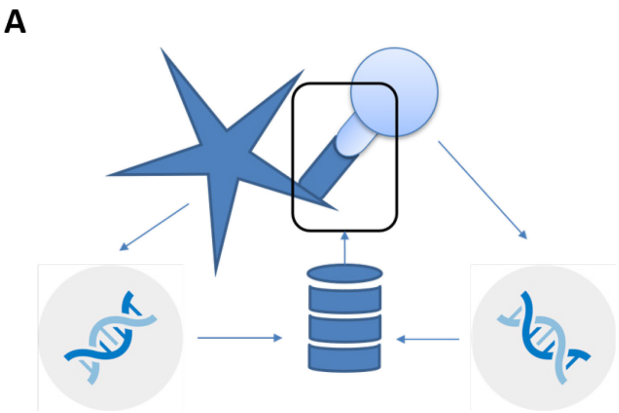

Fig 3.1.5 Ligand-receptor pairing by complementary transcriptome analysis (**A**) Scheme depicting the general workflow in complementary transcriptomics for ligand receptor pairing. In short, transcriptomes are generated from purely sorted stroma or (memory) lymphocytes preparations. The program is then comparing present genes[105] with curated databases of known *trans*-interactions (e.g. from KEGG) to predict possible ones (black frame) (**B**) Exemplary readout for the comparison of CD45$^-$ VCAM-1$^+$PECAM-1$^-$ stroma with long-lived plasma cells. All boxes are ligands/receptors in the KEGG Cytokine/Chemokine pathway [hsa04060] (left). A blue box indicates the presence of a given gene in stroma whereas red box shows presence in plasma cells, as outlined for the known interaction of CXCL12/CXCR4 (right).

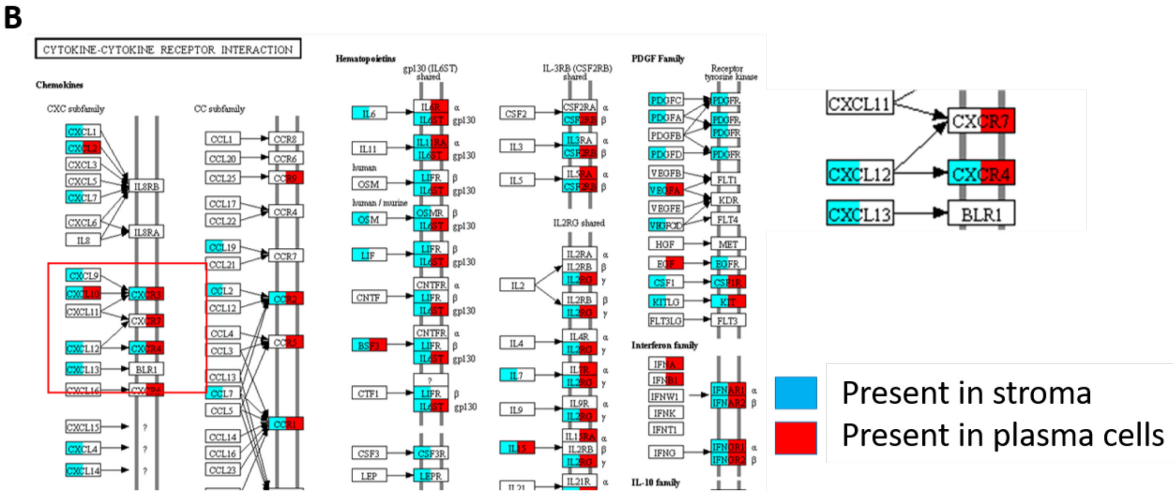

In line with contemporary literature, one interaction that can be observed from both transcriptomes is that of stroma-derived CXCL12/SDF-1 and its cognate receptor CXCR4 on long-lived plasma cells (*Fig 3.1.5B*, inlet and magnified on bottom right). In the curated list of known cytokine/chemokine and corresponding receptors, we have each molecule split into two boxes to show whether the transcript was present or absent in either transcriptome (stroma: blue, plasma cells: red).

3.2 Assessing the heterogeneity of murine bone marrow IL-7$^+$ stroma cells

Having established a digestion protocol for quantitative isolation enabled us to look at the majority of the stroma cells without extensive cell death during the preparation. Also, analyzing the stromal gene expression despite low cell numbers from FAC-sorted cells seemed feasible as the transcriptomes in *Fig. 3.1.5* showed. However, as these compared stromal to endothelial cells as characterized by their differing germ layer origins, the differentially expressed genes were not immediately informative for the stromal niche composition and heterogeneity. Naturally, we wanted to explore the heterogeneity within a stromal subset whose function was already established. IL-7 is known to play a crucial role in the survival and maintenance in memory T lymphocytes and early B cell lineage progression.

3.2.1 IL-7$^+$ stromal cells have significantly higher Prrx1 levels than IL-7$^-$ counterparts

As intracellular staining of IL-7 didn't prove feasible due to low steady state concentrations and because it interferes with sorting/RNA preparations, heterozygous reporter mice in which GFP has been knocked into the Il7 gene (*Fig. 3.2.1A*) were used instead. In the heterozygous genotype, the remaining functional IL-7 seemed to be sufficient to drive T and B cell lymphopoiesis as their numbers were not drastically altered (data not shown). Hence, it's assumed to mimic the wild-type accordingly without influencing the niches in the bone marrow.

Mice have been sacrificed as previously described for bulk stromal transcriptomes and pure cells sorted from FACS™ (*Fig. 3.2.1B-C*). The comparison of differentially expressed genes between GFP$^+$PECAM-1$^-$ and GFP$^-$PECAM-1$^-$ samples shows that they cluster according to phenotype and differ significantly (*Fig. 3.2.1D*).

The top list of differentially expressed genes according to the ranking by HPCDA score first of all revealed that these transcriptomes are vastly more similar to one another as seen by their relatively lower HPCDA scores in contrast to the bulk stroma vs. endothelial cell analysis (*Tab. S3*). The fact however that many of the top genes are supposedly myeloid genes (Ly6C, NGP, Lyz1, MPO) argues for considerable contamination by these cells that didn't show up in the sorting controls. We were therefore critical of the data and didn't follow it up for candidate markers.

Another reason for concern was that despite sorting for GFP$^+$ and GFP$^-$ cells, Il7 transcript could be determined independently by two Affymetrix probes in the GFP$^-$ sorted cells (*Fig. 3.2.1E*).

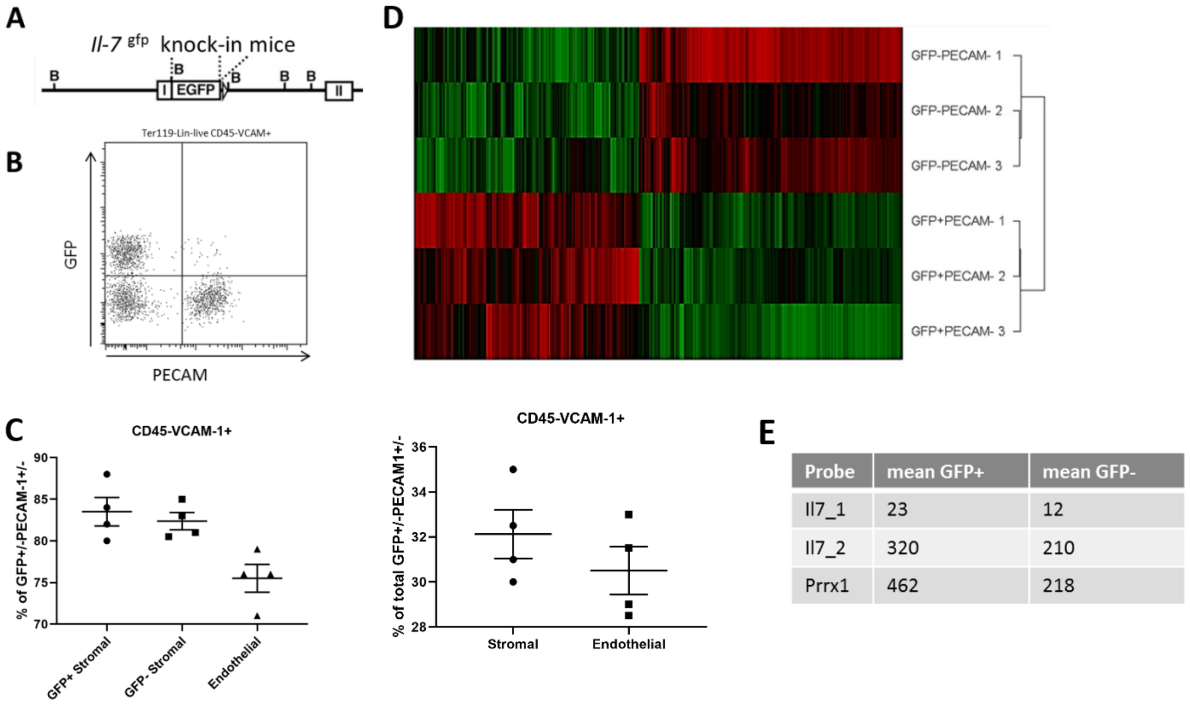

Probe	mean GFP+	mean GFP-
Il7_1	23	12
Il7_2	320	210
Prrx1	462	218

Fig. 3.2.1: Gene expression analysis of Interleukin-7 reporter GFP stromal cells (**A**) Schematic depiction of the IL7KI design used with boxes being exons/cDNAs and 'B' depicting BamHI cutting sites. (**B**) Cells were isolated from heterozygous IL7KI mice and analyzed for their GFP fluorescence in the VCAM-1$^+$ population; gated on live, Ter119$^-$Lineage$^-$CD45$^-$VCAM-1$^+$ singlets**.** (**C**) Purity (left) and total recovery (right) after cell isolation and sort; (**D**) Heatmap comparing the gene expression of GFP$^+$PECAM$^-$ with GFP$^-$PECAM$^-$ sorted cells. Data from 3 independent arrays from 4 mice. zScore of log2 expression values in the range from -2.1 (green) to 2.1 (red). Genes selected are limma $p < 0.05$ and $-1.3 <$ fold change <1.3; **(E)** Overview of Il7 and Prrx1 probe mean signals between GFP$^+$PECAM-1$^-$ and GFP$^-$PECAM-1$^-$ sorted cells

However, among the controversial list of top genes we could also find the stromal master transcription factor Prrx1 that is readily used in stromal reporter mice. Surprisingly, it is expressed twice as high in the GFP$^+$ fraction of stromal cells than it is in the GFP$^-$ cells (*Fig. 3.2.1E*).

3.2.2 *Ex vivo* co-expression of immune regulatory hematopoietic surface markers on stromal cells

As gene expression analysis via micro arrays is always a population-level approach to assess diversity, we were wondering whether it was possible to miss small stromal subsets due to unproportional bias of larger ones in the gene expression.

Therefore, an unbiased surface marker screening approach based on flow cytometry was chosen (LEGENDScreen™, Mouse Kit, BioLegend). This managed to combine a population-spanning with a single-cell level approach. To get further insight into how the availability of IL-7 might also determine stromal marker expression via feedback loops, the analysis was done on both IL7KI heterozygous and homozygous mice. Given the kit's bias towards hematopoietic cells as mostly canonical "cluster of

differentiation (CD)" antibodies are included, still a considerable amount of these CDs seemed to be expressed by bulk stromal cells and GFP^+ cells.

Of those markers expressed, different general expression modes could be observed. While some markers only showed expression among GFP^- stromal cells (e.g. CD55, Tim-1), others could be found on both GFP^+ and GFP^- stromal cells such as CD1d or CD63. There was hardly a scenario where a marker was exclusively expressed by the GFP^+ compartment although general enrichment in this population could be seen (see CD73 intermediates or CD54). Expression is rarely confined to the stromal population but can be found in same or differing levels on endothelial cells (blue populations) or $CD45^+$ hematopoietic cells that served as an internal reference population for gating (data not shown). Interestingly, stromal marker and/or GFP expression appear mutually exclusive for several of the tested surface markers (CD160, APRIL, PD-1, PDC-TREM).

Of note, it is rarely the case that markers are vastly differentially expressed between stroma and endothelial cells (CD140a/b, CD105, CD54) which makes using any of the tested markers as an elusive surrogate marker in the mouse problematic.

Apart from the persistent observation that there are haplotype-dependent expression level differences of GFP (further noted in section 3.2.8), the lack of a functional wild-type IL-7 allele didn't seem to impact vastly on surface marker phenotype. Minimally altered expression patterns can be found for CD73, PD-1 among others. CD55/DAF stands out in the homozygous scenario as a considerable GFP^+ stromal population can be observed in that haplotype.

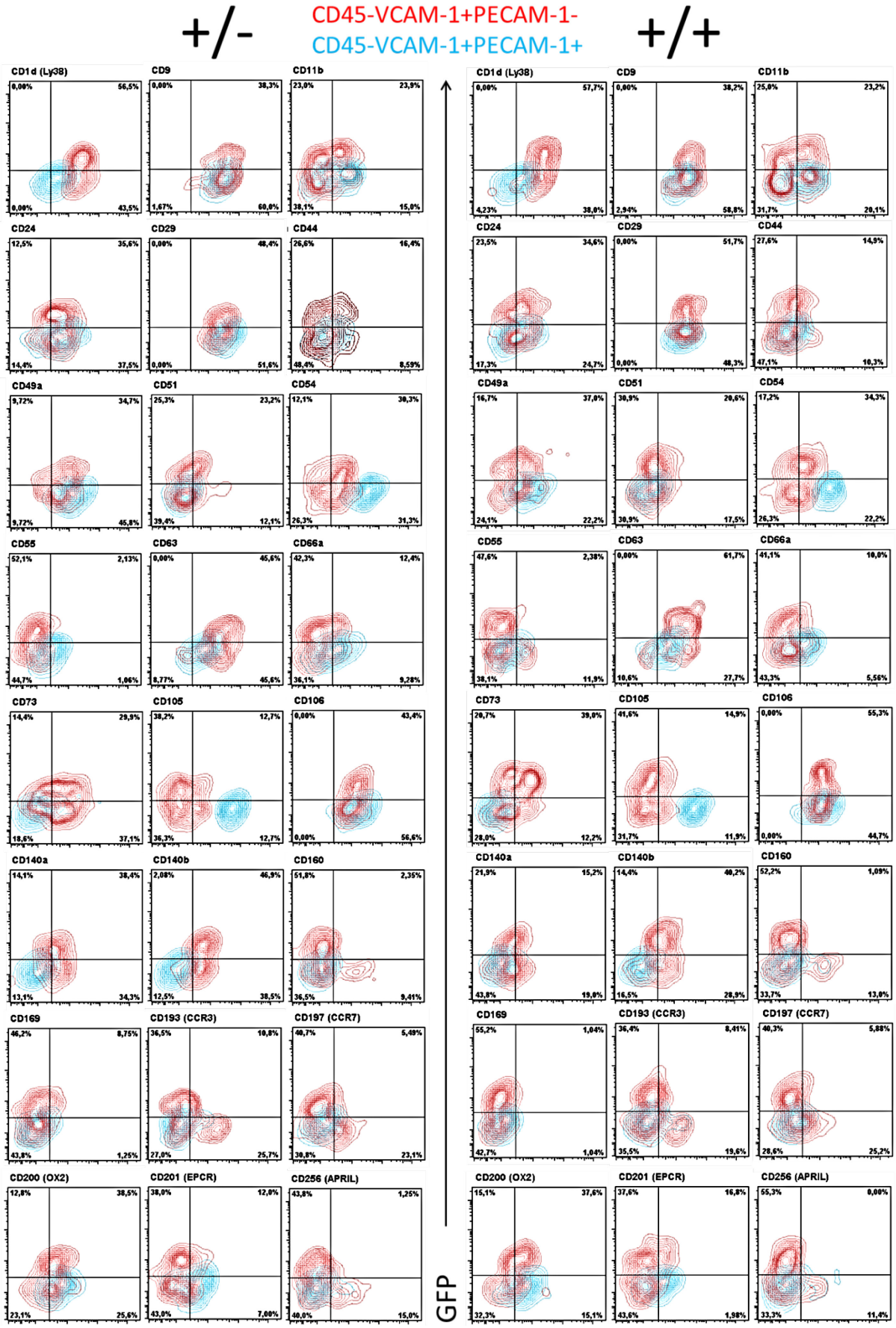
+/-
CD45-VCAM-1+PECAM-1-
CD45-VCAM-1+PECAM-1+
+/+
CD1d (Ly38)
CD9
CD11b
CD24
CD29
CD44
CD49a
CD51
CD54
CD55
CD63
CD66a
CD73
CD105
CD106
CD140a
CD140b
CD160
CD169
CD193 (CCR3)
CD197 (CCR7)
CD200 (OX2)
CD201 (EPCR)
CD256 (APRIL)
GFP

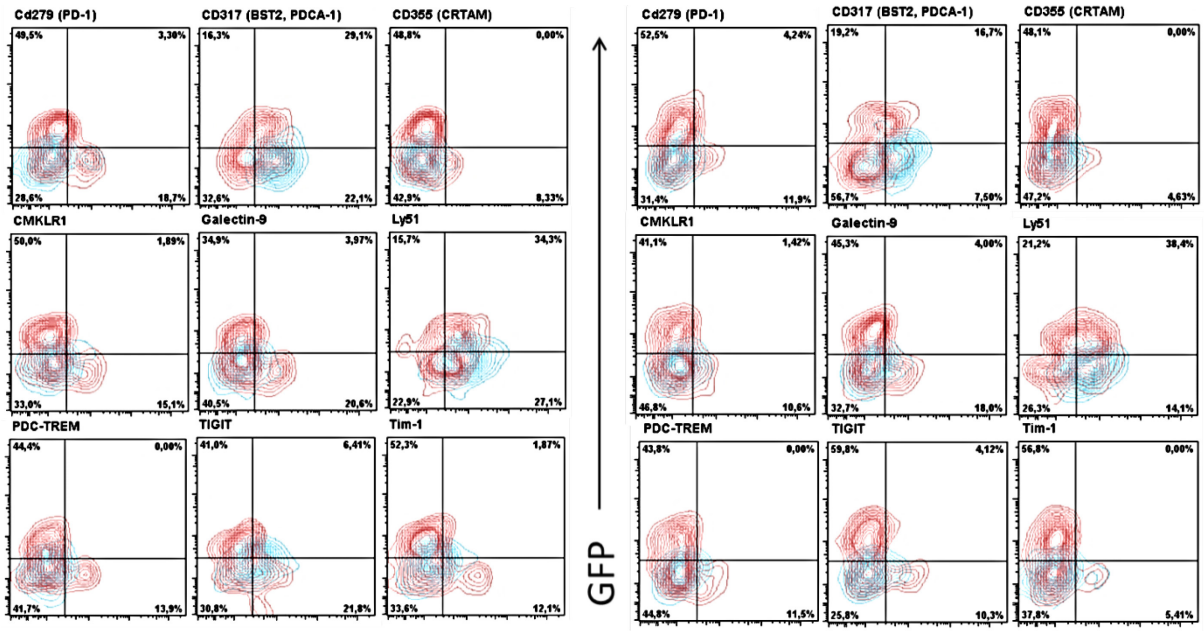

Fig. 3.2.2.1: Differential surface marker expression on CD45$^-$VCAM-1$^+$ PECAM-1$^{+/-}$GFP$^{+/-}$ BMSCs between IL7KI haplotypes Representative contour plots of marker vs GFP between IL7KI heterozygous (+/-) or homozygous (+/+) mice (n=3); CD45-VCAM-1$^+$ cells either being PECAM-1 positive (blue) or negative (red); gates were set according to isotype controls and/or FMO; samples were gated for viable, non-lineage (at least Ter119$^-$) singlets

Upon verifying some of the markers from the screening in a multiplexed approach in a follow-up flow cytometry experiment using the same hybridoma clones on wild-type C57Bl/6 mice we could confirm the very limited stromal heterogeneity on a per-cell level, at least for the clones/markers tested (*Fig. 3.2.2.2*).

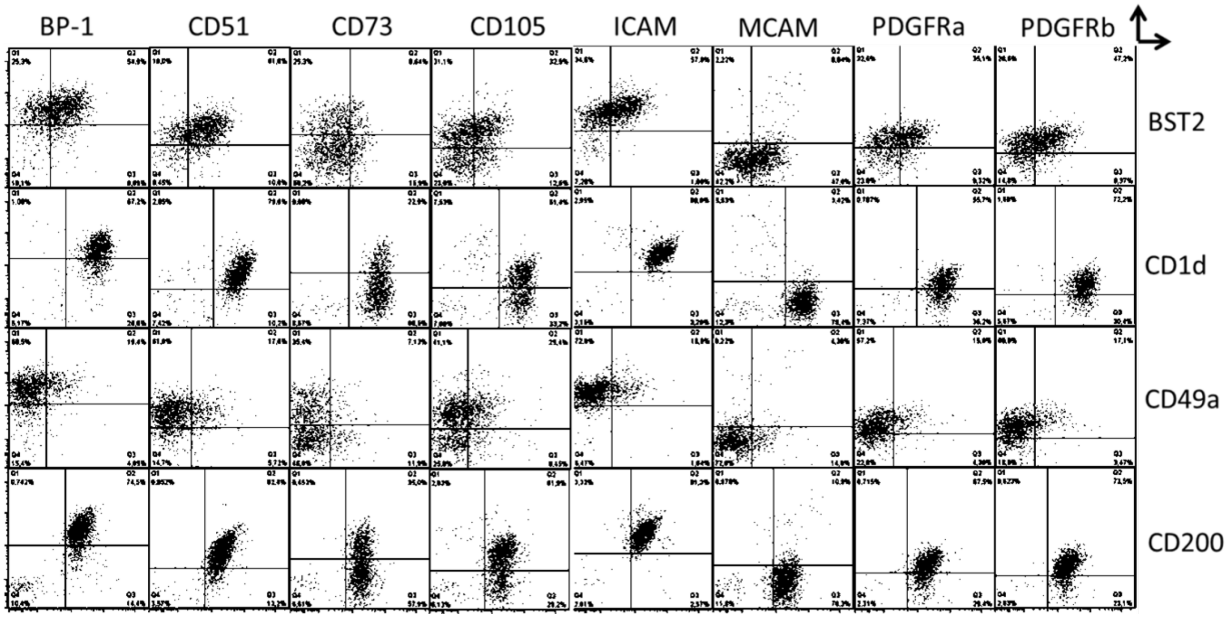

Fig. 3.2.2.2: Considerable population overlap in surface marker expression of stroma-related surface molecules on CD45$^-$VCAM-1$^+$ BMSCs in multiplexing flow-cytometric analysis Dotplots of CD45-VCAM-1$^+$ cells from C57Bl/6 mice with top and side labels corresponding to y- and x-axis, respectively; samples were gated for viable, non-lineage singlets according to FMO control

It is pretty apparent when looking at CD200 or CD1d counterstains with the other markers, only one pronounced population can be determined – the exception for both being CD73 and CD105 where a clear separation into two subpopulations can be seen. A much wider distribution of marker combinations can be seen in the case of BST2 vs CD73/CD105, although cells don't show a bimodal expression pattern in either scenario. That recapitulates the staining pattern of CD73 vs GFP in the prior screening experiment.

3.2.3 CD1d as surrogate marker for VCAM-1$^+$PECAM-1$^-$ stromal cells

A potential goal of this screening approach was not only to find substantial sub-populations among stromal cells but also to identify surrogate markers for known population. One problem with our established staining protocol has always been the reliance on VCAM-1 to identify stromal/endothelial cells and additionally PECAM-1 to exclude endothelial cells from the gating. While confirming the expression of CD1d on stromal cells, it could also be shown that its expression is considerably higher on the majority of stromal cells (*Fig. 3.2.3.1*, upper right, Q1). A different gating on CD45$^-$CD1d^{hi} cells revealed to contain the majority of the VCAM-1$^+$PECAM-1$^-$ stromal compartment with only negligible amounts of PECAM-1$^+$ or double-negative cells to be included in line with the initial screening results.

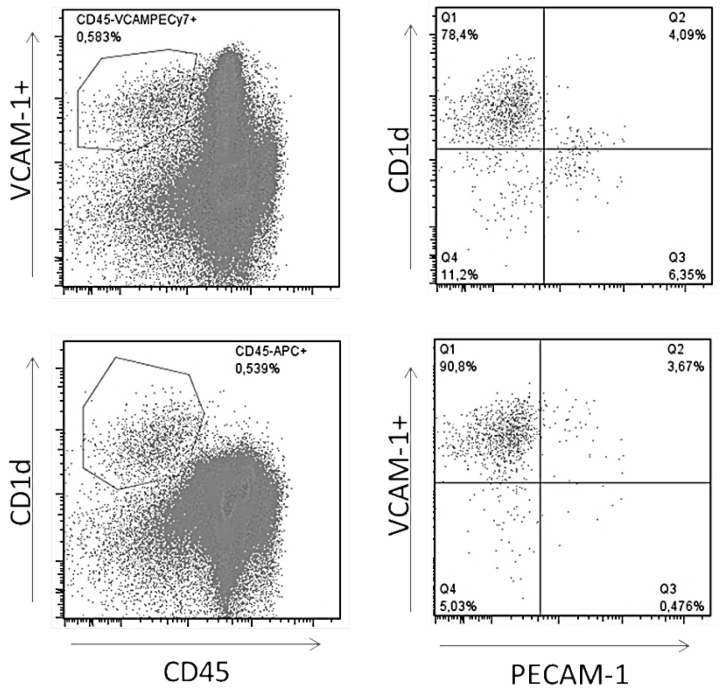

Fig. 3.2.3.1: CD1d is a surrogate marker for VCAM-1$^+$PECAM-1$^-$ cells First row: Dotplots of bulk VCAM-1$^+$ CD45$^-$ stroma that is largely CD1d$^+$; 2nd row: CD45$^-$CD1d$^+$ cell do include the majority of VCAM-1$^+$ cells while barely staining for PECAM-1); samples were gated for viable, non-lineage singlets according to FMO

CD1d also proved to be expressed *in situ* on *bona fide* stroma cells as evidenced by their radioresistance in Ubiquitin:RFP mice that have been sub-lethally irradiated and which have been reconstituted with C57Bl/6 bone marrow – rendering all non-proliferating cells such as stroma endothelium or memory cells fluorescent (see *Fig. 3.2.3.1*, RFP).

As the flow-cytometric analysis of CD1d vs CD45 indicated that CD1d is not restricted to the stromal compartment but also expressed on hematopoietic cells, especially antigen-presenting cells. This explains why in addition to a stromal overlap (*Fig. 3.2.3.2, arrows*), a surface staining on hematopoietic cells (*Fig. 3.2.3.2, composite*) can be observed. The nuclei of the stromal show the notable pyramid/spindle shape which sets them apart from polymorphonuclear (granulocytes) and circular (lymphocyte) and flat (endothelium) phenotypes.

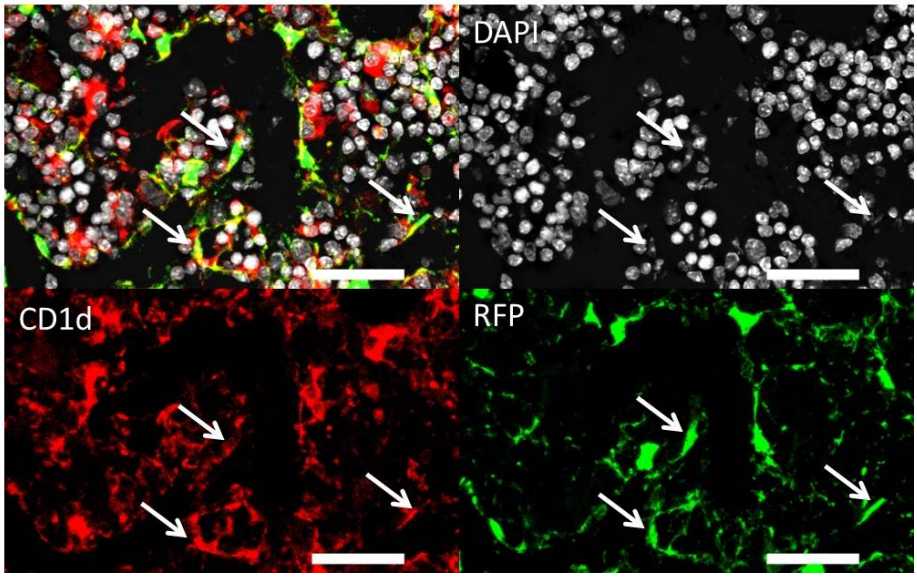

Figure 3.2.3.2: CD1d is expressed on radioresistant stromal cells in the bone marrow Femur slides of BM chimeras where stained for CD1d and RFP and nuclei (DAPI); arrows indicate substantial signal overlap on cell bodies and processes; scale: 50 µm

3.2.4 IL-7^{+} stromal cells are enriched in CD200^{int}/BP-1^{+}/CD73^{+}/CD105^{-} compartment

As laid out in section 3.2.1, IL-7 has proven difficult to stain intracellularly at physiological concentrations in our hands as well as in the literature. Although the gene-expression and surface marker screening approach didn't reveal an exclusive antigen to stain instead, a characteristic surface marker combination shows to enrich for the desired stromal subpopulation (see *Fig. 3.2.4*). Among the many markers to emerge from the screening kit, three were particularly enriched in the GFP/IL-7^{+} stroma cells. Firstly, GFP^{+} expression was found exclusively enriched in the CD200 intermediate fraction. Secondly, BP-1^{+} and CD73^{+} seemed to be enriched for GFP^{+} cells at least. Some stromal markers also proved to be mutually exclusive with regards to GFP levels. Endoglin/CD105 for example was only expressed on GFP^{-} stromal cells, thus serving as a negative marker of IL-7 stroma. When gating on the marker-positive cells among non-hematopoietic cells, GFP^{+} cells still comprised a considerable number of cells for CD200, BP-1 and CD73 arguing for their important role in stromal biology.

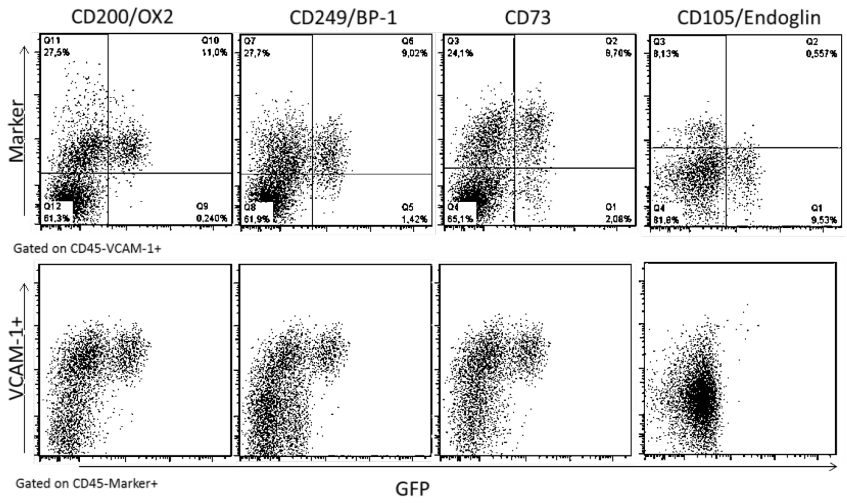

Fig. 3.2.4: IL7/GFP is enriched in CD200^{int}CD249^{+} CD73^{+}CD105^{-} stromal cells in heterozygous IL7KI mice Dot plots indicating marker co-expression with GFP on CD45^{-}VCAM-1^{+} (top row) or VCAM-1 expression on CD45^{-}Marker^{+} cells (bottom row); samples were further gated for viable, non-lineage singlets

3.2.5 IL-7 abundance feeds back on stromal marker expression unrelated to lack of mature lymphocytes

One of the differentially expressed genes originally identified from the comparison of bulk stroma cells and endothelial cells was Cadherin-11, also termed OB-Cadherin derived from its prominent expression in osteoblasts. It was later observed to be expressed on reticular stroma as well.

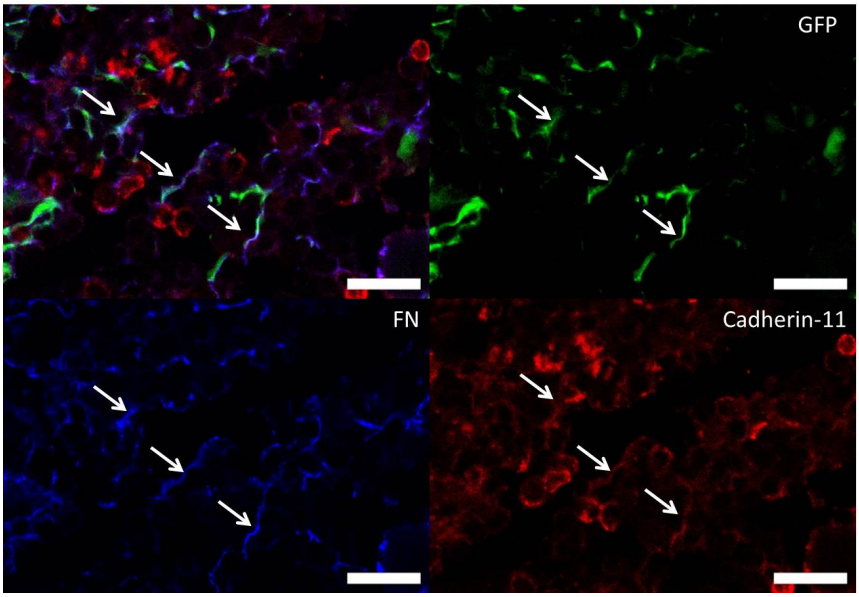

Fig. 3.2.5.1: Cadherin-11 is expressed on radioresistant stromal cells Composite image of femoral slides indicate substantial signal overlap of GFP stroma (green), stromal Fibronectin/FN (blue) and Cadherin-11 (red). Arrows: Stromal processes that are triple positive; scale: 20µm

While the broad cytometric screening approach of surface markers didn't yield considerable differences between IL7KI haplotypes in the initial experiment, stromal markers BP-1 and Cadherin-11 revealed a correlation of expression profile and haplotype. Notably, both MFI and percentage of BP-1^{+} cells are considerably higher in the IL7KI$^{-/-}$ haplotype whereas for Cadherin-11 the opposite holds true - regardless of whether one looks in GFP^{+} or GFP^{-} stromal populations.

As a homozygous knock-in mouse is a virtual knock-out of IL-7 due to absence of a functional wild-type allele (as apparent by lack of lymph nodes in the animals), it was hypothesized that the availability or rather the absence of IL-7 might feedback to these stromal markers. Another possibility could have

been an indirect feedback loop via mature lymphocyte as absence of IL-7 also leads to T and B cells progenitors not progressing to mature stages due to their reliance on IL-7 as a survival factor. To analyze whether the presence of mature lymphocyte is needed for the observed BP-1/Cadherin-11 phenotype, the Rag1 knock-out model was chosen. Here, cells can't recombine their genome for T/B cell receptor thus also not being able to progress to mature stages. IL-7 expression by stroma, however, is not impaired.

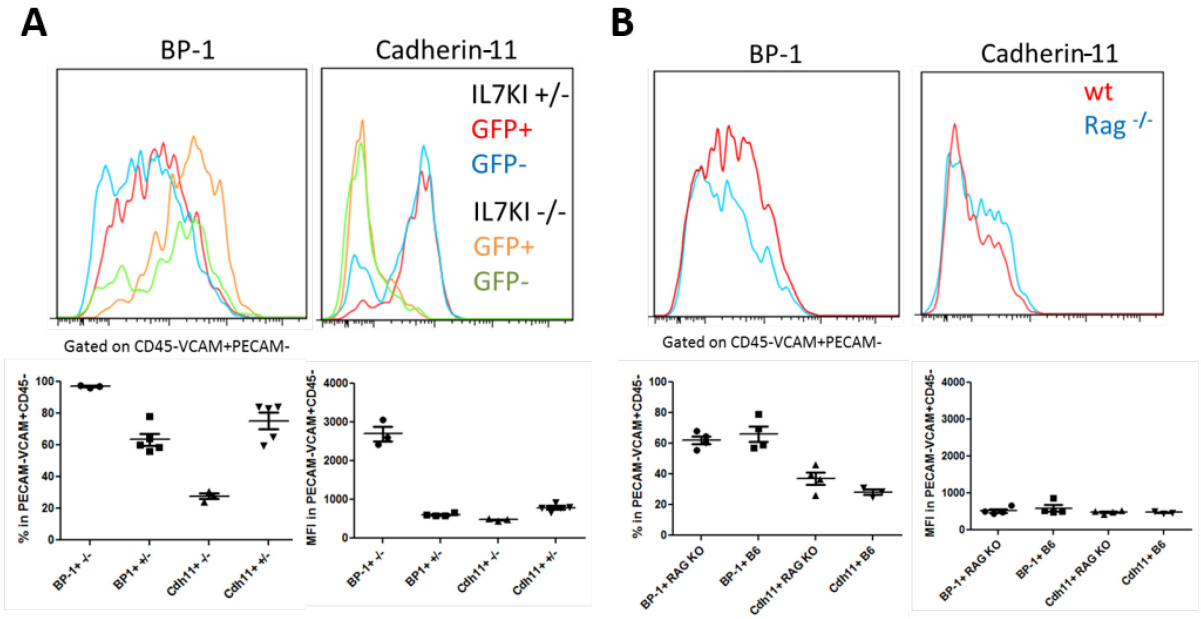

Fig. 3.2.5.2: Differential stromal expression of BP-1 and Cadherin-11 in the presence or absence of IL-7 is not due to lack of mature lymphocytes A: Histograms for BP-1 and Cadherin-11 on VCAM-1$^+$PECAM-1$^-$ cells separated by haplotype and GFP expression **B:** Histograms for BP-1 or Cadherin-11 expression on VCAM-1$^+$PECAM-1$^-$ cells of wild-type C57Bl/6 (red line) or RagKO mice (blue line); samples were gated for viable, non-lineage singlets; below: percentage and MFI of BP-1$^+$ and Cadherin-11$^+$ cells, respectively; data are mean ± SEM

Surprisingly, when comparing BP-1 and Cadherin-11 levels between Rag KO and wild-type C57Bl/6 mice no difference can be observed anymore.

3.2.6 IL-7 expression shows features of monoallelic expression

Although surface marker expression differences were marginal (apart from BP-1/Cadherin-11) between hetero- and homozygous IL7KI genotypes, a striking phenotype with respect to GFP expression could be seen in general. Surprisingly and contrary to assumptions the homozygous mice didn't just have higher mean fluorescence intensity due to more GFP being produced per cell but they also had a higher overall percentage of GFP$^+$ cells (see *Fig 3.2.6*).

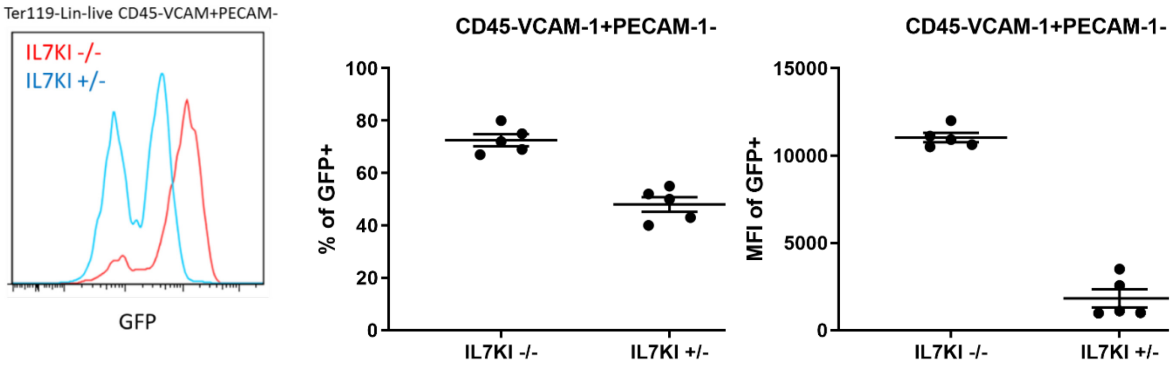

Fig. 3.2.6: GFP levels in IL7KI mice display features of monoallelic expression Left: Representative histogram for GFP expression levels in IL7KI heterozygous (blue) or homozygous mice (red); samples were gated for viable, non-lineage singlets and indicated population; Center/Right: percentage and MFI of GFP in hetero- & homozygous mice; data are mean ± SEM

This is remarkable as a potential explanation might be a generally monoallelic expression pattern wherein IL-7$^+$ stromal cells would only or at least partially transcribe only one allele thus resulting in higher GFP$^+$ percentage due to stochastics.

3.2.7 Substantial stroma marker *in situ* overlap revealed by confocal microscopy & semi-automated image analysis

While the confocal microscopy offers the unlimited advantage to get a hold on the *in situ* lifestyle of stromal cells and their nearest neighbors and ECM environment, it comes with the disadvantage that at the current state of the art, a staining panel is limited to five fluorescent channels at a time and quantification of these pictures doesn't allow for assessing potential marker overlap apart from subjective judgment. There are technological approaches that are aiming to change that in the future by repetitively staining and bleaching one and the same histology slide to allow for advanced multiplexing.

As the amount of data from these stainings will only increase, we devised a macro in ImageJ that enables us to visually plot two stainings vs each other, mark the overlapping area and quantify these single and overlapping areas in a plot similar to a Venn diagram. In addition, the black area inside the frame underneath depicts the total image area not occupied by the stainings so that one also gets an idea of absolute frequencies and not just those relative between two markers.

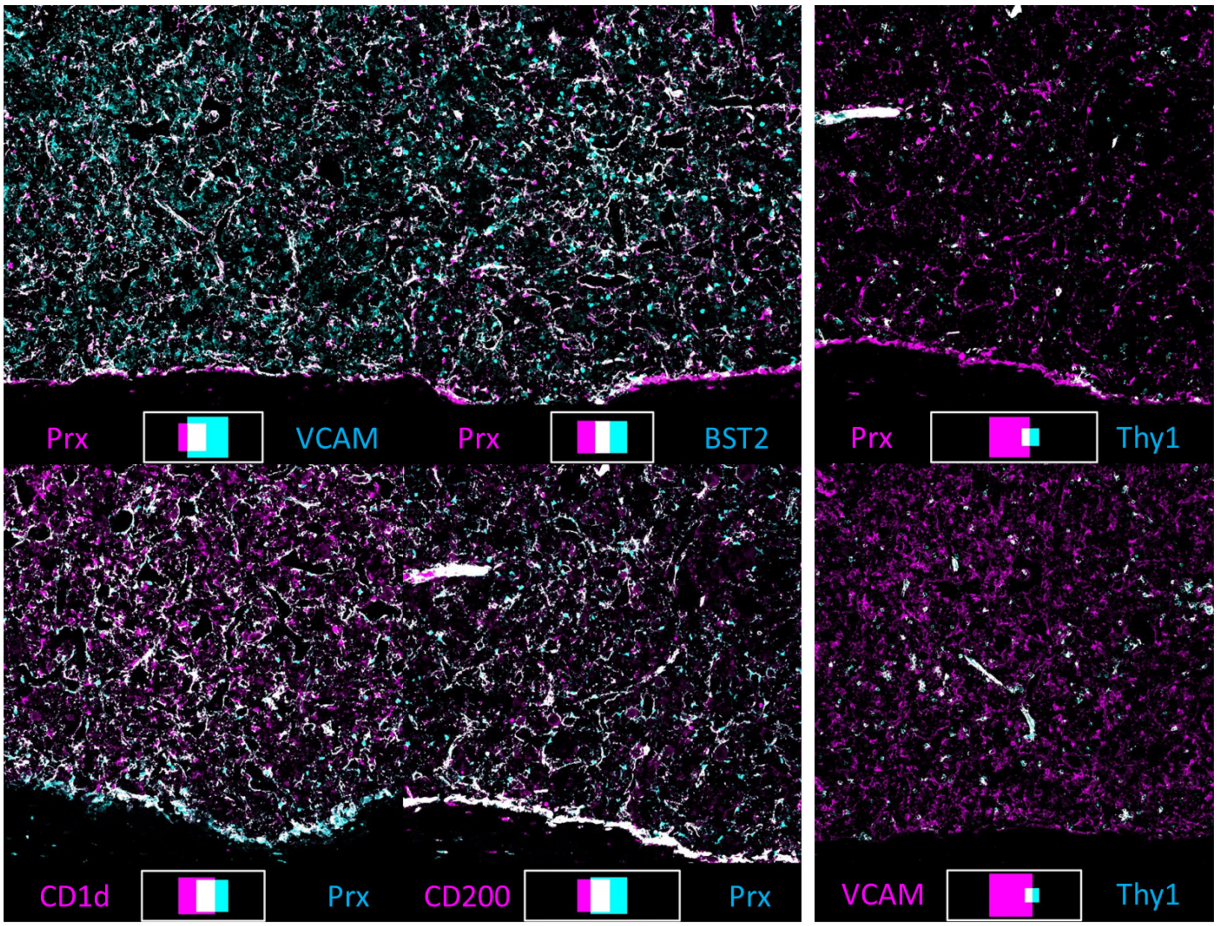

Fig. 3.2.7.1: Visual quantification of histological overlap of Prx, VCAM-1, CD1d, CD200 and Thy1 in murine bone marrow False-color images of 6 µm slides of longitudinally cut PrxRFP femora. Tissues were incubated with antibodies against RFP, VCAM-1, CD1d, CD200; antigens are depicted in corresponding colors beneath the image; area inside the frame corresponds to all pixels in the image with the contribution of each channel in corresponding color and overlap in white; image width: 708 µm

As expected, all stromal markers show a substantial overlap with Prx that serves as the gold standard for mesenchymal (hence stromal) identity. It is also not surprising that each of the stromal markers display a non-overlapping signal with Prx. The reasons are two-fold. Firstly, most of them are known to be expressed on hematopoietic cells as well which is especially obvious in the case of BST2 (on B cell progenitors) and VCAM-1 (abundant on granulocytes). Secondly, one has to keep in mind that the RFP is a cytosolic protein while the stromal marker stain is a surface stain. This is best accounted for by the fact that the soma of stromal cells can only be visualized by Prx but is never visible by surface marker stains.

While the algorithm can serve as a tool to quickly identify overlapping population from high throughput imaging, another approach can also be seen in the counterstain of Prx, VCAM-1 and Thy1, respectively. Thy1 also known as CD90 is described as a pan-T lymphocyte marker. When compared to the overlap of stromal markers, not only is it apparent that the signal contributes less to total pixels but also the overlap with Prx is considerably less. Although it appears as roughly 50% in both comparisons on can

see from the elongated overlap signals that these are mainly due to vessels where both Prx and Thy1 are expressed in adjacent pericytes and endothelial cells, respectively.

An even more advanced approach was developed in coordination with Wimasis to address questions beyond mere overlap and colocalization in fluorescent confocal stainings. One such example is depicted in *Fig. 3.2.7.2* with its original images (A) and corresponding segmentation (B).

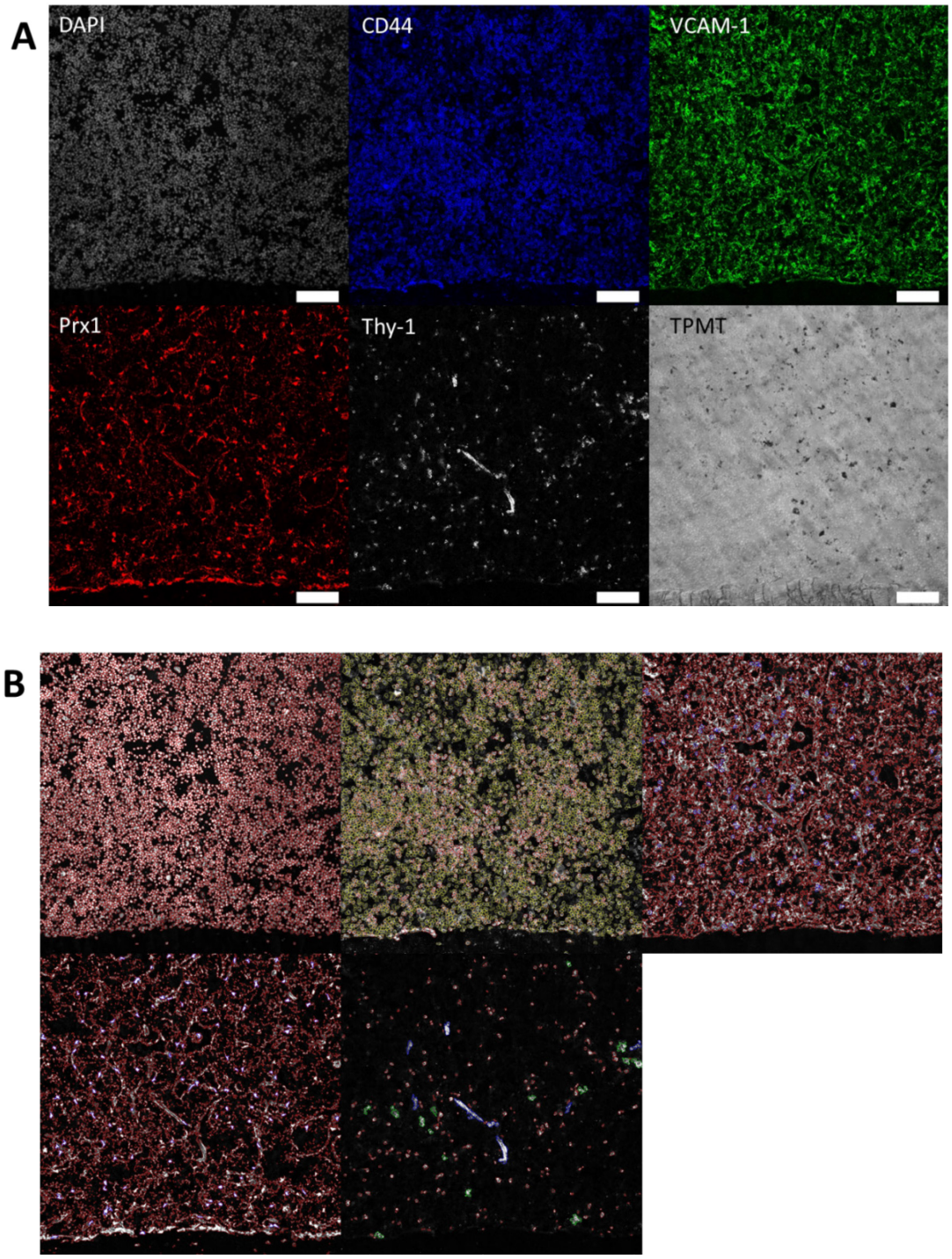

Fig. 3.2.7.2: Advanced image segmentation of hematopoietic and stromal stainings for colocalization and overlap analysis Slides of longitudinally cut femora from PrxRFP reporter mice were incubated with antibodies against RFP (anti-RFP-Biotin/anti-rabbit-A555, red), CD44 (A488, blue), VCAM-1 (A647, green), Thy1 (A594,

white), nuclear staining (DAPI, grey) and transmissive channel for morphology (TPMT on 405 laser), respectively; **A:** stainings in separate channels; **B:** Image segmentation of corresponding images in A provided by Wimasys was run and recognized structures marked in varying colors (DAPI: nuclei encircled in red, CD44: surface expression intensity was graded from green to red, VCAM-1: irregular shapes from stroma were marked in red while circular granulocytes are marked blue, Prx: irregular signal was marked in red while stromal soma are marked blue, Thy1: circular single cells were marked in red while clusters are denoted green and elongated macro-structures blue); Scale: 50 µm

3.2.8 Stromal markers are conserved between organs but depict less compartmentalization in bone marrow

While the overall focus of this thesis was to determine the heterogeneity within the bone marrow stromal cells, the original interest in the stromal cells stemmed from the fact that the bone marrow seemed to be a preferential homing and maintenance place for memory lymphocyte precursors. Hence the very initial question that arose was what differentiated a splenic stromal cell from that of the BM.

A staining panel that elucidates these differences is one including Annexin A2, gas6 (growth arrest specific 6) and CD1d. Gas6 (fold change: 19) was originally identified as differentially higher expressed genes in the bulk stroma vs endothelium analysis (see *section 3.1.4*).

Annexin A2 is considered a pleiotropin[106] but has been implicated in the stromal HSC niche due to its interactions with CXCL12[107, 108]. gas6 was similarly correlated to improved HSC maintenance by *in vitro* data and was found to exert its effect via cell-cell interactions[109] through its cognate receptors Axl/MerTK/Sky[110]. Both gas6 and ANXA2 have been linked to the homing and dormancy induction of prostate cancer cells to the bone marrow[111].

The staining in the bone marrow visualizes the vast reticular stroma pattern that is typically observed in the bone marrow with extensive overlap of the three markers on stromal processes (*Fig. 3.2.8*, top).

The same staining in the spleen does reveal that the markers are expressed there as well but whereas Annexin A2 is almost as equally spread as in the BM, gas6$^+$ and CD1d$^+$ stroma cells are localized in a very distinctive pattern (*Fig. 3.2.8*, bottom). This becomes especially visible with regards to the follicles (*Fig. 3.2.8*, dashed circle). While gas6 is exclusively expressed outside of them, CD1d is enriched on cells of the follicle boundaries.

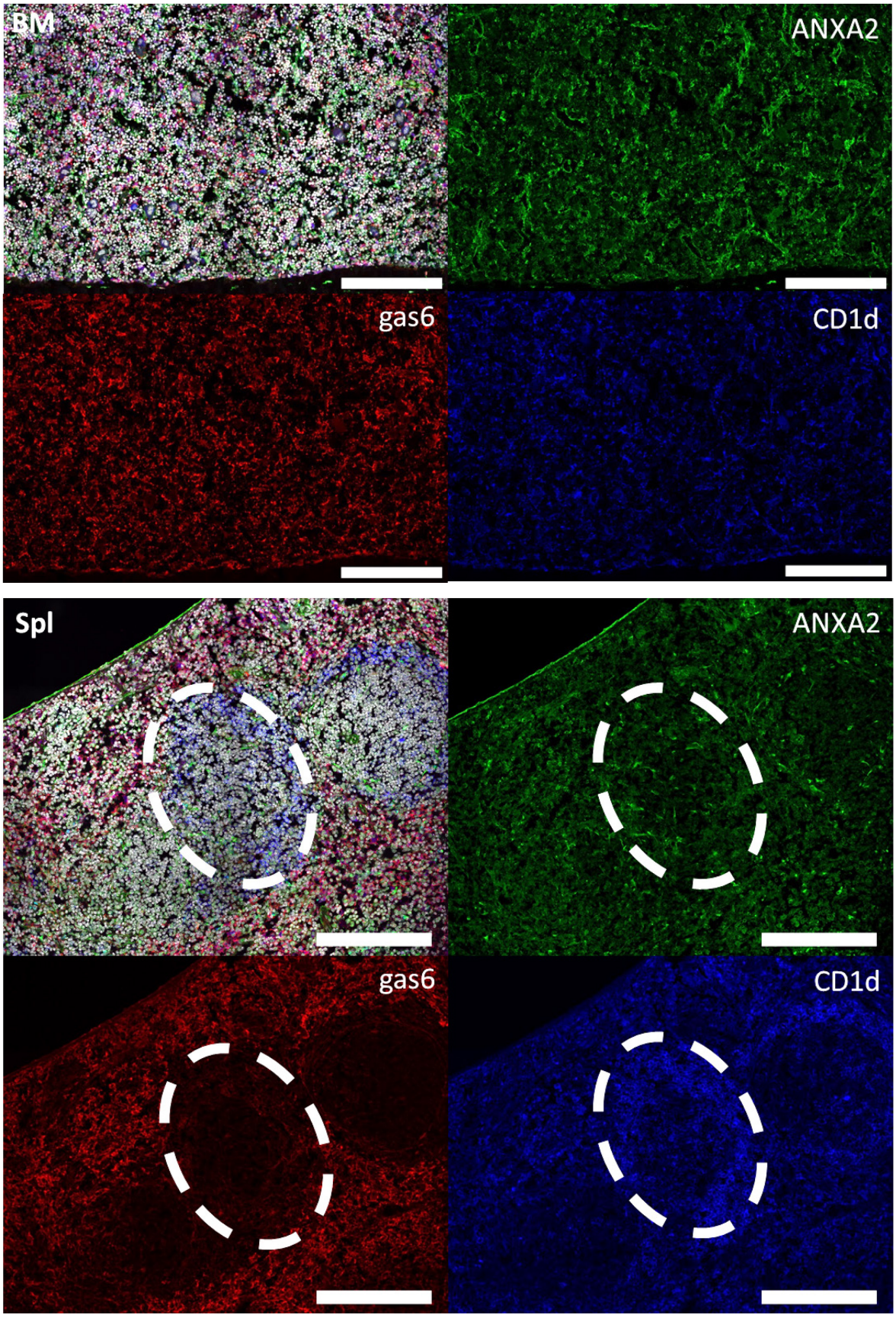

Figure 3.2.8: Organ-specific compartmentalization of stromal cells in murine bone marrow and spleen Slides of longitudinally cut femora and spleen from B6 mice were incubated with DAPI (white) and antibodies against Annexin A2 (ANXA2, green), gas6 (red) and CD1d (blue); dashed circles indicate a follicle; scale: 200µm

3.2.9 A potential role for Annexin A2/ Annexin A2 receptor for the homing and interaction of stromal cells and HSCs and B cell lineage

Since Annexin A2 was identified to be expressed on stromal cells and colocalize with a handful of markers (including CD1d and gas6) and was implicated in the literature to play a role in the homing and attachment of prostate cancer cells in the bone marrow we hypothesized that it might also play a role in physiological interactions of lymphocytes and stroma cells. Initially assuming that its cognate receptor ANXA2R might be expressed on memory T lymphocytes ($Thy1^{+}CD44^{hi}$) did not appear to be the case (*Fig 3.2.9.1A*). It even seemed not to be expressed on the T lymphocyte lineage at all.

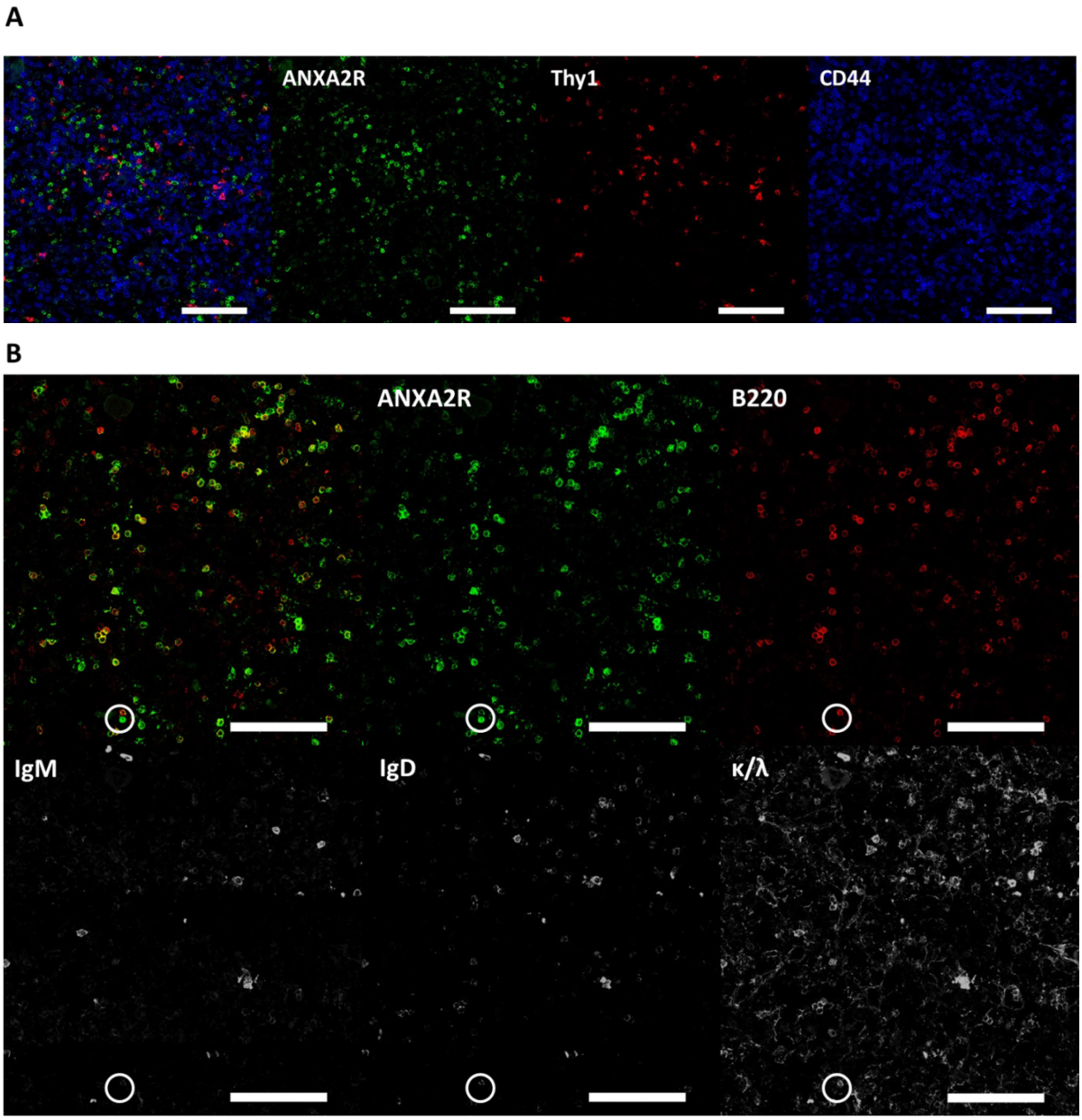

Fig. 3.2.9.1: Annexin A2 receptor is almost exclusively expressed in the B lymphocyte lineage in the bone marrow **A:** Histological slides from C57Bl/6 femora were incubated with antibodies against Annexin A2 receptor (ANXA2R, green), Thy1 (red), CD44 (blue); **B:** ANXA2R (green), B220 (red), IgM/IgD/κ + λ light chain (light grey); white circle: rare phenotype of $B220^{-}ANXA2R^{hi}(IgM^{-}IgD^{-}\kappa/\lambda^{-})$ cell; scale: 50 µm

Notably, when counterstained with B220 to account for all of the B cell lineage except for plasma cells, it showed a high degree of colocalization with B220 (*Fig. 3.2.9.1B*, composite image).

While no further analysis was pursued to narrow down the hematopoietic populations wherein ANXA2R is expressed, it should be noted that an infrequent phenotype that could be found in those stainings was that of a $B220^{-}ANXA2R^{hi}(IgM^{-}IgD^{-}\kappa/\lambda^{-})$ cell (*Fig. 3.2.9.1B*, white circle). Whether this could be HSCs or downstream, uncommitted lymphopoietic progenitors remains to be elucidated.

Another recurring observation (n=4) was that $ANXA2R^{+}$ cells that seemed to be in the vasculature of the bone marrow as outlined by lining CD1d stroma pericytes and lack of adjacent DAPI signal always had a substantially higher surface signal ($ANXA2R^{hi}$, *Fig. 3.2.9.2*, red circles) compared to those within the tissue (*Fig. 3.2.9.2*, green circles).

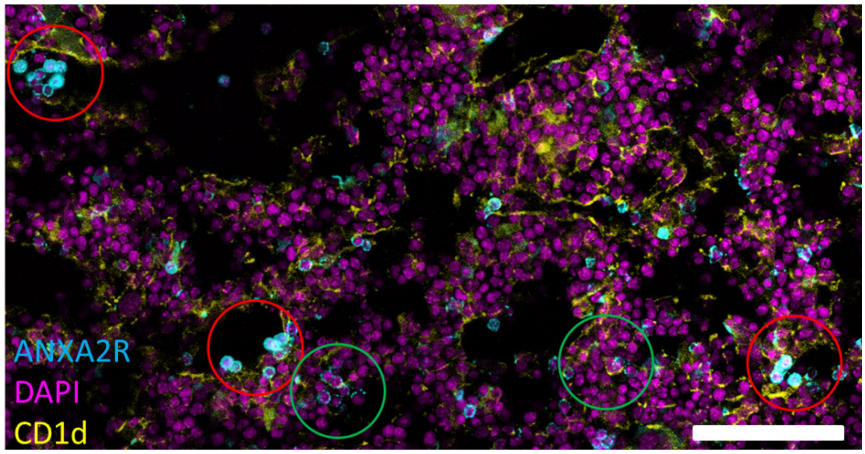

Fig. 3.2.9.2: ANXA2R surface expression is higher in vasculature-borne cells than tissue-resident in murine bone marrow Representative slide of longitudinally-cut femora from C57Bl/6 mice (n=4) were stained for ANXA2R (light blue), CD1d (yellow) or nuclei (DAPI/purple); red circles: ANXA2Rhi cells in vasculature; green circles: tissue-resident ANXA2Rlo cells; Scale: 50 µm

4 Discussion

The initial goal of this study was to enhance the isolation outcome of VCAM-1$^+$ stromal cells from fresh murine bone marrow. An early increase could be achieved by digesting flushed bone marrow and empty bone independently from each other and combine suspensions afterwards as implied in earlier work of our group[112]. Due to their strong adherence to plastic surfaces formerly used for cultivation purposes the cytoskeleton was targeted in a subsequent attempt to recover stromal cells after digestion. The F-actin destabilizing agents Cytochalasin D and Latrunculin B could increase the recovery furthermore. The enhanced protocol enabled broader investigation of stromal cells in general. On the one hand, stromal cells were sorted to elucidate their gene expression profile and to gain insight into their commitment to several subsets. On the other hand, and partially in conjunction with gene expression data, several surface markers known to be expressed on stromal subsets were stained in flow cytometry and histology.

Histological quantification of Prx reporter mice long bones showed that stromal reticular cells make up about 2% of total nucleated bone marrow cells. It needs to be noted that this estimate is rather a conservative one as it doesn't account for bone lining osteoblasts and might have missed some pericytes as those don't have the "extended/dendritic" phenotype that is typical for PrxRFP$^+$ cell bodies of reticular stroma. Nevertheless, initial isolations fell even short of this goal by yielding less than 0.1% of CD45$^-$VCAM-1$^+$ cells among all live Ter119$^-$ cells analyzed. The major hindrance during isolation seems to be their embedding in extracellular matrix which was subsequently addressed by a set of digestion enzymes with which cells are incubated. Their susceptibility to mechanical stress might as well be attributed to the rupture of gap junctions that are expressed on mesenchymal stroma[113].

Stromal cell-derived stem cells are plastic-adherent as shown by Friedenstein and coworkers[11]. This issue was addressed by adding F-Actin destabilizing agents Cytochalasin D and Latrunculin B. Surprisingly, as they both have different working principles of disturbing cytoskeleton integrity, their influence on stromal yield is different. In other words, depriving the cell of G-Actin (Latrunculin B) seems to be more efficient than capping already formed filaments (Cytochalasin D). This is even more notable as serum-sensitive effects of Latrunculin B cannot be excluded in these experiments. It can also be ruled out that this effect is simply contributed to toxicity of the compounds as percentages in viability didn't differ drastically.

However, both reagents were chosen for digestion as they were shown to synergize[97]. The reversibility of their action leads to the question whether cells might be lost due to adherence again after subsequent washing steps. This issue hasn't been addressed in the scope of this thesis but is worth pursuing although reversing kinetics for stromal cells are not known so far. It could however be observed that bone marrow that was objected to a digestion including inhibitors took longer to

reattach on plastic surfaces after plating compared to BM digested without additives (data not shown). Hence, the effect seems to be prolonged enough not to cause cell to attach again after switch to LatB-free buffers.

In the next step, cell suspensions obtained with the improved protocol were stained for VCAM-1 and Lineage markers to be sorted via FACS™ in the following step. Although sufficiently pure fractions of VCAM-1^{+}PECAM-1$^{+/-}$ could be sorted, the recovery was far from complete. As a result of the rare phenotype of stromal cells in full bone marrow, sorting of BM from one mouse took approximately 1.5h. Hence, some cells might have died due to sedimentation in the sample tube or sorting tubes. System-wide cooling of the tubing system was applied to address this issue. In addition, the sample tube was resuspended repeatedly to avoid density-related effects. Applying isopycnic sample medium can be another suitable approach to further prevent sedimentation from happening in the future. Initial tests with Percoll-adjusted sorting buffer proved feasible and didn't influence the fluidics or stainings despite increased viscosity of the suspension (data not shown).

Besides optimization of the isolation protocol the biological question of this thesis ultimately was to shed light on the heterogeneity of murine bone marrow stromal cells. Due to the diversity of stromal markers published and used for proper isolation, this thesis first focused on VCAM-1. VCAM-1 has been described to be expressed on stromal cells supporting the maintenance of several long-lived or memory lymphocyte subsets *in vivo*[114]. Interestingly, the stromal subsets do seem to overlap but not always co-express survival-promoting signals (IL-7 or CXCL12 for CD4 memory or long-lived plasma cells, respectively). With the memory niche concept possibly applicable for other lymphocyte subsets as well, bone marrow stroma becomes an interesting target to characterize.

It has been well recognized in recent years that the infection route of antigen matters resulting in tissue-resident, topological memory lymphocytes as a first line of defense for future encounters[115, 116]. However, our group established that memory lymphocytes for systemic antigens like Measles, Mumps and Rubella (MMR) seem to favor homing to the bone marrow over other organs for the resting phase[117]. Although some argued that the bone marrow is a calm environment that favors resting populations, the very fact of thriving hematopoiesis and even acute phase *in situ* proliferation[118] has called that assumption into question. Still, it seemed rather inefficient that especially plasmablasts and long-lived plasma cells should relocate from spleen to BM. Hence, our initial question to be addressed with the stromal cells was that of genotypic and phenotypic differences between common splenic stromal cells[119] (FRC, MRC, FDC) and BMSCs. Unfortunately, at the time of generating these transcriptomes, we were not able to obtain sufficient numbers of VCAM-1^{+}PECAM-1^{-} stromal cells from the spleen. In an attempt to at least understand BMSC signature gene expression, micro arrays were prepared from stromal PECAM-1^{-} versus endothelial PECAM-1^{+} cell RNA. As both originate from

different germ layers (mesoderm versus endoderm, respectively), a vastly differential expression was expected beforehand and verified in the results.

Genes that are significantly higher expressed in PECAM-1$^-$ cells seem to confirm their multi-lineage differentiation potential. Being able to give rise to adipocytes, osteoblasts and chondrocytes among other mesenchymal cell types led to the term "mesenchymal stem cells" for their *in vitro* cultured counterparts[120]. Of the lineage commitments observed for stromal cells in the bone marrow the most prominent relate to osteoblasts and adipocytes. Of importance is the transitional phenotype of some genes differentially expressed. Adiponectin or Follistatin-like 1 for example are expressed at highest on pre-adipocytes both decreasing rapidly upon further commitment[54, 121]. As for the early adipocyte markers one needs to take into account that cytoskeleton-destabilizing agents such as Latrunculin B and Cytochalasin D might have side effects on the cell physiology. As the shape of the cell changes adipogenesis is likely to be triggered[53, 54, 122]. This was further corroborated by the enriched gene sets of cell adherence. Although the time scale for the morphological transition is not reached within the experiment, transcriptional upregulation of genes could be triggered this early. Such side-effects could be prevented by addition of Actinomycin D in all buffers to block *de novo* transcription in future studies. That could additionally rule out effects by exposing the cells to normoxia when they have been shown to reside in a tissue of pronounced hypoxia[41, 123, 124, 125].

The early committing phenotype might also be true for the osteogenic lineage that is reportedly induced by FGFR2[126, 127] and/or Cadherin-11 together with N-Cadherin[128, 129]. Nevertheless, the osteoblast phenotype is more pronounced with maturity markers such as bone sialoprotein, osteopontin or osteoglycin being highly expressed. However, this observation could only be confirmed for *runx2* on the master transcription factor (TF) level but not for the hallmark TF *osterix*. A common concern of course is that of exclusivity of markers for certain lineages as Cadherin-11 could be shown in this thesis to be expressed on reticular stroma as well and lineage-tracing with Osterix shows Osterix$^+$ cells contribute to reticular stroma perinatally[130]. So it is not surprising to find genes known to inhibit osteoblast maturation (e.g. SFRP4[131, 132], IGFBP5[133, 134]) are expressed at the same time. This finding - together with the presence of adipocyte, myoblast/vSMC and chondroblast markers - hints at a highly versatile and multi-lineage stromal cell pool.

In line with the introductory outline of VCAM-1$^+$ stromal cells as bone marrow niche supporting cells, one can confirm the expression of the corresponding survival signals CXCL12, kit ligand and IL-7. The latter was found to be expressed at low yet differential levels matching earlier reports[135].

Considering the successful isolation of bulk stromal cells, another issue to be addressed is their survival *ex vivo*. An important step is the sorting procedure at the FACS™ devices. There, cells pass nozzle with

a diameter classically being around 60 µm. Given the sheer stress susceptibility even in the cytoskeleton-disturbed condition, switching to higher nozzle diameters such as 100 µm proved beneficial for viability after sort (data not shown). The disadvantage in such a scenario however was that as sorting speed is limited to 2000 events per second, a pre-enrichment becomes necessary further impacting on the recovery of stromal cells.

Despite having isolated seemingly pure populations of $GFP^{+/-}$ stromal cells from the IL7KI reporter mice, we were surprised to find a majority of leukocyte contaminating genes in the differentially regulated genes. The fact that the Il7 transcript seemed to be present in both sorted fractions made us additionally cautious. Different possibility arose from the finding. Firstly, we could have had GFP^+ cells contaminate our GFP^- population. This was considered unlikely as the clustering still worked perfectly and the sort check didn't show any GFP^+ cells in the GFP^- fraction. It is possible that GFP^+ cells lose their GFP fluorescence signal during sorting due to quenching or proteasomal degradation. Secondly, monoallelic expression is possible and would serve as an explanation how a cell could transcribe from the wild-type allele without having to use the knock-in allele. We could see that this is also implied by the GFP expression shift between IL7KI heterozygous and homozygous animals. In case of a biallelic expression pattern, only the GFP mean fluorescence intensity should change as more GFP would be expressed per cell. What we do find is that not only the MFI changes but the percentage of GFP^+ stromal cells as well. This rather fits to the assumption that at least some cells express IL-7 monoallelically which in the homozygous setting would manifest in higher probability of cells choosing the knock-in allele as observed. Further work needs to be done to further explore that claim but preliminary follow-up experiments seem to confirm the monoallelic expression that is well known by other members of the IL-2 family[136] (Richard Addo, unpublished data).

The last and equally likely scenario to explain the Il7 signal in the GFP^- sorted transcriptomes is the probe design. From what we could determine, Affymetrix designed their probes in Exon 3 or 4 of the Il7 gene which are both unaltered in the wild-type (WT) and knock-in as the insert is directly after Exon 1 (see *Fig. 3.2.1A* and unpublished data, Richard Addo). Regardless of the shortcomings of those transcriptomes it was surprising to see Prx (Prrx1) as the only HPCDA-ranked gene to be higher expressed in the GFP^+ sorted fraction. Assuming that the signal was not just diluted out by leukocyte genes in $GFP^-PECAM\text{-}1^-$ cells, it would mean that the mesenchymal master transcription factor is higher expressed in the presumed $IL\text{-}7^+$ cells. As the Prx reporter mice are designed as a terminal excision by cre/loxP system, we were lacking information up to what point in differentiation stromal cells expressed Prx. Recent data implicating it in the inhibition of adipogenic[137] and osteogenic[138] pathways, respectively, argue for a role of Prx as a correlate of stromal "stemness". It is thus intriguing to see the expression of the survival niche factor IL-7 in such an "undifferentiated" population in the bone

marrow. It will be interesting to see whether Prx will be equally enriched in another sorted stromal subpopulation and since the advent of single-cell sequencing especially on a per-cell level.

When looking at the results of the surface marker screening kit of heterozygous vs homozygous IL7KI mice, one has to keep in mind that by definition and history, the CD nomenclature is biased towards hematopoietic cells. The manufacturer even markets it for that purpose. Hence, although we did get an unbiased screening approach, it was to be expected that not all included markers would be expressed. Furthermore, the results of the screening need some cautious consideration: Since we pooled bone marrow stroma from 3 different mice each and compared two different haplotypes, the total cell number for each stain was rather low (approx. 10^5 cells). Still, the studied stromal and endothelial populations could clearly be considered statistically as such at a minimum of 200 cells/ $CD45^-VCAM\text{-}1^+$ gate. It cannot be ruled out that the individual mice contributed different populations to the analysis. However, assessing variation between individuals was not the scope of the approach. In addition, the manufacturer provided the antibodies as is in a pre-titrated fashion that might be suitable for hematopoietic suspensions but not for rare cells like stroma. We adjusted the gates for FMO and isotype controls to account for that fact. Finally, as the staining was carried out in a multiplexed fashion, the staining procedure was harmonized for all antibodies, i.e. performed on ice. For some markers, especially chemokine receptors (CCRs, CXCRs), manufacturers and scientists recommend staining at 37 °C to increase brightness. Hence, signal intensity with these antibodies might underestimate expression or introduce unwanted background.

Despite these confounding variables, it was still rather surprising to find the expression of more than 25 surface markers, some of which have never been linked to stromal cells or non-hematopoietic cells in general. The functional implications depend on the corresponding molecule.

CD1d is a non-classical member of the MHC family and present lipids to NKT and to a lesser degree γδ T cells, especially by professional antigen-presenting cells[139, 140]. This partially reignites the discussion in the field whether stroma cells are *bona fide* antigen-presenting cells. It is known that while they don't express MHC II in steady state, they quickly upregulate its expression after exposure to IFNγ[141, 142, 143]. This conditional expression appears to be beneficial in a systemic inflammation setting but CD1d in contrast is expressed constitutively. NKT cells don't require peripheral CD1d/TCR triggering for their survival but rely on IL-15 and IL-7 for homeostasis[144] much akin to CD8 memory lymphocytes[145] (where the concept is debated[146], however). Whether that entails competition for a similar niche would be in interesting question. Another member of the CD1 family, CD201/EPCR, was found to expressed on stroma cells as well. While it's not involved in lipid presentation to NKT cells it has been shown to play a role in HSC maintenance[147], further adding to the list of well-described interactions there.

A prominent category of markers expressed encompasses cell-ECM and cell-cell adhesion. Most notably, we find substantial expression of the Integrin subunits αM (CD11b), αV (CD51) and α1/β1 (CD49a/CD29) of the VLA1 heterodimer. The latter is important for binding to a variety of Collagens and Laminin. Integrin αV is a common subunit of dimers binding to vitronectin, fibronectin or – like CD105/Endoglin – to TGFβ1-3. Integrin αM was shown to bind ICAM-1 (CD54) which is also produced by a subpopulation of stroma identifying a possible new stroma-stroma interaction. Like ICAM-1, CD44 is a very broadly expressed glycoprotein capable of binding fibrin, fibrinogen, and hyaluronan. Other targets exclusive to CD44 include Osteopontin and Selectins due to its diverse glycosylation patterns. One such glycoform (HCELL) could even be shown to confer bone marrow homing to transferred MSCs[148] much like the CXCL12/CXCR4 axis. CRTAM, which only shows a very minor population in the GFP^- stroma cells was only recently described to be essential for epithelial and fibroblast cell adhesion[149]. Another member is CEACAM-1 (CD66a) that has been implicated in homophilic and heterophilic interactions on epithelia, endothelia and leukocytes. Surprisingly, it also shows interaction with Annexin A2. CD24 is a cell adhesion molecule that has been studied as a differentiation molecule in lymphocytes. Its absence predisposes mice to developing EAE[150] implicating a protective role in autoimmune diseases. Sialoadhesin/Siglec-1 (CD169) binds to sialic acid modifications of surface proteins on other cells. It has been implicated on macrophages in the retention of HSCs in the niche[151].

CD9 and CD63 are members of the tetraspanin family and found on a variety of cells, including nerve, muscle cells and many cells of hematopoietic origin. CD9 is found to participate in forming a large molecular cell complex with other member proteins (e.g. MHC class II, CD19, CD5 etc.) and could be beneficial in case of antiviral responses. CD9 was reported to be expressed on human progenitor MSCs recently[152]. CD63 is enriched on exosomes and MSC exosomes proved immunosuppressive in an uveitis model[153].

CD73 is known as an ecto-enzyme converting AMP to Adenosine and Phosphate. While it has been shown to be expressed in MSCs and osteoblasts[154, 155] it is more classically known from lymphocyte differentiation[156] and recently (cancer) metabolism and immune suppression[157, 158]. Since stromal cells and their *in vitro* MSC descendants in particular are known to be immunosuppressive in physiological, transplantation and co-transfer settings[159], the expression of other markers than CD73 known to be involved in these pathways (CD24[150], CD200[160], CD55[161], TIGIT[162], Tim-1[163], CD160[164, 165], PD-1[166], Galectin-9[167, 168, 169]) broadly recapitulates this phenotype on the population level in our hands although we cannot yet comment on the overlap between these populations. What is remarkable though, is that almost all of these inhibitory markers (with the exception of CD73) show a mutually exclusive expression with regards to IL-7/GFP. This distinction seems to be plausible for the dual biological roles stromal cells have been implicated in. On one hand, they favor survival and expansion of hematopoietic

precursors, especially of HSCs and the B cell lineage. On the other hand, they are known to suppress proliferation & induce quiescence. Separating these factors – receptors & ligands alike – spatiotemporally might keep that delicate balance in check in the bone marrow. Of those inhibitory markers expressed by a subset of GFP^- stromal cells CD55/DAF stands out as it is entirely absent on homozygous IL7KI reporter BMSCs. There is no mechanistic link that readily explains this in the literature. But since DAF was shown to modulate T cell activation by quenching T- and antigen-presenting cell (APC)-derived C3a/C5a[170, 171], it might simply be the absence of mature T lymphocytes that abrogates the upregulation of DAF in the first place.

This, however did not seem to be the case for BP-1 and Cadherin-11 that showed differential expression between IL7KI haplotypes. Because we assumed that if the absence of mature lymphocytes is the cause for the different expression modes, a RagKO mouse where recombination/maturation of lymphocytes is similarly stalled should recapitulate the observed phenotype. Although that wasn't the case, an additional puzzling aspect was that although the WT vs RagKO staining of Cadherin-11 was similar, the percentage (20-30% Cadherin-11^+) rather reflected the level previously observed in the $IL7KI^{-/-}$ mice in contrast to the expected heterozygous percentage (70-80% Cadherin-11^+). It remains to be shown how Cadherin-11 might be linked to IL-7 expression in the IL7KI setting. While BP-1 did show the same expression between heterozygous IL7KI, wild-type and RagKO it has both higher percentage and MFI in the homozygous BM stroma. In B cell progenitors it is upregulated after IL-7/IL-7R signaling[172], hence would be expected to display a lower MFI in the homozygous haplotype. We did however not find any CD127/IL-7Rα chain expression in the surface marker screening on either haplotype (data not shown). Thus - assuming that absence of CD127 is not due to recent engagement with IL-7 and/or due to its absence - what is upstream of BP-1 in stroma is unknown. It should also be noted that the mice for the surface marker screening were considerably younger compared to those from which different BP-1 and Cadherin-11 expression could be observed. Considering how flexible contributions to the stromal niche are perinatally already[130], it cannot be ruled out that a phenotypic change takes place within stroma during aging in line with clear-cut differences of MSCs isolated from young vs old donors/mice[173].

CMKLR1 (ChemR23) was previously described as an adipokine receptor in white adipose tissue together with its ligand Chemerin[174]. Chemerin in turn is negatively regulated by Prx[137]. When expressed on macrophages, mainly on M1 polarized cells, it can be detrimental for inflammation or beneficial depending on the ligands it binds[175]. Since it can heteromerize with CXCR4 and CCR7, negatively regulating their affinity for their respective ligands[176], it is likely that the small subset of 15% will have an altered signaling threshold with regards to these pathways.

Despite a strict lineage (CD45, Ly6G/C, B220) exclusion gating strategy we were surprised to find a variety of markers expressed on stroma cell subsets that are commonly attributed to plasmacytoid dendritic cells (pDCs) in the mouse. That is true for BST2/PDCA-1, PDC-TREM, CCR7 [177]. The broad myeloid Integrin αX (CD11c) was not expressed on stroma (data not shown). As counterstains are not available one can only speculate whether these markers are co-expressed on the same cells. Taken together with the fast Interferon response of BMSCs and their ability to upregulate MHC II in infection settings[178] an antiviral functional overlap between these two distinctive lineages would be intriguing, surely. The question that remains is why chemotactic receptors like CCR7 or CCR3 (rather known from eosinophils) are expressed on immobile stroma cells at all – assuming the staining is accurate. A possible hint comes from the fact that BMSCs have been implicated as motile osteoprogenitors that provide a local pool of osteoblast precursors in bone fracture settings[179] in line with their description as stem cells. Since an early fracture is usually accompanied with tissue-damaged induced inflammation, this set of markers might lead to adequate homing of BMSCs to sites of injury.

Similar to CXCL12 and IL-7, APRIL/CD256 was identified as a survival factor for plasmablasts in the bone marrow[180]. Apart from this function it appears to be dispensable for the immune system as APRIL-deficient mice develop normally[181]. While its secretion is usually attributed to macrophages in a 2D *in vitro* enrichment of adherent primary BMSCs[180], these experiments might miss the *in situ* expression of APRIL on stromal cells due to loss of ECM/3D structure & physiology akin to CXCL12[182, 183]. While only present on 10-15% of *ex vivo* stromal cells, their presumably equal distribution and embedding in the marrow makes them better niche-providing cells than mobile macrophages.

Ultimately, the surface marker screening could reconfirm some stromal populations described in literature (CD106/VCAM-1, CD140a/b, CD73, CD200/OX2, CD54/ICAM etc.) but also identified new stroma populations hitherto unknown on BM stroma (CD1d, CD55) and some to be downriched in absence of IL-7 as achieved via IL7KI haplotype. It needs to be noted, however, that these findings are far superior to previous studies in elucidating the *in situ* phenotype in that we obtained the data for freshly isolated *ex vivo* BM stromal cells. Previous studies have looked at whole-population lysates and subsequent mass spectrometry[152] or analyzed plated and/or passaged MSCs (hence depleted of non-adherent cells) and have since changed their proliferation status, surface marker phenotype and size[184].

Since the advent of the "-omics" approaches in life sciences the amount of data that is generated with each experiment continuously surpasses what is manually feasible to analyze. That was also true in two scenarios during this thesis and the reason for cooperation with DRFZ bioinformaticians Pawel Durek and Ralf Köhler, respectively.

Together with Pawel Durek, we addressed the question how our knowledge of the niche constituents – namely stroma and memory lymphocytes – could be exploited from their corresponding transcriptome data that was readily available in our group. In short, we were looking for possible overlooked ligand-receptor interactions from either cell type. This approach of course has limitations. As we have to rely on curated lists of ligand/receptor interactions, orphan candidates might be missed. Additionally, the algorithm still needs some refinement with regards to homotypic interactions and cis/trans-binding, i.e. that the same molecule on one cell type shouldn't be detected as a pair and possible ligand/receptor pairs on one cell shouldn't be counted as an interaction with the other cell, respectively.

We faced a similar hurdle during overlap analysis of histological stroma marker stain. Histology in contrast to flow cytometry suffers from a subjective bias when it comes to adjusting the image acquisition settings and subsequent comparison of image files from different stains. That is not to say that histology is not set in accordance to an isotype control and to maximum brightness distribution. But especially in stromal histology, we are interested in the filigree processes of the reticular stroma which at times requires oversaturating part of the image to get the full scope. Hence, we devised an ImageJ macro with Ralf Köhler from the Hauser lab that can automatically extract channels from **.lsm* files convert it to binary by thresholding, due a pixel-by-pixel overlap analysis and present the results as false-color histology as well as Venn diagram overview. This way, manual input is minimized to the settings on the microscope. The macro is limited by the fact that it quantifies entirely on a per-pixel basis. The problem is apparent when looking at the stainings of VCAM-1, BST2 and Thy1, respectively. All three have stromal contributions but show a considerable expression on hematopoietic cells as well. Any overlap/colocalization macro will hence severely over-/underestimate the actual stromal marker overlap with these markers. Here, segmentation – i.e. the trained recognition of particular image/cell features will need to be implemented in the future. This was actively started with Ralf Köhler and in corporation with Wimasis, Munich.

An exemplary staining with subsequent segmentation can be seen in *Fig. 3.2.7.2*. Besides DAPI, it includes Prx and VCAM-1 to assess stroma cells and Thy1 and CD44 for T cells in general and the $Thy1^{+}CD44^{hi}$ pool in particular (*Fig. 3.2.7A*). The segmentation of each channel is provided in *Fig. S4B*. In addition to simply detecting and counting nuclei (DAPI), the segmentation can rank CD44 signal per cell by expression level as we are most interested in $CD44^{hi}$ cells of a memory phenotype. Also, it can separate the hematopoietic (VCAM-1, blue) from stromal (VCAM-1, red outline) VCAM-1 signal. Equally, it is possible to assess Prx cell bodies (Prx, blue outline) and processes (Prx, red outline) separately. Thy1 is even more complex. As previously mentioned, Thy1 is expressed on T cells as well as arteriolar cells. The elongated arteriolar contribution (Thy1, blue outline) can thus be separated.

Additionally, a recurring observation with Thy1 in the BM is that both singular cells (Thy1, red outline) as well as clusters can be found (Thy1, green outline). This advanced segmentation could thus answer questions in the direction of whether memory T cells are more frequently found in clusters and whether those rather colocalize with Prx cell bodies or processes which can help in formulating better hypotheses to test in subsequent experiments.

We hope that it will be useful beyond this thesis as a potential use case was already considered the in-house multi-epitope ligand cartography (MELC) that the Hauser lab developed. There, histology can be multiplexed by repetitive staining and bleaching of antibody conjugates.

Annexin A2 and its cognate receptor ANXA2R seem to be a promising new ligand-receptor interaction between stroma cells and the B cell lineage according to the preliminary findings of this thesis. While it remains to be clarified which B cell progenitors do express the receptor and whether it plays a role in the homing and maturation of these cells. It would come as no surprise to see that lymphocytes make use of the same mechanisms as has been described for prostate cancer cells in the bone marrow. There, the triad of CXCL12/CXCR4, ANXA2/ANXA2R and gas6/Axl is supposed to keep the cells in place[107, 108, 185]. Keeping in mind how important CXCL12 is for B cell progenitors this insinuates a viable hypothesis to test. As for the differential surface expression levels that coincide with their localization in or out of the vasculature, one could equally argue with a crosstalk of CXCL12 and ANXA2. CXCL12 is most highly expressed in the bone marrow stroma while its concentration drops sharply in the vasculature. What the functional relevance of this mechanism is remains elusive.

The two paramount aims of this project were, firstly, to understand what makes the bone marrow a preferential homing organ for memory lymphocytes compared to spleen or liver and secondly what separates a benign/protective bone marrow niche from a malign/autoreactive one in an autoimmune disorder and whether there even is such a difference as the cells could be qualitatively the same except for constant antigen exposure. While this thesis cannot comment on the latter question, initial comparative stainings of some stromal markers (CD1d, ANXA2, gas6) have shown that the key to understand stroma biology might lie in their (co-)localization and compartmentalization in the respective tissue. It is true that splenic follicles have no counterpart in BM and memory niches lack considerable representation in spleen, making these presumptions fallible. What the depicted stainings show, however, is that in general majority of markers are present in each of the tissues but not necessarily on the same cells. The bone marrow seems to be unique in that regard as the broad overlap or at least proximity of markers seems to be decisive in enabling niches. As a considerable reservoir of memory B cells in the human spleen[186] and tissue-resident memory lymphocytes show, one should not be too stringent in calling the bone marrow the sole harbor of immunological memory. It helps to keep in mind that the HSC niche, for example, adaptively relocalizes in mammals several

times during embryonal development (yolk sac --> aorta-gonad-mesonephros --> fetal liver --> bone marrow medulla) and can even be extramedullary in physiological and pathological conditions [187]. This implies that no “one/restricted” cell type is capable of providing niches but comparison between those stages might elucidate minimal requirements.

5 Outlook

Having identified a variety of markers – among them many previously attributed to hematopoietic cells – on stromal cells, this thesis contributed to the deeper understanding of how the stromal network of the murine bone marrow might shape the hematopoietic environment and development in the crowded microcosm that is the bone.

It remains to be seen how many of the markers identified herein show an equal expression pattern on human stromal cells, however. Empirically, it can be expected that not all will be expressed and if they are, their functions might differ. A good example for that is CD105 in the human where it is considered a *bona fide* stroma marker while in the mouse it almost exclusively localizes to endothelial cells.

Another aspect this work could not address due to time constraints is the kinetics and overall time course of the marker expression with age and for example in an acute immune reaction. Considering the well-established fact that HSCs get a myeloid skew the older the mice get and that this process has been linked to stromal contributions[188] such as an intrinsic adipogenic skew[189, 190] , it would only be logical to assume that the overall stroma expression pattern varies and feeds back to environmental cues. In the concept of "inflamm-aging"[191], aging and an acute immune reaction can even be linked to one another. That genomic damage seems to contribute to a similar degree becomes obvious from how well irradiation damage recapitulates the "old bone marrow" phenotype[192]. Future fate-mapping studies will likely contribute to our understanding in this regard.

Rather omitted from this thesis but seemingly a consequence of the architecture of the bone marrow is the finding it might be fundamentally wrong to treat stroma cells as multiple isolated cells sitting together in a shared ECM entirely detached from the rest of the body. It should not be forgotten that stroma cells are tightly inter-connected by gap junctions, i.e. Connexins which are even implicated in modulating CXCL12 secretion[193, 194, 195]. Now if you consider a network that can easily exchange second messengers and hormones[196] the question arises why you would even expect clearly separated populations in the first place as all cells are eventually subjected to differing degrees of the same stimulus in this setting. It is true that the clear-cut sub-population view is reinforced by observed bimodal distributions from flow cytometry but it wouldn't be too surprising to learn that stromal marker expression is in a spatiotemporal flux in response to external stimuli from ECM and lymphocytes as the IL-7 data imply. Notably, the concept of stable maintenance in a niche is irreconcilable with a flexible stromal network so it remains to be shown how these interactions that can last a lifetime in humans (as evidenced by stable childhood disease antibody titers[197, 198]) survive the turbulent surroundings of the bone marrow.

6 Supplement

Tab. S1: Overview of RNA quantity and quality from FAC sorted sub-populations of bulk stroma cells

Sample	# mice	CD45$^-$VCAM-1$^+$PECAM-1$^-$		CD45$^-$VCAM-1$^+$PECAM-1$^+$	
		RNA content [ng]	RIN	RNA content [ng]	RIN
1	3	135	8.0	89	8.2
2a	2	63	8.6	80	7.8
2b	3	56		61	
3a	2	69	5.0	68	8.9
3b	2	63		60	

Tab. S2: Significantly differentially expressed genes in VCAM-1$^+$PECAM-1$^-$ BMSCs in comparison with VCAM-1$^+$PECAM-1$^+$ control cells ranked by HPCDA score Table denotes gene (first column) and corresponding originating tissue (second column); multiple appearances of a gene indicate more than one positive probe-set; Sig S: mean corrected signal intensity of PECAM$^-$ chip samples; Sig E: mean corrected signal intensity of PECAM$^+$ chip samples; FC: fold change; data is derived from 3 different experiments

Gene	Expression site	Sig S	Sig E	FC	HPCDA-Score
MMP13	stroma[199, 200], osteoblasts[201]	17306	32	**1626**	**51989**
C1 inhibitor	fibroblasts[202], megakaryocytes/ platelets[203]	22611	113	**182**	**44026**
Insulin-like growth factor binding protein 5	myoblasts[204]	30651	195	**134**	**35428**
Adiponectin	pre-adipocyte[205]	16823	86	**172**	**31284**
Ceruloplasmin	stroma[206]	12869	38	**243**	**25294**
CXCL12	stroma[207]	32047	430	**82**	**22717**
Cytochrome P450, 1B1	adipocytes[208, 209], vSMCs[210]	12672	30	**528**	**22468**
Bone sialoprotein	osteoblasts	16796	82	**188**	**20817**
Tenascin C	osteoblasts[211]	14317	74	**203**	**18964**
Osteopontin	osteoblasts, osteoclasts	24785	160	**164**	**16416**
Procollagen I, α2	osteoblasts[212]	22068	187	**128**	**15724**
PTPRD	pre-B cells[213]	5900	38	**135**	**13234**
Cadherin-11	osteoblasts, fibroblasts[214]	9550	25	**357**	**13061**
Endoglyx-1	endothelial[100]	125	11052	**-279**	**12651**
Seprase	stroma[215, 216]	4728	47	**86**	**12055**
Zac1	chondrocytes[217], myocytes[218]	6288	18	**607**	**11939**
Follistatin-like 1	pre-adipocytes[121], myocytes[219, 220]	8649	65	**112**	**11845**
Endothelial cell-specific molecule 1	adipocytes[102]	8557	48	**193**	**11798**
PTPRD	pre-B cells[213]	4355	34	**141**	**11403**
Glycoprotein m6a	neurons[221]	134	10273	**-194**	**11389**
PDGFRb	stroma[88], pericytes[222]	8909	47	**218**	**11203**
Glia-derived nexin	skeletal muscle[223]	17607	164	**93**	**11042**
kit ligand	stroma, osteoblasts[224]	11822	72	**161**	**10807**
Procollagen VI, α1	muscle, adipocytes, chondrocytes	4851	25	**211**	**10624**
Kininogen 1	-	4754	8	**719**	**10614**
Leptin receptor	stroma[225]	8267	248	**30**	**10543**
Rap guanine nucleotide exchange factor (GEF) 5	-	97	1798	**-16**	**10426**
Osteoglycin	osteoblasts, vSMCs	4927	12	**516**	**9754**
Glutathione peroxidase 3	plasma, adipose tissue	9428	109	**86**	**9547**
ACAM	adipocytes[103]	1740	75	**23**	**9466**
Mannose receptor, C type 1	myoblasts[226]	152	10963	**-108**	**9069**

Fatty acid binding protein 4, adipocyte	endothelium[227]	1363	35686	**-35**	**8988**
Stabilin 2	endothelium[228, 229]	212	11911	**-101**	**8773**
Anthrax toxin receptor 1	endothelium[230]	5488	194	**27**	**8689**
FAT tumor suppressor homolog 1	vSMCs[231]	4048	42	**99**	**8600**
VEGFC	macrophages[232], osteoclasts	4295	48	**86**	**8513**
Secreted frizzled-related protein 4	-	9536	80	**118**	**8495**
Lysyl oxidase-like 1	vSMCs[233]	4694	9	**481**	**8482**
Aquaporin 1	erythrocytes, endothelium[234]	173	6266	**-33**	**8271**

Tab. S3: Overview of RNA quantity and quality from FAC sorted sub-populations of IL7KI GFP$^{+/-}$ stromal cells

Sample	# mice	CD45$^-$VCAM-1$^+$GFP$^+$PECAM-1$^-$		CD45$^-$VCAM-1$^+$GFP$^-$PECAM-1$^-$	
		RNA content [ng]	RIN	RNA content [ng]	RIN
1	1	107	N/A	139	N/A
2	2	212	N/A	163	N/A
3	1	146	N/A	119	N/A

Tab. S4: Significantly differentially expressed genes in GFP$^+$PECAM-1$^-$ BMSCs in comparison with GFP$^-$PECAM-1$^-$ control cells ranked by HPCDA score Table denotes gene (names) and corresponding originating); multiple appearances of a gene indicate more than one positive probe set; Sig S: mean corrected signal intensity of GFP+PECAM$^-$ chip samples; Sig E: mean corrected signal intensity of GFP-PECAM$^-$ chip samples; FC: fold change; data is derived from 3 different experiments

Gene	Gene name	Sig S	Sig E	FC	HPCDA-Score
S100a8	S100 calcium binding protein A8 (calgranulin A)	24021.3	49716.6	-2.30	**2630.49**
S100a9	S100 calcium binding protein A9 (calgranulin B)	17320.4	43289.5	-2.38	**2619.40**
Ngp	neutrophilic granule protein	4852.5	21509	-4.00	**2487.33**
Camp	cathelicidin antimicrobial peptide	4329.1	21460.6	-5.10	**2390.79**
Mpo	myeloperoxidase	2264.9	13826.5	-8.00	**1749.58**
Lyz1	lysozyme	823.9	10737	-4.29	**1605.34**
Hmgn2	high mobility group nucleosomal binding domain 2	3571.1	14169.5	-4.21	**1512.86**
Chi3l3	chitinase 3-like 3	2547.05	15175.4	-5.76	**1504.80**
Srgn	serglycin	1869.25	9582.5	-5.46	**1468.63**
Lyz1	lysozyme	3119.8	14065.3	-4.29	**1427.03**
Prtn3	proteinase 3	1526.25	9309.2	-8.00	**1420.97**
Rps6	ribosomal protein S6	7522.3	11809.6	-1.62	**1367.89**
Rps6	ribosomal protein S6	6279.85	10238.5	-1.62	**1323.26**
Chi3l3 /Chi3l4	chitinase 3-like 3 / 4	1729.9	12314.2	-6.73	**1269.91**
Lyz2	lysozyme	2580.2	11881.5	-4.84	**1250.85**
Tacc3	transforming, acidic coiled-coil containing protein 3	51.35	192.3	-3.86	**1077.03**
Tkt	transketolase	2981.05	10548.5	-3.93	**1069.43**
Ly6c1 /Ly6c2	lymphocyte antigen 6 complex, locus C1/2	1129.25	6650.15	-6.61	**963.09**
Lair1	leukocyte-associated Ig-like receptor 1	54.5	248.75	-3.61	**959.99**
Ear1	eosinophil-associated, ribonuclease A family, member 1	510.9	4012.25	-24.25	**953.26**
Ube2c	ubiquitin-conjugating enzyme E2C	195.15	601.4	-3.48	**942.50**
Arhgap30	Rho GTPase activating protein 30	48.95	302.75	-5.66	**929.91**

Ctsg	cathepsin G	810.9	5078.65	-7.73	**925.39**
Prrx1	paired related homeobox 1	462.7	218.35	2.18	**919.41**
Svip	Small VCP Interacting Protein	70.15	244.4	-3.67	**878.96**
Ear2	eosinophil-associated, ribonuclease A family, member 2	377.05	2868.9	-11.92	**835.05**
Dmp1	dentin matrix protein 1	92.55	291.75	-3.08	**831.47**
Ear1	eosinophil-associated, ribonuclease A family, member 1	106.55	1572.05	-8.57	**828.58**
Mpeg1	macrophage expressed gene 1	208.3	500.55	-2.69	**822.47**
Far2	male sterility domain containing 1	42.9	180.3	-3.93	**819.38**
Lcn2	lipocalin 2	1593.15	7781.5	-4.59	**818.72**
Serpinb1a	serine (or cysteine) peptidase inhibitor, clade B, member 1a	475.25	4989.25	-9.51	**813.24**
Tuba4a	tubulin, alpha 4A	917.75	5890.2	-6.96	**813.04**
Arhgap9	Rho GTPase activating protein 9	83.55	230.15	-2.42	**804.46**
Prg2	proteoglycan 2, bone marrow	204.45	2188.5	-15.19	**797.19**
Gpx1	glutathione peroxidase 1	2294.95	6813.3	-3.08	**792.71**
Nup210	nucleoporin 210	73.05	336.8	-4.21	**775.32**
Tcfec	transcription factor EC	8.2	262.1	-34.90	**768.19**
Hmgb2	high mobility group box 2	980.25	4753.65	-4.59	**760.10**
Strbp	spermatid perinuclear RNA binding protein	32.05	117.4	-2.73	**754.51**
Ms4a3	membrane-spanning 4-domains, subfamily A, member 3	457.45	3460.75	-9.85	**753.59**
Dkc1	dyskeratosis congenita 1, dyskerin homolog (human)	246.3	514.7	-1.93	**748.23**
B4galnt1	beta-1,4-N-acetyl-galactosaminyl transferase 1	6.5	115	-8.00	**736.02**
Hnrnpf	heterogeneous nuclear ribonucleoprotein F	1249.15	2306.9	-1.65	**731.70**
Msra	methionine sulfoxide reductase A	221.75	385.1	-2.14	**729.93**

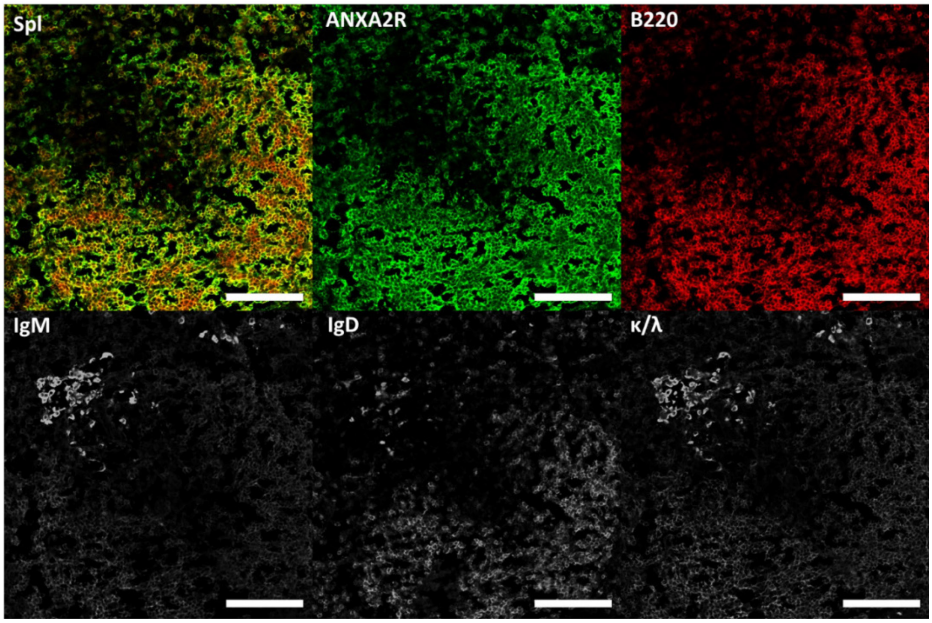

Fig. S1: Annexin A2 receptor is expressed in the B lymphocyte lineage in the spleen **A:** Histological slides from C57Bl/6 femora were incubated with antibodies against Annexin A2 receptor (ANXA2R, green), Thy1 (red), CD44

(blue); **B:** ANXA2R (green), B220 (red), IgM/IgD/kappa + lambda light chain (light grey); white circle: rare phenotype of B220-ANXA2Rhi(IgM-IgD-k/l-) cell; scale: 50 µm

7 References

1. Travlos, G.S. Normal structure, function, and histology of the bone marrow. *Toxicologic pathology* **34**, 548-565 (2006).

2. Munka, V.G., A. *Folia morphologica*, 13 edn, 1965.

3. Beutler, E. & Williams, W.J. *Williams hematology 6. Ed*. McGraw-Hill, Medical Publishing Division, 2001.

4. Katayama, Y. *et al.* Signals from the sympathetic nervous system regulate hematopoietic stem cell egress from bone marrow. *Cell* **124**, 407-421 (2006).

5. Mendez-Ferrer, S., Battista, M. & Frenette, P.S. Cooperation of beta(2)- and beta(3)-adrenergic receptors in hematopoietic progenitor cell mobilization. *Annals of the New York Academy of Sciences* **1192**, 139-144 (2010).

6. Mendez-Ferrer, S., Lucas, D., Battista, M. & Frenette, P.S. Haematopoietic stem cell release is regulated by circadian oscillations. *Nature* **452**, 442-447 (2008).

7. Dorshkind, K., Green, L., Godwin, A. & Fletcher, W.H. Connexin-43-type gap junctions mediate communication between bone marrow stromal cells. *Blood* **82**, 38-45 (1993).

8. Schajnovitz, A. *et al.* CXCL12 secretion by bone marrow stromal cells is dependent on cell contact and mediated by connexin-43 and connexin-45 gap junctions. *Nature immunology* **12**, 391-398 (2011).

9. Le Blanc, K. & Mougiakakos, D. Multipotent mesenchymal stromal cells and the innate immune system. *Nature reviews. Immunology* **12**, 383-396 (2012).

10. Dominici, M. *et al.* Minimal criteria for defining multipotent mesenchymal stromal cells. The International Society for Cellular Therapy position statement. *Cytotherapy* **8**, 315-317 (2006).

11. Friedenstein, A.J., Petrakova, K.V., Kurolesova, A.I. & Frolova, G.P. Heterotopic of bone marrow. Analysis of precursor cells for osteogenic and hematopoietic tissues. *Transplantation* **6**, 230-247 (1968).

12. Friedenstein, A.J., Chailakhjan, R.K. & Lalykina, K.S. The development of fibroblast colonies in monolayer cultures of guinea-pig bone marrow and spleen cells. *Cell and tissue kinetics* **3**, 393-403 (1970).

13. Sanchez-Ramos, J. *et al.* Adult bone marrow stromal cells differentiate into neural cells in vitro. *Experimental neurology* **164**, 247-256 (2000).

14. Morikawa, S. *et al.* Prospective identification, isolation, and systemic transplantation of multipotent mesenchymal stem cells in murine bone marrow. *The Journal of experimental medicine* **206**, 2483-2496 (2009).

15. Mendez-Ferrer, S. *et al.* Mesenchymal and haematopoietic stem cells form a unique bone marrow niche. *Nature* **466**, 829-834 (2010).

16. Dahlstrand, J., Zimmerman, L.B., McKay, R.D. & Lendahl, U. Characterization of the human nestin gene reveals a close evolutionary relationship to neurofilaments. *Journal of cell science* **103 (Pt 2)**, 589-597 (1992).

17. Isern, J. *et al.* The neural crest is a source of mesenchymal stem cells with specialized hematopoietic stem cell niche function. *eLife* **3**, 1-28 (2014).

18. Xie, L., Zeng, X., Hu, J. & Chen, Q. Characterization of Nestin, a Selective Marker for Bone Marrow Derived Mesenchymal Stem Cells. *Stem Cells Int* **2015**, 762098 (2015).

19. Park, D. *et al.* Endogenous bone marrow MSCs are dynamic, fate-restricted participants in bone maintenance and regeneration. *Cell stem cell* **10**, 259-272 (2012).

20. Tokoyoda, K., Egawa, T., Sugiyama, T., Choi, B.I. & Nagasawa, T. Cellular niches controlling B lymphocyte behavior within bone marrow during development. *Immunity* **20**, 707-718 (2004).

21. Sugiyama, T., Kohara, H., Noda, M. & Nagasawa, T. Maintenance of the hematopoietic stem cell pool by CXCL12-CXCR4 chemokine signaling in bone marrow stromal cell niches. *Immunity* **25**, 977-988 (2006).

22. Omatsu, Y. *et al.* The essential functions of adipo-osteogenic progenitors as the hematopoietic stem and progenitor cell niche. *Immunity* **33**, 387-399 (2010).

23. Nagasawa, T. *et al.* Defects of B-cell lymphopoiesis and bone-marrow myelopoiesis in mice lacking the CXC chemokine PBSF/SDF-1. *Nature* **382**, 635-638 (1996).

24. Nagasawa, T. Microenvironmental niches in the bone marrow required for B-cell development. *Nature reviews. Immunology* **6**, 107-116 (2006).

25. Hara, T. *et al.* Identification of IL-7-producing cells in primary and secondary lymphoid organs using IL-7-GFP knock-in mice. *Journal of immunology* **189**, 1577-1584 (2012).

26. Cordeiro Gomes, A. *et al.* Hematopoietic Stem Cell Niches Produce Lineage-Instructive Signals to Control Multipotent Progenitor Differentiation. *Immunity*, 1-13 (2016).

27. Peschon, J.J. *et al.* Early lymphocyte expansion is severely impaired in interleukin 7 receptor-deficient mice. *The Journal of experimental medicine* **180**, 1955-1960 (1994).

28. von Freeden-Jeffry, U. *et al.* Lymphopenia in interleukin (IL)-7 gene-deleted mice identifies IL-7 as a nonredundant cytokine. *The Journal of experimental medicine* **181**, 1519-1526 (1995).

29. Acar, M. *et al.* Deep imaging of bone marrow shows non-dividing stem cells are mainly perisinusoidal. *Nature* (2015).

30. Zhou, Bo O., Yue, R., Murphy, Malea M., Peyer, J.G. & Morrison, Sean J. Leptin-Receptor-Expressing Mesenchymal Stromal Cells Represent the Main Source of Bone Formed by Adult Bone Marrow. *Cell stem cell* **15**, 154-168 (2014).

31. Weiss, L. The hematopoietic microenvironment of the bone marrow: an ultrastructural study of the stroma in rats. *The Anatomical record* **186**, 161-184 (1976).

32. Blocki, A. *et al.* Not All MSCs Can Act as Pericytes: Functional In Vitro Assays to Distinguish Pericytes from Other Mesenchymal Stem Cells in Angiogenesis. *Stem cells and development* **22**, 2347-2355 (2013).

33. Corselli, M., Chen, C.-W., Crisan, M., Lazzari, L. & Péault, B. Perivascular Ancestors of Adult Multipotent Stem Cells. *Arteriosclerosis, Thrombosis, and Vascular Biology* **30**, 1104-1109 (2010).

34. Crisan, M. *et al.* A Perivascular Origin for Mesenchymal Stem Cells in Multiple Human Organs. *Cell stem cell* **3**, 301-313 (2008).

35. Chen, W.C.W. *et al.* Cellular Kinetics of Perivascular MSC Precursors. *Stem Cells International* **2013**, 1-18 (2013).

36. Corselli, M., Chen, C.W., Crisan, M., Lazzari, L. & Péault, B. Perivascular ancestors of adult multipotent stem cells. *Arteriosclerosis, Thrombosis, and Vascular Biology* **30**, 1104-1109 (2010).

37. Cooke, Vesselina G. *et al.* Pericyte Depletion Results in Hypoxia-Associated Epithelial-to-Mesenchymal Transition and Metastasis Mediated by Met Signaling Pathway. *Cancer Cell* **21**, 66-81 (2012).

38. Asada, N. *et al.* Differential cytokine contributions of perivascular haematopoietic stem cell niches. *Nat Cell Biol* **19**, 214-223 (2017).

39. Kunisaki, Y. *et al.* Arteriolar niches maintain haematopoietic stem cell quiescence. *Nature* **502**, 637-643 (2013).

40. Cox, G. *et al.* High abundance of CD271(+) multipotential stromal cells (MSCs) in intramedullary cavities of long bones. *Bone* **50**, 510-517 (2012).

41. Tormin, A. *et al.* CD146 expression on primary nonhematopoietic bone marrow stem cells is correlated with in situ localization. *Blood* **117**, 5067-5077 (2011).

42. Mauch, T.J. & Schoenwolf, G.C. Developmental Biology. Sixth Edition. By Scott F. Gilbert. *American Journal of Medical Genetics* **99**, 170-171 (2001).

43. Komori, T. Regulation of osteoblast differentiation by Runx2. *Advances in experimental medicine and biology* **658**, 43-49 (2010).

44. Nakashima, K. *et al.* The novel zinc finger-containing transcription factor osterix is required for osteoblast differentiation and bone formation. *Cell* **108**, 17-29 (2002).

45. Baron, R. & Kneissel, M. WNT signaling in bone homeostasis and disease: from human mutations to treatments. *Nature medicine* **19**, 179-192 (2013).

46. Ehninger, A. & Trumpp, A. The bone marrow stem cell niche grows up: mesenchymal stem cells and macrophages move in. *The Journal of experimental medicine* **208**, 421-428 (2011).

47. Visnjic, D. *et al.* Hematopoiesis is severely altered in mice with an induced osteoblast deficiency. *Blood* **103**, 3258-3264 (2004).

48. Zhang, J. *et al.* Identification of the haematopoietic stem cell niche and control of the niche size. *Nature* **425**, 836-841 (2003).

49. Calvi, L.M. *et al.* Osteoblastic cells regulate the haematopoietic stem cell niche. *Nature* **425**, 841-846 (2003).

50. Lymperi, S. *et al.* Strontium can increase some osteoblasts without increasing hematopoietic stem cells. *Blood* **111**, 1173-1181 (2008).

51. Zhu, J. *et al.* Osteoblasts support B-lymphocyte commitment and differentiation from hematopoietic stem cells. *Blood* **109**, 3706-3712 (2007).

52. Jilka, R.L. The Relevance of Mouse Models for Investigating Age-Related Bone Loss in Humans. *The journals of gerontology. Series A, Biological sciences and medical sciences* (2013).

53. Rubin, C.T. *et al.* Adipogenesis is inhibited by brief, daily exposure to high-frequency, extremely low-magnitude mechanical signals. *Proceedings of the National Academy of Sciences of the United States of America* **104**, 17879-17884 (2007).

54. Sen, B. *et al.* Mechanical strain inhibits adipogenesis in mesenchymal stem cells by stimulating a durable beta-catenin signal. *Endocrinology* **149**, 6065-6075 (2008).

55. Spiegelman, B.M. PPAR-gamma: adipogenic regulator and thiazolidinedione receptor. *Diabetes* **47**, 507-514 (1998).

56. Naveiras, O. *et al.* Bone-marrow adipocytes as negative regulators of the haematopoietic microenvironment. *Nature* **460**, 259-263 (2009).

57. Worthylake, R.A. & Burridge, K. Leukocyte transendothelial migration: orchestrating the underlying molecular machinery. *Current opinion in cell biology* **13**, 569-577 (2001).

58. Kopp, H.G., Hooper, A.T., Avecilla, S.T. & Rafii, S. Functional heterogeneity of the bone marrow vascular niche. *Annals of the New York Academy of Sciences* **1176**, 47-54 (2009).

59. Trumpp, A., Essers, M. & Wilson, A. Awakening dormant haematopoietic stem cells. *Nature reviews. Immunology* **10**, 201-209 (2010).

60. Osawa, M., Hanada, K., Hamada, H. & Nakauchi, H. Long-term lymphohematopoietic reconstitution by a single CD34-low/negative hematopoietic stem cell. *Science* **273**, 242-245 (1996).

61. Orkin, S.H. & Zon, L.I. Hematopoiesis: an evolving paradigm for stem cell biology. *Cell* **132**, 631-644 (2008).

62. Maruyama, M., Lam, K.P. & Rajewsky, K. Memory B-cell persistence is independent of persisting immunizing antigen. *Nature* **407**, 636-642 (2000).

63. Polic, B., Kunkel, D., Scheffold, A. & Rajewsky, K. How alpha beta T cells deal with induced TCR alpha ablation. *Proceedings of the National Academy of Sciences of the United States of America* **98**, 8744-8749 (2001).

64. Schluns, K.S. & Lefrancois, L. Cytokine control of memory T-cell development and survival. *Nature reviews. Immunology* **3**, 269-279 (2003).

65. Kondrack, R.M. *et al.* Interleukin 7 regulates the survival and generation of memory CD4 cells. *The Journal of experimental medicine* **198**, 1797-1806 (2003).

66. Lodolce, J.P. *et al.* IL-15 receptor maintains lymphoid homeostasis by supporting lymphocyte homing and proliferation. *Immunity* **9**, 669-676 (1998).

67. Kennedy, M.K. *et al.* Reversible defects in natural killer and memory CD8 T cell lineages in interleukin 15-deficient mice. *The Journal of experimental medicine* **191**, 771-780 (2000).

68. Becker, T.C. *et al.* Interleukin 15 is required for proliferative renewal of virus-specific memory CD8 T cells. *The Journal of experimental medicine* **195**, 1541-1548 (2002).

69. Tan, J.T. *et al.* Interleukin (IL)-15 and IL-7 jointly regulate homeostatic proliferation of memory phenotype CD8+ cells but are not required for memory phenotype CD4+ cells. *The Journal of experimental medicine* **195**, 1523-1532 (2002).

70. Benson, M.J. *et al.* Cutting edge: the dependence of plasma cells and independence of memory B cells on BAFF and APRIL. *Journal of immunology* **180**, 3655-3659 (2008).

71. Hauser, A.E. *et al.* Chemotactic responsiveness toward ligands for CXCR3 and CXCR4 is regulated on plasma blasts during the time course of a memory immune response. *Journal of immunology* **169**, 1277-1282 (2002).

72. Cassese, G. *et al.* Plasma cell survival is mediated by synergistic effects of cytokines and adhesion-dependent signals. *Journal of immunology* **171**, 1684-1690 (2003).

73. Murphy, K.P., Travers, P., Walport, M. & Janeway, C. *Janeway's immunobiology*. Garland Science, 2008.

74. Tokoyoda, K. *et al.* Professional memory CD4+ T lymphocytes preferentially reside and rest in the bone marrow. *Immunity* **30**, 721-730 (2009).

75. Holt, R.D. & Barfield, M. Habitat selection and niche conservatism. *Israel Journal of Ecology & Evolution* **54**, 295-309 (2008).

76. Yao, Z., Jones, J., Kohrt, H. & Strober, S. Selective resistance of CD44hi T cells to p53-dependent cell death results in persistence of immunologic memory after total body irradiation. *Journal of immunology* **187**, 4100-4108 (2011).

77. Di Maggio, N. *et al.* Fibroblast growth factor-2 maintains a niche-dependent population of self-renewing highly potent non-adherent mesenchymal progenitors through FGFR2c. *Stem cells* **30**, 1455-1464 (2012).

78. Fukiage, K. *et al.* Expression of vascular cell adhesion molecule-1 indicates the differentiation potential of human bone marrow stromal cells. *Biochemical and biophysical research communications* **365**, 406-412 (2008).

79. Digirolamo, C.M. *et al.* Propagation and senescence of human marrow stromal cells in culture: a simple colony-forming assay identifies samples with the greatest potential to propagate and differentiate. *British journal of haematology* **107**, 275-281 (1999).

80. Banfi, A. *et al.* Proliferation kinetics and differentiation potential of ex vivo expanded human bone marrow stromal cells: Implications for their use in cell therapy. *Experimental hematology* **28**, 707-715 (2000).

81. Sasaki, T., Takagi, M., Soma, T. & Yoshida, T. 3D culture of murine hematopoietic cells with spatial development of stromal cells in nonwoven fabrics. *Cytotherapy* **4**, 285-291 (2002).

82. Tormin, A. *et al.* CD146 expression on primary nonhematopoietic bone marrow stem cells is correlated with in situ localization. *Blood* **117**, 5067-5077 (2011).

83. Churchman, S.M. *et al.* Transcriptional profile of native CD271+ multipotential stromal cells: evidence for multiple fates, with prominent osteogenic and Wnt pathway signaling activity. *Arthritis and rheumatism* **64**, 2632-2643 (2012).

84. Cox, G. *et al.* High abundance of CD271(+) multipotential stromal cells (MSCs) in intramedullary cavities of long bones. *Bone* **50**, 510-517 (2012).

85. Fonsatti, E. & Maio, M. Highlights on endoglin (CD105): from basic findings towards clinical applications in human cancer. *Journal of translational medicine* **2**, 18 (2004).

86. Braun, J. *et al.* Concerted Regulation of CD34 and CD105 Accompanies Mesenchymal Stromal Cell Derivation from Human Adventitial Stromal Cell. *Stem cells and development* (2012).

87. Winkler, E.A., Bell, R.D. & Zlokovic, B.V. Pericyte-specific expression of PDGF beta receptor in mouse models with normal and deficient PDGF beta receptor signaling. *Molecular neurodegeneration* **5**, 32 (2010).

88. Tokunaga, A. *et al.* PDGF receptor beta is a potent regulator of mesenchymal stromal cell function. *Journal of bone and mineral research : the official journal of the American Society for Bone and Mineral Research* **23**, 1519-1528 (2008).

89. Hara, T. *et al.* Identification of IL-7-producing cells in primary and secondary lymphoid organs using IL-7-GFP knock-in mice. *Journal of immunology (Baltimore, Md. : 1950)* **189**, 1577-1584 (2012).

90. Zehentmeier, S. Static and dynamic components cooperate to form a stable survival niche for memory plasma cells in the bone marrow:
a microanatomical study *Naturwissenschaftliche Fakultät I, Humboldt Universität Berlin* (2013).

91. Rock, J. *et al.* CD303 (BDCA-2) signals in plasmacytoid dendritic cells via a BCR-like signalosome involving Syk, Slp65 and PLCgamma2. *European journal of immunology* **37**, 3564-3575 (2007).

92. Biesen, R. *et al.* Sialic acid-binding Ig-like lectin 1 expression in inflammatory and resident monocytes is a potential biomarker for monitoring disease activity and success of therapy in systemic lupus erythematosus. *Arthritis and rheumatism* **58**, 1136-1145 (2008).

93. Shimizu, T.K.M. A method for preparing 2- to 50-µm-thick fresh-frozen sections of large samples and undecalcified hard tissues. *Histochem Cell Biol* (2000).

94. Wakatsuki, T., Schwab, B., Thompson, N.C. & Elson, E.L. Effects of cytochalasin D and latrunculin B on mechanical properties of cells. *Journal of cell science* **114**, 1025-1036 (2001).

95. Cooper, J.A. Effects of cytochalasin and phalloidin on actin. *The Journal of cell biology* **105**, 1473-1478 (1987).

96. Morton, W.M., Ayscough, K.R. & McLaughlin, P.J. Latrunculin alters the actin-monomer subunit interface to prevent polymerization. *Nat Cell Biol* **2**, 376-378 (2000).

97. Foissner, I. & Wasteneys, G.O. Wide-ranging effects of eight cytochalasins and latrunculin A and B on intracellular motility and actin filament reorganization in characean internodal cells. *Plant & cell physiology* **48**, 585-597 (2007).

98. Schroeder, A. *et al.* The RIN: an RNA integrity number for assigning integrity values to RNA measurements. *BMC molecular biology* **7**, 3 (2006).

99. Domen, J. & Weissman, I.L. Hematopoietic stem cells need two signals to prevent apoptosis; BCL-2 can provide one of these, Kitl/c-Kit signaling the other. *The Journal of experimental medicine* **192**, 1707-1718 (2000).

100. Huber, M.A. *et al.* Expression of stromal cell markers in distinct compartments of human skin cancers. *Journal of cutaneous pathology* **33**, 145-155 (2006).

101. Collins, T. *et al.* Structure and chromosomal location of the gene for endothelial-leukocyte adhesion molecule 1. *The Journal of biological chemistry* **266**, 2466-2473 (1991).

102. Wellner, M. *et al.* Endothelial cell specific molecule-1--a newly identified protein in adipocytes. *Hormone and metabolic research = Hormon- und Stoffwechselforschung = Hormones et metabolisme* **35**, 217-221 (2003).

103. Eguchi, J. *et al.* Identification of adipocyte adhesion molecule (ACAM), a novel CTX gene family, implicated in adipocyte maturation and development of obesity. *The Biochemical journal* **387**, 343-353 (2005).

104. Raschperger, E., Engstrom, U., Pettersson, R.F. & Fuxe, J. CLMP, a Novel Member of the CTX Family and a New Component of Epithelial Tight Junctions. *Journal of Biological Chemistry* **279**, 796-804 (2004).

105. OICR. Whole Genome Sequencing. In: icon-whole-transcriptome-seq, editor.; 2018.

106. C.-Y., W. & C.-F., L. Annexin A2: Its molecular regulation and cellular expression in cancer development. *Disease Markers* **2014** (2014).

107. Jung, Y. *et al.* Annexin-2 is a regulator of stromal cell-derived factor-1/CXCL12 function in the hematopoietic stem cell endosteal niche. *Experimental hematology* **39**, 151-166.e151 (2011).

108. Jung, Y. *et al.* Annexin 2-CXCL12 interactions regulate metastatic cell targeting and growth in the bone marrow. *Molecular cancer research : MCR* **13**, 197-207 (2015).

109. Dormady, S.P., Zhang, X.M. & Basch, R.S. Hematopoietic progenitor cells grow on 3T3 fibroblast monolayers that overexpress growth arrest-specific gene-6 (GAS6). *Proceedings of the National Academy of Sciences of the United States of America* **97**, 12260-12265 (2000).

110. Immunol, A.R. TAM Receptor Signaling in Immune Homeostasis. 355-391 (2015).

111. Shiozawa, Y. *et al.* GAS6/AXL axis regulates prostate cancer invasion, proliferation, and survival in the bone marrow niche. *Neoplasia (New York, N.Y.)* **12**, 116-127 (2010).

112. Schulz, D. Isolation and ex vivo characterization of stromal cells involved in the maintenance of memory lymphocytes from murine bone marrow. M.Sc. thesis, University of Potsdam, Potsdam, 2014.

113. Umezawa, A., Harigaya, K., Abe, H. & Watanabe, Y. Gap-junctional communication of bone marrow stromal cells is resistant to irradiation in vitro. *Experimental hematology* **18**, 1002-1007 (1990).

114. Tokoyoda, K. & Radbruch, A. Signals controlling rest and reactivation of T helper memory lymphocytes in bone marrow. *Cellular and molecular life sciences : CMLS* **69**, 1609-1613 (2012).

115. Schenkel, J.M. & Masopust, D. Tissue-resident memory T cells. *Immunity* **41**, 886-897 (2014).

116. Mei, H.E. *et al.* Steady-state generation of mucosal IgA+ plasmablasts is not abrogated by B-cell depletion therapy with rituximab. *Blood* **116**, 5181-5190 (2010).

117. Okhrimenko, A. *et al.* Human memory T cells from the bone marrow are resting and maintain long-lasting systemic memory. *Proceedings of the National Academy of Sciences of the United States of America* **111**, 9229-9234 (2014).

118. Siracusa, F. *et al.* Nonfollicular reactivation of bone marrow resident memory CD4 T cells in immune clusters of the bone marrow. *Proceedings of the National Academy of Sciences of the United States of America* **115**, 1334-1339 (2018).

119. den Haan, J.M., Mebius, R.E. & Kraal, G. Stromal cells of the mouse spleen. *Front Immunol* **3**, 201 (2012).

120. Dominici, M. *et al.* Minimal criteria for defining multipotent mesenchymal stromal cells. The International Society for Cellular Therapy position statement. *Cytotherapy* **8**, 315-317 (2006).

121. Wu, Y., Zhou, S. & Smas, C.M. Downregulated expression of the secreted glycoprotein follistatin-like 1 (Fstl1) is a robust hallmark of preadipocyte to adipocyte conversion. *Mechanisms of development* **127**, 183-202 (2010).

122. Gerlach, J.C. *et al.* Adipogenesis of human adipose-derived stem cells within three-dimensional hollow fiber-based bioreactors. *Tissue engineering. Part C, Methods* **18**, 54-61 (2012).

123. Berniakovich, I. & Giorgio, M. Low oxygen tension maintains multipotency, whereas normoxia increases differentiation of mouse bone marrow stromal cells. *International Journal of Molecular Sciences* **14**, 2119-2134 (2013).

124. Kim, S., Chaudhry, A., Lee, I. & Frank, J.a. Effects of long-term hypoxia and pro-survival cocktail in bone marrow-derived stromal cell survival. *Stem cells and development* **23**, 530-540 (2014).

125. Valorani, M.G. *et al.* Hypoxia increases Sca-1/CD44 co-expression in murine mesenchymal stem cells and enhances their adipogenic differentiation potential. *Cell and Tissue Research* **341**, 111-120 (2010).

126. Miraoui, H. *et al.* Fibroblast growth factor receptor 2 promotes osteogenic differentiation in mesenchymal cells via ERK1/2 and protein kinase C signaling. *The Journal of biological chemistry* **284**, 4897-4904 (2009).

127. Miraoui, H., Severe, N., Vaudin, P., Pages, J.C. & Marie, P.J. Molecular silencing of Twist1 enhances osteogenic differentiation of murine mesenchymal stem cells: implication of FGFR2 signaling. *Journal of cellular biochemistry* **110**, 1147-1154 (2010).

128. Di Benedetto, A. *et al.* N-cadherin and cadherin 11 modulate postnatal bone growth and osteoblast differentiation by distinct mechanisms. *Journal of cell science* **123**, 2640-2648 (2010).

129. Kii, I., Amizuka, N., Shimomura, J., Saga, Y. & Kudo, A. Cell-cell interaction mediated by cadherin-11 directly regulates the differentiation of mesenchymal cells into the cells of the osteo-lineage and the chondro-lineage. *Journal of bone and mineral research : the official journal of the American Society for Bone and Mineral Research* **19**, 1840-1849 (2004).

130. Mizoguchi, T. *et al.* Osterix Marks Distinct Waves of Primitive and Definitive Stromal Progenitors during Bone Marrow Development. *Developmental Cell* **29**, 340-349 (2014).

131. Cho, S.W. *et al.* Differential effects of secreted frizzled-related proteins (sFRPs) on osteoblastic differentiation of mouse mesenchymal cells and apoptosis of osteoblasts. *Biochemical and biophysical research communications* **367**, 399-405 (2008).

132. Nakanishi, R. *et al.* Osteoblast-targeted expression of Sfrp4 in mice results in low bone mass. *Journal of bone and mineral research : the official journal of the American Society for Bone and Mineral Research* **23**, 271-277 (2008).

133. Mukherjee, A. & Rotwein, P. Insulin-like growth factor-binding protein-5 inhibits osteoblast differentiation and skeletal growth by blocking insulin-like growth factor actions. *Molecular endocrinology (Baltimore, Md.)* **22**, 1238-1250 (2008).

134. Peruzzi, B. *et al.* c-Src and IL-6 inhibit osteoblast differentiation and integrate IGFBP5 signalling. *Nature communications* **3**, 630 (2012).

135. Mazzucchelli, R.I. *et al.* Visualization and identification of IL-7 producing cells in reporter mice. *PloS one* **4**, e7637 (2009).

136. Holländer, G.A. *et al.* Monoallelic expression of the interleukin-2 locus. *Science (New York, N.Y.)* **279**, 2118-2121 (1998).

137. Du, B. *et al.* The transcription factor paired-related homeobox 1 (Prrx1) inhibits adipogenesis by activating transforming growth factor-beta (TGFbeta) signaling. *The Journal of biological chemistry* **288**, 3036-3047 (2013).

138. Lu, X. *et al.* Identification of the homeobox protein Prx1 (MHox, Prrx-1) as a regulator of osterix expression and mediator of tumor necrosis factor alpha action in osteoblast differentiation.

Journal of bone and mineral research : the official journal of the American Society for Bone and Mineral Research **26**, 209-219 (2011).

139. Chun, T. *et al.* CD1d-expressing dendritic cells but not thymic epithelial cells can mediate negative selection of NKT cells. *The Journal of experimental medicine* **197**, 907-918 (2003).

140. Uldrich, A.P. *et al.* CD1d-lipid antigen recognition by the γδ TCR. *Nature immunology* **14**, 1137-1145 (2013).

141. Romieu-Mourez, R., François, M., Boivin, M.N., Stagg, J. & Galipeau, J. Regulation of MHC class II expression and antigen processing in murine and human mesenchymal stromal cells by IFN-γ, TGF-β, and cell density. *The Journal of Immunology* **179**, 1549 (2007).

142. Schnabel, L.V., Pezzanite, L.M., Antczak, D.F., Felippe, M.J. & Fortier, L.A. Equine bone marrow-derived mesenchymal stromal cells are heterogeneous in MHC class II expression and capable of inciting an immune response in vitro. *Stem Cell Res Ther* **5**, 13 (2014).

143. Tang, K.C. *et al.* Down-Regulation of MHC II in Mesenchymal Stem Cells at High IFN- Can Be Partly Explained by Cytoplasmic Retention of CIITA. *The Journal of Immunology* **180**, 1826-1833 (2008).

144. Slauenwhite, D. & Johnston, B. Regulation of NKT Cell Localization in Homeostasis and Infection. *Frontiers in immunology* **6**, 255 (2015).

145. Tan, J.T. Interleukin (IL)-15 and IL-7 Jointly Regulate Homeostatic Proliferation of Memory Phenotype CD8+ Cells but Are Not Required for Memory Phenotype CD4+ Cells. *Journal of Experimental Medicine* **195**, 1523-1532 (2002).

146. Sercan Alp, Ö. *et al.* Memory CD8(+) T cells colocalize with IL-7(+) stromal cells in bone marrow and rest in terms of proliferation and transcription. *European journal of immunology* **45**, 975-987 (2015).

147. Pepler, L., Yu, P., Dwivedi, D.J., Trigatti, B.L. & Liaw, P.C. Characterization of mice harboring a variant of EPCR with impaired ability to bind protein C: novel role of EPCR in hematopoiesis. *Blood* **126**, 673-682 (2015).

148. Sackstein, R. *et al.* Ex vivo glycan engineering of CD44 programs human multipotent mesenchymal stromal cell trafficking to bone. *Nature medicine* **14**, 181-187 (2008).

149. Garay, E. *et al.* CRTAM: A molecule involved in epithelial cell adhesion. *Journal of cellular biochemistry* **111**, 111-122 (2010).

150. Tan, Y., Zhao, M., Xiang, B., Chang, C. & Lu, Q. CD24: from a Hematopoietic Differentiation Antigen to a Genetic Risk Factor for Multiple Autoimmune Diseases. *Clinical reviews in allergy & immunology* **50**, 70-83 (2016).

151. Chow, A. *et al.* Bone marrow CD169+ macrophages promote the retention of hematopoietic stem and progenitor cells in the mesenchymal stem cell niche. *The Journal of experimental medicine* **208**, 261-271 (2011).

152. Holley, R.J. *et al.* Comparative quantification of the surfaceome of human multipotent mesenchymal progenitor cells. *Stem Cell Reports* **4**, 473-488 (2015).

153. Bai, L. *et al.* Effects of Mesenchymal Stem Cell-Derived Exosomes on Experimental Autoimmune Uveitis. *Sci Rep* **7**, 4323 (2017).

154. Bühring, H.-J. *et al.* Phenotypic characterization of distinct human bone marrow-derived MSC subsets. *Annals of the New York Academy of Sciences* **1176**, 124-134 (2009).

155. Zeevaart, J.G. *et al.* CD73-generated adenosine promotes osteoblast differentiation. **130**, 9492-9499 (2009).

156. Conter, L.J., Song, E., Shlomchik, M.J. & Tomayko, M.M. CD73 Expression Is Dynamically Regulated in the Germinal Center and Bone Marrow Plasma Cells Are Diminished in Its Absence. *PloS one* **9**, e92009 (2014).

157. Antonioli, L., Yegutkin, G.G., Pacher, P., Blandizzi, C. & Hasko, G. Anti-CD73 in cancer immunotherapy: awakening new opportunities. *Trends Cancer* **2**, 95-109 (2016).

158. Romio, M. *et al.* Extracellular purine metabolism and signaling of CD73-derived adenosine in murine Treg and Teff cells. *Am J Physiol Cell Physiol* **301**, C530-539 (2011).

159. De Miguel, M.P. *et al.* Immunosuppressive properties of mesenchymal stem cells: advances and applications. *Current molecular medicine* **12**, 574-591 (2012).

160. Vaine, C.A. & Soberman, R.J. The CD200-CD200R1 inhibitory signaling pathway: immune regulation and host-pathogen interactions. *Adv Immunol* **121**, 191-211 (2014).

161. Liu, J. *et al.* The complement inhibitory protein DAF (CD55) suppresses T cell immunity in vivo. *The Journal of experimental medicine* **201**, 567-577 (2005).

162. Manieri, N.A., Chiang, E.Y. & Grogan, J.L. TIGIT: A Key Inhibitor of the Cancer Immunity Cycle. *Trends in immunology* **38**, 20-28 (2017).

163. Kane, L.P. T cell Ig and mucin domain proteins and immunity. *Journal of immunology* **184**, 2743-2749 (2010).

164. Del Rio, M.L. *et al.* Modulation of cytotoxic responses by targeting CD160 prolongs skin graft survival across major histocompatibility class I barrier. *Translational research : the journal of laboratory and clinical medicine* **181**, 83-95.e83 (2017).

165. D'Addio, F. *et al.* CD160Ig fusion protein targets a novel costimulatory pathway and prolongs allograft survival. *PloS one* **8**, e60391 (2013).

166. Sharpe, A.H. & Pauken, K.E. The diverse functions of the PD1 inhibitory pathway. *Nature reviews. Immunology* **18**, 153-167 (2018).

167. Liu, F.T. & Rabinovich, G.a. Galectins: Regulators of acute and chronic inflammation. *Annals of the New York Academy of Sciences* **1183**, 158-182 (2010).

168. Madireddi, S. *et al.* Galectin-9 controls the therapeutic activity of 4-1BB-targeting antibodies. *The Journal of experimental medicine* **211**, 1433-1448 (2014).

169. Ungerer, C. *et al.* Galectin-9 is a suppressor of T and B cells and predicts the immune modulatory potential of mesenchymal stromal cell preparations. *Stem cells and development* **23**, 755-766 (2014).

170. Strainic, M.G. *et al.* Locally produced complement fragments C5a and C3a provide both costimulatory and survival signals to naive CD4+ T cells. *Immunity* **28**, 425-435 (2008).

171. Heeger, P.S. *et al.* Decay-accelerating factor modulates induction of T cell immunity. *The Journal of experimental medicine* **201**, 1523-1530 (2005).

172. Welch, P.A., Burrows, P.D., Namen, A., Gillis, S. & Cooper, M.D. Bone marrow stromal cells and interleukin-7 induce coordinate expression of the BP-1/6C3 antigen and pre-B cell growth. *International immunology* **2**, 697-705 (1990).

173. Ganguly, P. *et al.* Age-related Changes in Bone Marrow Mesenchymal Stromal Cells: A Potential Impact on Osteoporosis and Osteoarthritis Development. *Cell Transplant* **26**, 1520-1529 (2017).

174. Goralski, K.B. *et al.* Chemerin, a novel adipokine that regulates adipogenesis and adipocyte metabolism. *The Journal of biological chemistry* **282**, 28175-28188 (2007).

175. Herova, M., Schmid, M., Gemperle, C. & Hersberger, M. ChemR23, the receptor for chemerin and resolvin E1, is expressed and functional on M1 but not on M2 macrophages. *Journal of immunology* **194**, 2330-2337 (2015).

176. de Poorter, C., Baertsoen, K., Lannoy, V., Parmentier, M. & Springael, J.Y. Consequences of ChemR23 Heteromerization with the Chemokine Receptors CXCR4 and CCR7. *PloS one* **8**, 1-10 (2013).

177. Chistiakov, D.A., Orekhov, A.N., Sobenin, I.A. & Bobryshev, Y.V. Plasmacytoid dendritic cells: development, functions, and role in atherosclerotic inflammation. *Front Physiol* **5**, 279 (2014).

178. Stagg, J., Pommey, S., Eliopoulos, N. & Galipeau, J. Interferon-gamma – stimulated marrow stromal cells : a new type of nonhematopoietic antigen-presenting cell. *Victoria* **107**, 2570-2577 (2006).

179. Park, D. *et al.* Endogenous Bone Marrow MSCs Are Dynamic, Fate-Restricted Participants in Bone Maintenance and Regeneration. *Cell Stem Cell* **10**, 259-272 (2012).

180. Belnoue, E. *et al.* APRIL is critical for plasmablast survival in the bone marrow and poorly expressed by early-life bone marrow stromal cells. *Blood* **111**, 2755-2764 (2008).

181. Varfolomeev, E. *et al.* APRIL-Deficient Mice Have Normal Immune System Development. *Molecular and Cellular Biology* **24**, 997-1006 (2004).

182. Schajnovitz, A. *et al.* CXCL12 secretion by bone marrow stromal cells is dependent on cell contact and mediated by connexin-43 and connexin-45 gap junctions. *Nature immunology* **12**, 391-398 (2011).

183. Balandran, J.C. *et al.* Pro-inflammatory-Related Loss of CXCL12 Niche Promotes Acute Lymphoblastic Leukemic Progression at the Expense of Normal Lymphopoiesis. *Front Immunol* **7**, 666 (2016).

184. Rostovskaya, M. & Anastassiadis, K. Differential Expression of Surface Markers in Mouse Bone Marrow Mesenchymal Stromal Cell Subpopulations with Distinct Lineage Commitment. *PloS one* **7**, e51221 (2012).

185. Jung, Y. *et al.* Annexin II expressed by osteoblasts and endothelial cells regulates stem cell adhesion, homing, and engraftment following transplantation. *Blood* **110**, 82-90 (2007).

186. Mamani-Matsuda, M. *et al.* The human spleen is a major reservoir for long-lived vaccinia virus-specific memory B cells. *Blood* **111**, 4653-4659 (2008).

187. Kim, C.H. Homeostatic and pathogenic extramedullary hematopoiesis. *J Blood Med* **1**, 13-19 (2010).

188. Ergen, A.V., Boles, N.C. & Goodell, M.A. Rantes/Ccl5 influences hematopoietic stem cell subtypes and causes myeloid skewing. *Blood* **119**, 2500-2509 (2012).

189. Rubin, C.T. *et al.* Adipogenesis is inhibited by brief, daily exposure to high-frequency, extremely low-magnitude mechanical signals. *Proceedings of the National Academy of Sciences of the United States of America* **104**, 17879-17884 (2007).

190. Takeshita, S., Fumoto, T., Naoe, Y. & Ikeda, K. Age-related marrow adipogenesis is linked to increased expression of RANKL. *The Journal of biological chemistry* **289**, 16699-16710 (2014).

191. Pangrazzi, L. *et al.* "Inflamm-aging" influences immune cell survival factors in human bone marrow. *European journal of immunology* **47**, 481-492 (2017).

192. Green, D.E. & Rubin, C.T. Consequences of irradiation on bone and marrow phenotypes, and its relation to disruption of hematopoietic precursors. *Bone* **63**, 87-94 (2014).

193. Dorshkind, K., Green, L., Godwin, a. & Fletcher, W.H. Connexin-43-type gap junctions mediate communication between bone marrow stromal cells. *Blood* **82**, 38-45 (1993).

194. Montecino-Rodriguez, E., Leathers, H. & Dorshkind, K. Expression of connexin 43 (Cx43) is critical for normal hematopoiesis. *Blood* **96**, 917-924 (2000).

195. Park, J.M. *et al.* Exogenous CXCL12 activates protein kinase C to phosphorylate connexin 43 for gap junctional intercellular communication among confluent breast cancer cells. *Cancer letters* **331**, 84-91 (2013).

196. Jiang, J.X., Siller-Jackson, A.J. & Burra, S. Roles of gap junctions and hemichannels in bone cell functions and in signal transmission of mechanical stress. *Front Biosci* **12**, 1450-1462 (2007).

197. Leyendeckers, H. *et al.* Correlation analysis between frequencies of circulating antigen-specific IgG-bearing memory B cells and serum titers of antigen-specific IgG. *European journal of immunology* **29**, 1406-1417 (1999).

198. Taub, D.D. *et al.* Immunity from smallpox vaccine persists for decades: a longitudinal study. *Am J Med* **121**, 1058-1064 (2008).

199. Lecomte, J. *et al.* Bone marrow-derived mesenchymal cells and MMP13 contribute to experimental choroidal neovascularization. *Cellular and molecular life sciences : CMLS* **68**, 677-686 (2011).

200. Lederle, W. *et al.* MMP13 as a stromal mediator in controlling persistent angiogenesis in skin carcinoma. *Carcinogenesis* **31**, 1175-1184 (2010).

201. Morrison, C. *et al.* Microarray and proteomic analysis of breast cancer cell and osteoblast co-cultures: role of osteoblast matrix metalloproteinase (MMP)-13 in bone metastasis. *The Journal of biological chemistry* **286**, 34271-34285 (2011).

202. Katz, Y. & Strunk, R.C. Synthesis and regulation of C1 inhibitor in human skin fibroblasts. *Journal of immunology* **142**, 2041-2045 (1989).

203. Schmaier, A.H., Amenta, S., Xiong, T., Heda, G.D. & Gewirtz, A.M. Expression of platelet C1 inhibitor. *Blood* **82**, 465-474 (1993).

204. James, P.L., Jones, S.B., Busby, W.H., Jr., Clemmons, D.R. & Rotwein, P. A highly conserved insulin-like growth factor-binding protein (IGFBP-5) is expressed during myoblast differentiation. *The Journal of biological chemistry* **268**, 22305-22312 (1993).

205. Lara-Castro, C., Fu, Y., Chung, B.H. & Garvey, W.T. Adiponectin and the metabolic syndrome: mechanisms mediating risk for metabolic and cardiovascular disease. *Current opinion in lipidology* **18**, 263-270 (2007).

206. Woodbury, D., Reynolds, K. & Black, I.B. Adult bone marrow stromal stem cells express germline, ectodermal, endodermal, and mesodermal genes prior to neurogenesis. *Journal of Neuroscience Research* **69**, 908-917 (2002).

207. Balduino, A. *et al.* Molecular signature and in vivo behavior of bone marrow endosteal and subendosteal stromal cell populations and their relevance to hematopoiesis. *Experimental cell research* **318**, 2427-2437 (2012).

208. Shin, S. *et al.* NRF2 modulates aryl hydrocarbon receptor signaling: influence on adipogenesis. *Mol Cell Biol* **27**, 7188-7197 (2007).

209. Zheng, W. *et al.* Stimulation of mouse Cyp1b1 during adipogenesis: characterization of promoter activation by the transcription factor Pax6. *Archives of biochemistry and biophysics* **532**, 1-14 (2013).

210. Kerzee, J.K. & Ramos, K.S. Constitutive and inducible expression of Cyp1a1 and Cyp1b1 in vascular smooth muscle cells: role of the Ahr bHLH/PAS transcription factor. *Circulation research* **89**, 573-582 (2001).

211. Morgan, J.M., Wong, A., Yellowley, C.E. & Genetos, D.C. Regulation of tenascin expression in bone. *Journal of cellular biochemistry* **112**, 3354-3363 (2011).

212. Weis, S.M. *et al.* Myocardial mechanics and collagen structure in the osteogenesis imperfecta murine (oim). *Circulation research* **87**, 663-669 (2000).

213. Mizuno, K. *et al.* MPTP delta, a putative murine homolog of HPTP delta, is expressed in specialized regions of the brain and in the B-cell lineage. *Mol Cell Biol* **13**, 5513-5523 (1993).

214. Chang, S.K. *et al.* Cadherin-11 regulates fibroblast inflammation. *Proceedings of the National Academy of Sciences of the United States of America* **108**, 8402-8407 (2011).

215. Roberts, E.W. *et al.* Depletion of stromal cells expressing fibroblast activation protein-alpha from skeletal muscle and bone marrow results in cachexia and anemia. *The Journal of experimental medicine* **210**, 1137-1151 (2013).

216. Tran, E. *et al.* Immune targeting of fibroblast activation protein triggers recognition of multipotent bone marrow stromal cells and cachexia. *The Journal of experimental medicine* **210**, 1125-1135 (2013).

217. Tsuda, T. *et al.* Zinc finger protein Zac1 is expressed in chondrogenic sites of the mouse. *Developmental dynamics : an official publication of the American Association of Anatomists* **229**, 340-348 (2004).

218. Valente, T., Junyent, F. & Auladell, C. Zac1 is expressed in progenitor/stem cells of the neuroectoderm and mesoderm during embryogenesis: differential phenotype of the Zac1-expressing cells during development. *Developmental dynamics : an official publication of the American Association of Anatomists* **233**, 667-679 (2005).

219. Nakatani, M., Kokubo, M., Ohsawa, Y., Sunada, Y. & Tsuchida, K. Follistatin-derived peptide expression in muscle decreases adipose tissue mass and prevents hepatic steatosis. *American journal of physiology. Endocrinology and metabolism* **300**, E543-553 (2011).

220. Ouchi, N. *et al.* Follistatin-like 1, a secreted muscle protein, promotes endothelial cell function and revascularization in ischemic tissue through a nitric-oxide synthase-dependent mechanism. *The Journal of biological chemistry* **283**, 32802-32811 (2008).

221. Mukobata, S. *et al.* M6a acts as a nerve growth factor-gated Ca(2+) channel in neuronal differentiation. *Biochemical and biophysical research communications* **297**, 722-728 (2002).

222. Song, S., Ewald, A.J., Stallcup, W., Werb, Z. & Bergers, G. PDGFRbeta+ perivascular progenitor cells in tumours regulate pericyte differentiation and vascular survival. *Nat Cell Biol* **7**, 870-879 (2005).

223. Festoff, B.W., Rao, J.S. & Hantai, D. Plasminogen activators and inhibitors in the neuromuscular system: III. The serpin protease nexin I is synthesized by muscle and localized at neuromuscular synapses. *Journal of cellular physiology* **147**, 76-86 (1991).

224. Broudy, V.C. Stem cell factor and hematopoiesis. *Blood* **90**, 1345-1364 (1997).

225. Thomas, T. *et al.* Leptin Acts on Human Marrow Stromal Cells to Enhance Differentiation to Osteoblasts and to Inhibit Differentiation to Adipocytes. *Endocrinology* **140**, 1630-1638 (1999).

226. Jansen, K.M. & Pavlath, G.K. Mannose receptor regulates myoblast motility and muscle growth. *The Journal of cell biology* **174**, 403-413 (2006).

227. Ghelfi, E. *et al.* Fatty acid binding protein 4 regulates VEGF-induced airway angiogenesis and inflammation in a transgenic mouse model: implications for asthma. *The American journal of pathology* **182**, 1425-1433 (2013).

228. Falkowski, M., Schledzewski, K., Hansen, B. & Goerdt, S. Expression of stabilin-2, a novel fasciclin-like hyaluronan receptor protein, in murine sinusoidal endothelia, avascular tissues, and at solid/liquid interfaces. *Histochem Cell Biol* **120**, 361-369 (2003).

229. Qian, H. *et al.* Stabilins are expressed in bone marrow sinusoidal endothelial cells and mediate scavenging and cell adhesive functions. *Biochemical and biophysical research communications* **390**, 883-886 (2009).

230. Bonuccelli, G. *et al.* ATR/TEM8 is highly expressed in epithelial cells lining Bacillus anthracis' three sites of entry: implications for the pathogenesis of anthrax infection. *American Journal of Physiology - Cell Physiology* **288**, C1402-C1410 (2005).

231. Hou, R., Liu, L., Anees, S., Hiroyasu, S. & Sibinga, N.E. The Fat1 cadherin integrates vascular smooth muscle cell growth and migration signals. *The Journal of cell biology* **173**, 417-429 (2006).

232. Kuwahara, G., Nishinakamura, H., Kojima, D., Tashiro, T. & Kodama, S. Vascular endothelial growth factor-C derived from CD11b+ cells induces therapeutic improvements in a murine model of hind limb ischemia. *Journal of vascular surgery* **57**, 1090-1099 (2013).

233. Kagan, H.M. & Li, W. Lysyl oxidase: properties, specificity, and biological roles inside and outside of the cell. *Journal of cellular biochemistry* **88**, 660-672 (2003).

234. Knepper, M.A. The aquaporin family of molecular water channels. *Proceedings of the National Academy of Sciences of the United States of America* **91**, 6255-6258 (1994).

Acknowledgements

(Danksagungen)

Ich möchte an dieser Stelle den vielen Menschen danken, die mich durch die ereignisreichen Jahre meiner Promotion begleitet und unterstützt haben. Vorweg gilt mein Dank Enrico Klotzsch, Andreas Thiel sowie Andreas Radbruch für die Erstellung der Gutachten zu dieser Arbeit sowie Emanuel Heitlinger und Thomas Stach für Ihre Bereitschaft, meiner Kommission beizuwohnen. Andreas Radbruch bin ich besonders dankbar, dass er mir nicht nur die Promotion als solche ermöglicht hat, sondern noch dazu zu einem so faszinierenden Thema wie der Stromazell-Biologie in einem immunologischen Setting.

Des Weiteren gilt mein Dank Özen dafür, dass sie mich an Stromazellen herangeführt und gutes, wissenschaftliches Arbeiten gelehrt hat. René für das Teilen seiner Flow-, Politik- und Gourmetkenntnisse, Claudi & Cam Loan für die Zeit als beste Banknachbarn und/oder Badminton-Experten. Richie für die lustigen Tage im Lab und die Kameradschaft bei einem Thema, mit dem man im DRFZ allein auf weiter Flur stand. Steffi für die Kaffeepausen und Privat-/Fachdiskussionen. Hyun-Dong, Padde & Farzin für die vielen offenen Ohren & Ratschläge, wenn Andreas mal wieder auf Dienstreise war. Ein Hoch auf flache Hierarchien. Gitta & Katrin für die lustigen Gespräche oder Hilfe im Labor. Mairi für ihre unglaublichen Histo- und Immunologiekenntnisse generell. Weijie für ihre unerschütterliche gute Laune. Ralf und Pawel für die starke Hilfe im bioinformatischen Arbeiten.

Natürlich möchte ich mich auch bei meiner Familie bedanke. Da wäre meine Oma Bianka, die bereits im jungen Alter meine Faszination für die Naturwissenschaften geweckt hat. Aber auch meinen Eltern, die mir das Studium überhaupt erst ermöglicht haben und mir stets unterstützend zur Seite standen. Das gilt natürlich in noch größerem Maße meiner Frau Sandra, die meinen Sturkopf und Prokrastinationswahn nun schon ein ganzes Weilchen ertragen muss und es hoffentlich noch viele weitere Jahre tun wird. Danke, dass du mich vorbehaltlos bei meinen Irrungen und Wirrungen unterstützt, auch wenn das halt mal ein paar Monate Arbeitslosigkeit zur Folge hatte. Danke, dass du mein Fels in der Brandung bist.

Statutory Declaration

(Selbstständigkeitserklärung)

Erklärung: Hiermit erkläre ich, die Dissertation selbstständig und nur unter Verwendung der angegebenen Hilfen und Hilfsmittel angefertigt zu haben. Ich habe mich anderwärts nicht um einen Doktorgrad beworben und besitze keinen entsprechenden Doktorgrad. Ich erkläre, dass ich die Dissertation oder Teile davon nicht bereits bei einer anderen wissenschaftlichen Einrichtung eingereicht habe und dass sie dort weder angenommen noch abgelehnt wurde. Ich erkläre die Kenntnisnahme der dem Verfahren zugrunde liegenden Promotionsordnung der Mathematisch-Naturwissenschaftlichen Fakultät I der Humboldt-Universität zu Berlin vom 27. Juni 2012. Weiterhin erkläre ich, dass keine Zusammenarbeit mit gewerblichen Promotionsberaterinnen/Promotions-beratern stattgefunden hat und dass die Grundsätze der Humboldt-Universität zu Berlin zur Sicherung guter wissenschaftlicher Praxis eingehalten wurden.

Declaration: I hereby declare that I completed the doctoral thesis independently based on the stated resources and aids. I have not applied for a doctoral degree elsewhere and do not have a corresponding doctoral degree. I have not submitted the doctoral thesis, or parts of it, to another academic institution and the thesis has not been accepted or rejected. I declare that I have acknowledged the Doctoral Degree Regulations which underlie the procedure of the Faculty of Mathematics and Natural Sciences of Humboldt-Universität zu Berlin, as amended on 27th June 2012. Furthermore, I declare that no collaboration with commercial doctoral degree supervisors took place, and that the principles of Humboldt-Universität zu Berlin for ensuring good academic practice were abided by.

---------- ----------

Date/Datum Signature/Unterschrift